Quasi-static Tearing Tests of Metal Plating

by

Jeffrey C. Woertz

B.S. Civil Engineering
University of Illinois Urbana-Champaign, 1992

Submitted to the Department of Ocean Engineering and
the Department of Mechanical Engineering
in partial fulfillment of the requirements for the degrees of

Master of Science in Naval Architecture and Marine Engineering
And
Master of Science in Mechanical Engineering
At the
MASSACHUSETTS INSTITUTE OF TECHNOLOGY
September 2002

Signature of Author.... .....
Department of Ocean Engineering and
The Department of Mechanical Engineering
09 August 2002

Certified by..... .....
Tomasz Wierzbicki
Professor of Applied Mechanics
Thesis Supervisor

Certified by..... .....
Frank A. McClintock
Professor of Mechanical Engineering
Thesis Reader

Accepted by..... .....
Professor Ain A. Sonin
Chairperson, Department Committee on Graduate Studies
Department of Mechanical Engineering

Accepted by..... .....
Professor Henrik Schmidt
Chairperson, Department Committee on Graduate Studies
Department of Ocean Engineering

Quasi-static Tearing Tests of Metal Plating

by

Jeffrey C. Woertz

Submitted to the Department of Ocean Engineering and
the Department of Mechanical Engineering
on 09 August 2002, in partial fulfillment of the
requirements for the degrees of

Master of Science of Naval Architecture and Marine Engineering
and
Master of Science in Mechanical Engineering

Abstract

Great effort is being focused on making the next generation of naval combatant ships more resistant to the effects of close-aboard explosions. The examination of the deformation modes in blast-loaded metal plating suggests that a physical model can be developed to simulate the force vs. displacement history produced by an impinging shock wave during the holing phase. Similar approaches have been successfully used to approximate damage due to grounding and ballistic penetrators.

In this case, the deformation of the clamped plate is modeled in two stages: (1) dishing, which leads to disking and (2) radial crack propagation, which results in petalling. In the first stage, a thin geometrically-scaled (0.90 mm, 1.15 mm, and 1.40 mm thick by 300 mm square) mild steel sheets are dished inward using spherical indenters of radii 20 mm, 50mm, and 75 mm. The sheets have an average tensile strength of 317 MPa and a Rockwell Superficial Hardness Number of 72 ($H_{N15T}72$).

This portion of the test approximates the initial material stretching done by a spherical wave at various standoff distances. The spherical indenter produces a circular hole, which simulates the disk of material normally ejected as a blast front penetrates a plate section. As the material reaches a critical necking thickness at the edges of the hole, radial cracks form creating petals. During the second stage, an oblique conical punch is used to simulate the expanding wave front, which drives open the petals, causing the cracks to propagate towards the plate's clamped boundaries. By measuring the resultant forces and minimizing the effects of friction, the total bending and membrane work can be reasonably estimated. Ultimately, the approximate blast damage for a given ship's hull may be related to a given charge size and standoff distance.

Thesis Supervisor: Tomasz Wierzbicki
Title: Professor of Applied Mechanics

Thesis Reader: Frank A. McClintock
Title: Professor of Mechanical Engineering

Acknowledgements

I would like to thank Professor Wierzbicki and Professor McClintock for their encouragement, enthusiasm, and guidance over the course of this project. It was a privilege to take advantage of their considerable wisdom and expertise.

I would like to thank Xiaoqing Teng for his assistance in both creating the preliminary ABAQUS model (finite element simulation) and in developing an analytical approach to flat plate conical stretching/dishing.

I would like to thank Dirk Mohr for his assistance in creating the LS-DYNA model and for his guidance during the early stages of testing.

I would like to thank the U.S. Navy for providing me with the chance to study at MIT. This has been one of many incredible opportunities afforded to me by this great organization.

Finally and most importantly, I wish to dedicate this work to my wife, Christy, and our two sons, Sam and Will, in thanks for their patience and support during our time here in Boston.

Table of Contents

List of Main Body Figures

List of Appendix Figures

List of Main Body Tables

List of Appendix Tables

Introduction

In response to the growing number of threat nations and the increased proliferation of anti-ship weaponry, the Office of Naval Research (ONR) has prompted new research in the areas of weapons effects and ship vulnerability. Mindful of budgetary pressures, the United States Navy is exploring the most cost-effective methods of increasing the damage resistance and improving the overall battle effectiveness of its warships. (Refer to Appendix A for more detailed prefatory material.)

To date, the plastic deformation resulting from a close-proximity explosion (either above or below the waterline) has not been the focus of any large-scale, publicly-accessible research project. Many organizations have intensely researched topics which apply similar mechanics, such as ballistic penetration, collision and grounding damage, and axial tube splitting. There has been preliminary work by both Wierzbicki (1996)/(1999) and Nurick (1996), which examined plate tearing and petalling done by on contact explosives. (A detailed review of past work in this area and the associated literature can be found in Appendix B)

In keeping with the goals of the U.S. Navy and ONR, this research focuses on the deformation and fracture of hull plating, which is subjected to either an underwater (UNDEX) or air explosion. Ultimately, the objective of the study is to provide a simplified method of gathering benchmark data to quantify a material's sensitivity to explosive damage. An inexpensive two-stage quasi-static indentation test is used to model the force vs. displacement history of a thin clamped steel sheet. These experimental results are then compared to both approximate analytical solutions and results obtained through Numerical simulations created in ABAQUS (Static Load with Pressure Boundary Conditions) and LS-DYNA (Quasi-static Load with Displacement Boundary Conditions).

Nomenclature

R	Plate Width
r	Hole Radius
R_b	Spherical Punch Radius
R_C	Clamped Plate Width
F_F	Frictional Force
P	Indenter Force
V	Indenter Velocity
μ	Frictional Coefficient
σ_Y	Material Yield Strength
σ_U	Material Ultimate Strength
σ_o	Material Flow Stress
δ	Plate Central Displacement
θ	Cone Punch Angle
φ_c	Indenter Wrapping Angle
t	Plate Thickness
E	Indenter Work
l	Petal Length

Statement of Problem

To improve blast damage resistance in future classes of combatant ships, the U. S. Navy and ONR are entertaining new concepts in both design and materials. Although, the characteristics of traditional mild and high strength steels have been studied extensively in naval applications, no simple, reliable method exists to predict hull panel blast damage due to a close proximity blast load. Blast holing prediction is a key factor in assessing ship survivability, including the number of flooded compartments, the ships residual section modulus, and probability of recovery. Blast damage computer codes are plentiful, but the accuracy of their results often remains in question. Consequently, nearly all trusted damage prediction is done through scaled live fire testing, which is both expensive and time consuming.

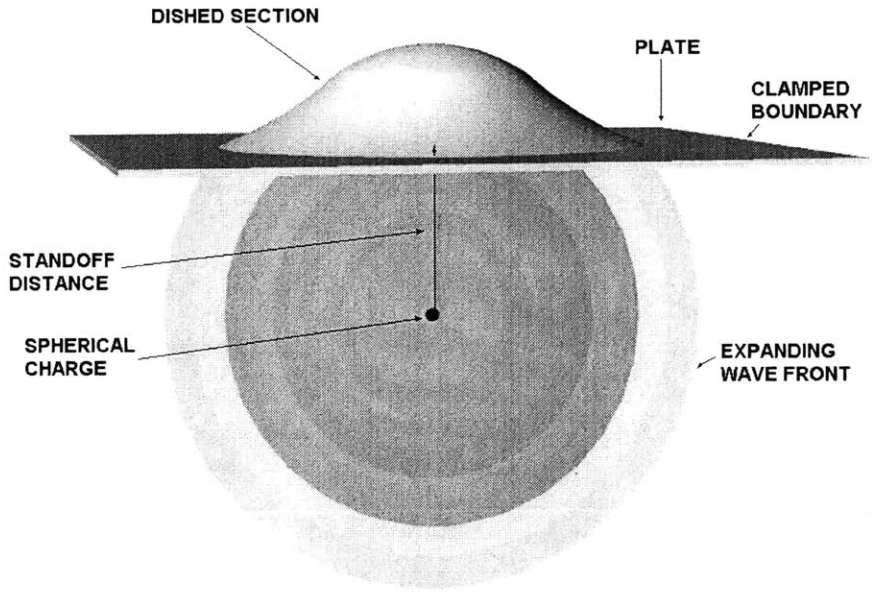

Figure 1: Simplified Blast Loaded Plate Geometry

The long-term challenge of this research is to combine theories from tearing fracture, plate cutting, petalling, and blast loading so as to provide a preliminary estimate of the damage caused by a given charge at some small distance from a clamped metal plate. The simplified physical model in Figure 1, presents the geometry of the problem. Figure 2 shows clear deformation and fracture similarities between dynamic (Rajendran (2000)) and quasi-static test specimens.

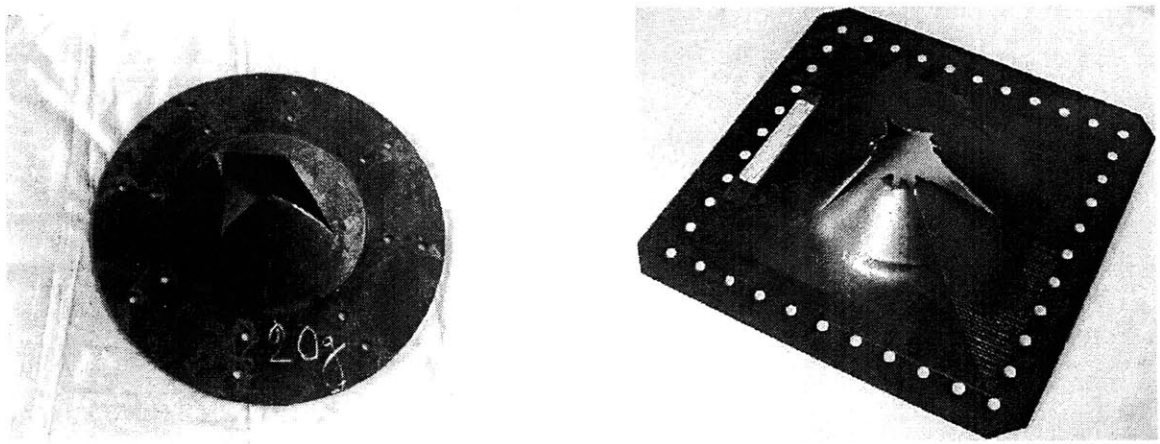

On Contact Blast Test (20 g PEK-1 explosive) Quasi-statically Indented Plate

Figure 2: Dynamically and Quasi-statically Fractured Specimens

The quasi-static tests have two immediate purposes. First, if the time-pressure history of an explosive can be related to the force displacement history of the proposed quasi-static tests, it becomes possible to relate the energy of the incident blast wave to the bending, stretching, and tearing work done in the material. Secondly, by examining crack initiation and propagation and measuring incremental strains during these quasi-static tests, one can develop a rudimentary crack-propagation criterion. Such a criterion could then be used to improve existing finite element codes and coupled hydro-codes. It is believed that these tools will lead to improve damage estimates (e.g. resultant hole size for a given charge). If

such estimates can be made quickly and inexpensively, research facilities could rapidly examine the suitability of a wide range of materials and structural arrangements with minimal resources.

Formulation of Problem

Experimental Approach

A series of penetrator tests is used to model the deformation which occurs in mild steel panels due to close proximity explosions. The modeling occurs in two stages. During the first stage, forces, displacements, and local strains are measured as a hemispherical punch is used to dish the center of a clamped thin mild steel sheet. As the material stretches and thins, a critical necking thickness will be reached near the center of the sheet. A circumferential crack then forms at the necked location. Radial cracks will subsequently form at the newly formed hole's edge. The initiation of radial cracks will mark the conclusion of the first stage.

In the second stage, an oblique conical punch is used to examine the behavior of the material while petalling. The cone is used to propagate either pre-cut or naturally formed radial cracks, causing several distinct outward-opening petals to form. With Teflon-based dry film lubricants baked onto both the test specimens and indenter contact surfaces, friction is kept to a minimum during the test. Fine grid markings (2.5 mm squares) are made on the plate in order to compute final local strains at periodic locations along the plate's radius. These strains can than be used to measure material stretching, petal displacement/curvature, bending work for the final deformed geometry. This total work can than be loosely related to the energy released during the first several milliseconds of an explosion.

Additionally, a series of successive photographs captures the formation and propagation of radial cracks through the mesh. In doing so, one can estimate the incremental strain on a given mesh element and estimate Crack Tip Opening Angle (CTOA) throughout the

propagation phase. When joined with a known force–displacement history, one can begin to draw conclusions about the material's ability to resist blast damage.

Numerical Approach

In order to gain insight into the fracture and displacements produced expected the quasi-static dishing experiment, a numerical model was created in ABAQUS. An axi-symmetric plate model was statically loaded with full-plate and half-radius pressures of varying magnitude. This analysis showed the (i) mode and location of fracture, (ii) whether fracture occurs buy thinning or necking, and (iii) an approximate deformed plate shape at fracture.

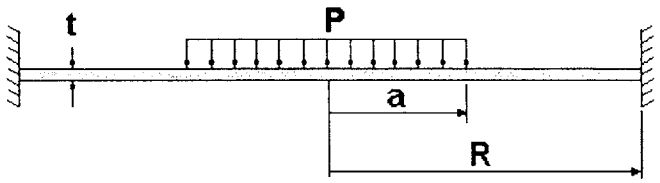

Figure 3: ABAQUS Numerical Model Representation

Additionally, a more comprehensive (and considerably more accurate) model was developed in LS-DYNA using displacement boundary conditions for a spherical punch.

Approximate Analytical Solutions

Approximate analytical methods have been previously developed for each of the quasi-static phases. Simonsen (2000) offers an approximate closed-form solution (under several assumptions) for plate displacement under hemispherical punch loading. With that solution, strains and dishing work can be computed with reasonable accuracy. These results are then compared with those obtain experimentally and numerically.

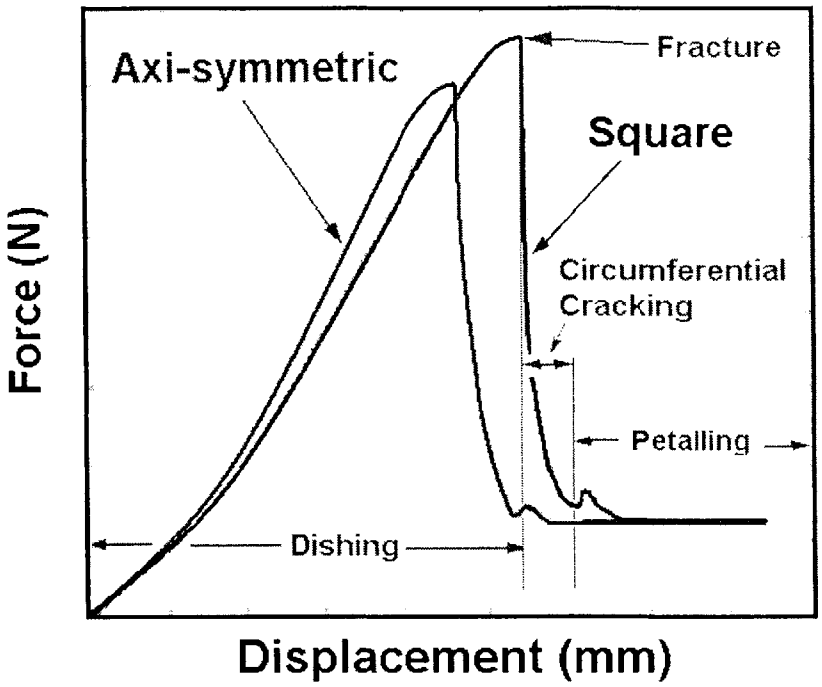

Figure 4: Generalized Force vs. Displacement History

With a closed-form solution derived originally for plate cutting, Wierzbicki (1993)/(1999) developed expressions for bending and membrane work done during the circumferential cracking/petalling phase. Combined, the various methods provide a reasonable estimate of the total work done in deforming the plate during a close-proximity explosion.

Still, knowing the work of macro-scale deformation is less important than identifying the overall force-displacement history. The deformed plate is the most obvious physical clue in surmising the wave front-plate interaction from the time of impact through to the petalling phase. It is this load-deformation relationship, combined with a suitable crack propagation criterion, which can most closely link the quasi-static conditions of a punch test to the dynamic conditions present in an explosive blast.

Approximate Analysis

Hemispherical Dishing and Circumferential Cracking Phase

As mentioned earlier, the dishing analysis is based on work done by Simonsen. The theory assumes an axi-symmetric plate is dished by a hemispherical punch of radius R_b. A Cartesian (w, r) coordinate system is used with φ_c being the angle from the center of the punch to the outermost contact point C. The total punch displacement is δ and the punch force is P. Figure 5 illustrates the geometry of the problem.

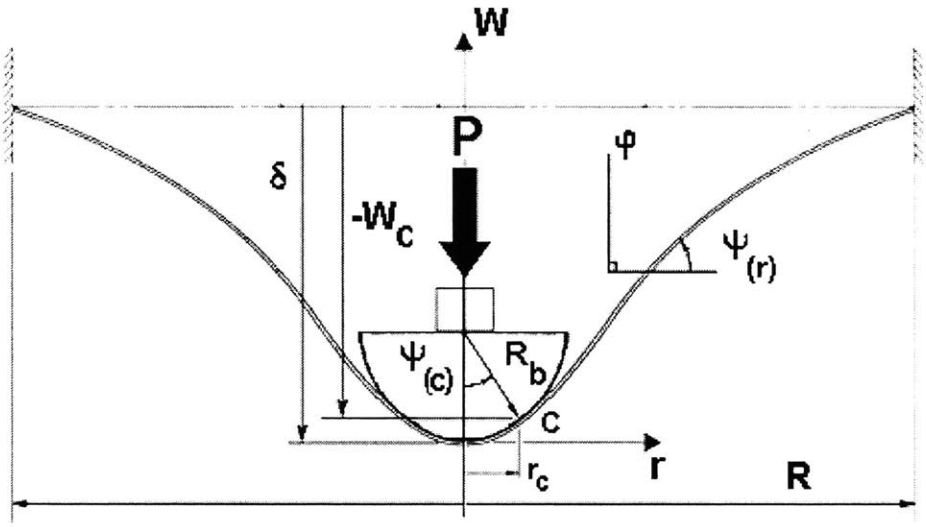

Figure 5: Spherical Dishing Geometry

Several assumptions are made in order to reach a closed-form solution. Plate bending is neglected, plate elements are considered to be displaced vertically, and the material is assumed to be rigid-plastic. Under the assumption of plane strain, the generalized radial membrane force is given by

$$N_o = \frac{2\sigma_o t_o}{\sqrt{3}} \tag{1}$$

The punch force (P) at point C can be expressed as:

$$P = 2\pi N_o R_b \sin^2 \psi(r) \tag{2}$$

where $\psi(r)$ is the wrapping angle function

Given the relation that:

$$\sin\psi = \frac{dw}{\sqrt{dw^2 + dr^2}} \tag{3}$$

The following differential equation can be surmised:

$$\frac{dw}{dr} = \frac{\sin^2 \psi_c}{\sqrt{\left(\frac{r}{R_b}\right)^2 - \sin^4 \psi_c}} \tag{4}$$

By applying the boundary condition $w(r) = 0$ at r = R, a solution for $w(r)$ can be reached by separation of variables:

$$w(r) = \frac{P}{2\pi N_o} \ln\left[\frac{r + \sqrt{r^2 - \sin^4 \psi_c}}{R + \sqrt{R^2 - \sin^4 \psi_c}}\right] \quad \text{for } r_c < r < R \tag{5}$$

Consequently, using the previously stated assumptions, one can determine the vertical displacement for all points on the plate and the force required to deform the plate. Of course, at some point the plate the plate will reach its material limits. Strain hardening characteristics must be introduced and the true stress strain curve is assumed to obey a power law:

$$\sigma = C_o \varepsilon^n \tag{6}$$

To predict necking localization and fracture, the maximum on the load-displacement curve is identified by setting $\frac{dP}{d\psi_c} = 0$. One can then solve for an approximate solution for φ_c at necking failure. The final expression given by Simonsen is:

$$\psi_{c\_fail} \approx .957 + .399n \tag{7}$$

Using this relation, additional expressions were derived to determine total displacement (δ_{fail}) and total work (E) up to the point of necking failure:

$$\delta_{fail} = 1.41n^{.33}R^{.48}R_b^{.52} \tag{8}$$

$$E = \pi C_o R R_b \left\{ .318\left(\frac{R}{R_b}\right)^{.607-.387\frac{R_b}{R}+1.2\left(\frac{R_b}{R}\right)^2} + .067(n-.2) \right\} \tag{9}$$

Conical Dishing

In some cases, a cone was used to dish a flat plate with a pre-cut starter hole in order to gain insight as when and to how the radial cracks form and propagate.

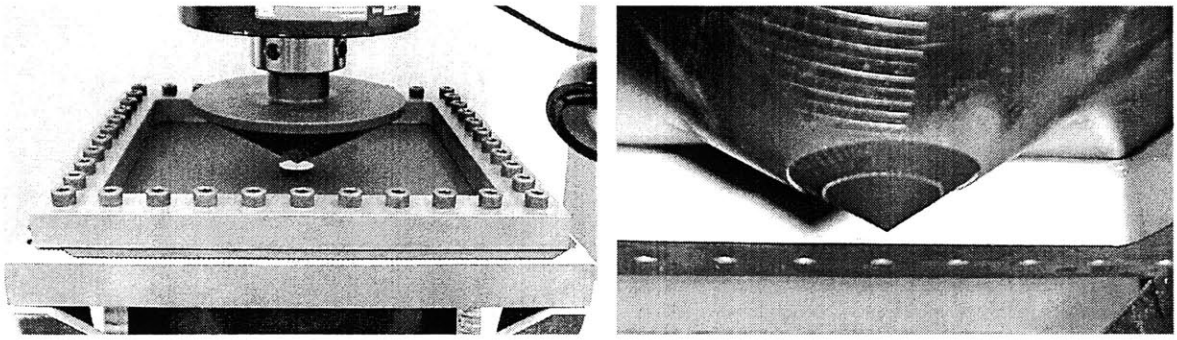

Figure 6: Conical Dishing Experiment

The problem's geometry is defined in Figure 7.

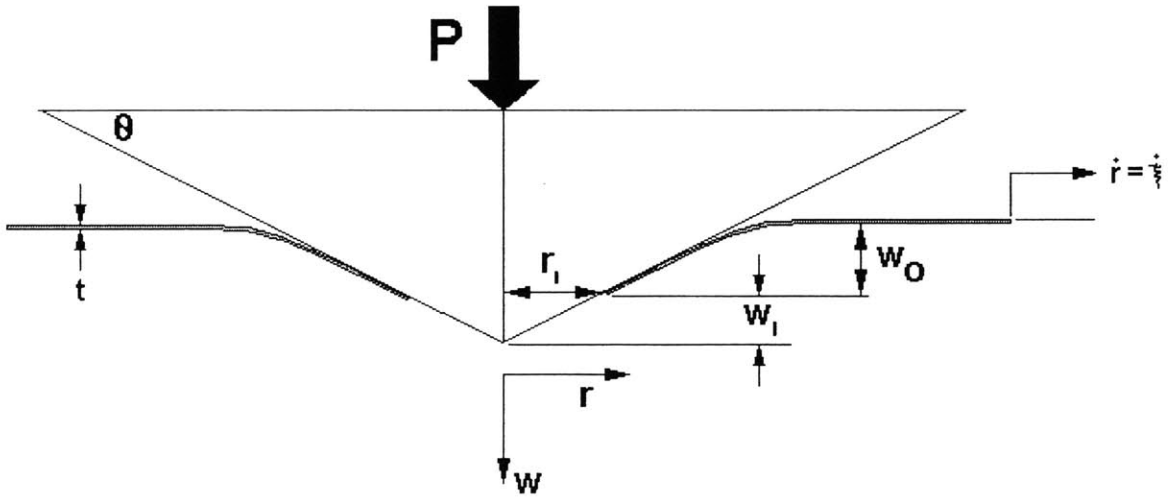

Figure 7: Conical Dishing Geometry

Again, the material is assumed to obey a true stress power law.

$$\sigma = C_o \varepsilon^n \tag{10}$$

Using the theory of moderately large deflections in thin plates and following Simonsen's assumption:

$$\varepsilon_r = \frac{1}{2}\left(\frac{\partial w}{\partial r}\right)^2 \tag{11}$$

Consequently,

$$\sigma = \frac{C_o (w')^{2n}}{2^n} \tag{12}$$

The generalized membrane stress then becomes:

$$N = \sigma t = \frac{C_o t (w')^{2n}}{2^n} \tag{13}$$

The governing equation is then:

$$(Nrw')' = \left(\frac{rC_o t (w')^{2n+1}}{2^n}\right)' = 0 \tag{14}$$

Subject to the boundary conditions, this equation has the general solution:

$$w = c_1 r^{\frac{2n}{2n+1}} + c_2 \tag{15}$$

The constants c_1 and c_2 can be found be applying the boundary condition $\frac{\partial w}{\partial r} = -\tan\theta$ at $r=r_1$. The expression for w then becomes:

$$w = \frac{2n+1}{2n} r_1^{\frac{1}{2n+1}} \tan\theta \left(\xi^{\frac{2n}{2n+1}} - r^{\frac{2n}{2n+1}}\right) \tag{16}$$

where ξ is the radius of the expanding plastically deformed zone.

The kinematic boundary condition (K.B.C.) is then applied at both r = ζ and r = r_1.

$$\text{K.B.C.:} \qquad \frac{dw}{dT} + \frac{d\xi}{dT} w' = 0 \qquad \text{at} \quad r=r_1 \qquad (\text{note } w' = -\tan\theta = \text{constant}) \tag{17}$$

where T is time and r_1 can be considered a time-like parameter.

Using this kinematic condition, ζ can now be expressed in terms of r_1:

$$\xi = r_1 \left(1 + \frac{2n}{2n+1} \right)^{\frac{2n+1}{2n}} \tag{18}$$

As a result, (16) becomes

$$w = \frac{2n+1}{2n} r_1 \tan\theta \left(\frac{4n+1}{2n+1} - \left(\frac{r}{r_1} \right)^{\frac{2n}{2n+1}} \right) \tag{19}$$

The vertical punch force, P, is given as the following:

$$P = 2\pi r_1 N \tan\theta = \frac{2\pi r_1 C_o t (\tan\theta)^{2n+1}}{2^n} \tag{20}$$

The punch displacement is:

$$\delta = w_o + r_1 \tan\theta = 2 r_1 \tan\theta \tag{21}$$

Substituting (20) into (21), the force-displacement relation is developed.

$$P = \frac{\pi C_o t (\tan\theta)^{2n} \delta}{2^n} \tag{22}$$

As an example, consider the following values:

C_o =460 MPa $\qquad$ θ =30° $\qquad$ n = .22 $\qquad$ t =.045"

P=48.5 kN

The analysis provides the force-displacement approximation show below in Figure 8.

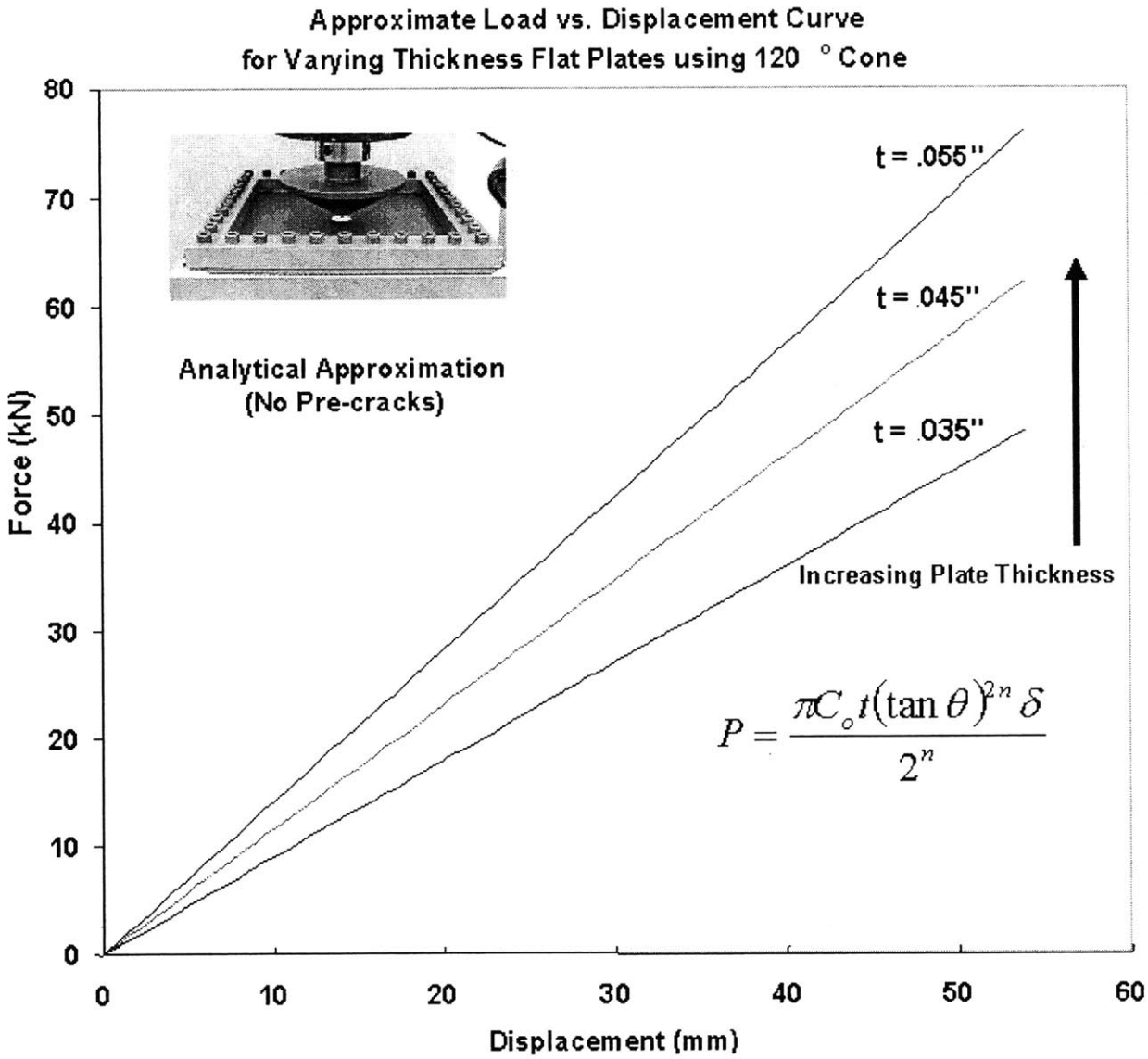

Figure 8: Analytical Approximation for Conical Dishing with Starter Hole

Radial Cracking and Petalling

The theory used in this section is derived in detail by Wierzbicki [1999]. He proposes that the total petalling work is due to crack propagation, petal bending, and membrane deformation. Further, these quantities are shown to be interdependent.

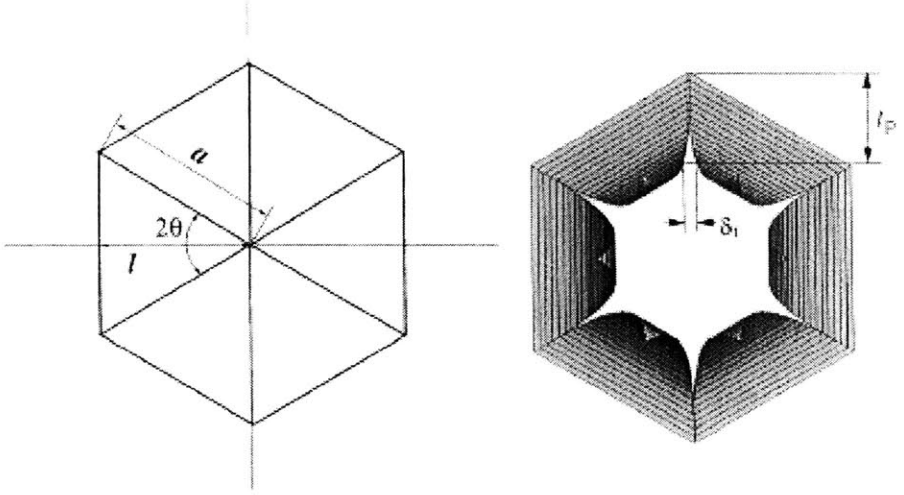

Figure 9: Theoretical Petalling Geometry

Due to physical limitations of the testing apparatus, fully dished plates could not be petalled during the series of experiments. Consequently, a flat plate was used to approximate the deformation and fracture conditions seen during petalling. Figure 6 shows an example of a six-petal geometry ($n_{petals}=6$). From the figure, the central angle, θ, is given as:

$$\theta = \frac{\pi}{n_{petals}} \tag{23}$$

and the instantaneous crack length, a, is related to the petal length, l, by

$$a = \frac{l}{\cos\theta} \tag{24}$$

The material is assumed to be rigid-plastic with an average flow stress, σ_o. The fully plastic bending moment per unit length, M_o, is calculated as:

$$M_o = \frac{\sigma_o t^2}{4} \tag{25}$$

Ultimately, the rate of bending work in a single petal can be computed as

$$\dot{W}_b = 4M\frac{\dot{l}}{\rho} l \tan\theta \tag{26}$$

where,

$$M = \eta M_o \tag{27}$$

M is the amplified bending Moment, which accounts for the increased bending resistance of a curved plate. In the flat plate approximation, $\eta = 1$. The per petal membrane work is then shown to be a function of crack tip opening displacement, δ_t:

$$\dot{W}_m = \frac{3.84 M_o \delta_t^{1/3} \rho^{2/3} \dot{l} (\sin\theta)^{-4/3}}{t\cos\theta} \tag{28}$$

where ρ is the instantaneous bending radius of the flaps.

Adding (26) and (28) to get total work:

$$W_t = W_b + W_m \tag{29}$$

then,

$$\frac{dW}{dT} = \frac{dl}{dT}\left[\frac{4Ml\tan\theta}{\rho} + \frac{3.84 M_o \delta_t^{1/3} \rho^{2/3} (\sin\theta)^{-4/3}}{t\cos\theta}\right] \tag{30}$$

The total work is then obtained by integrating the above expression with respect to l:

$$W_t = \frac{4Ml^2\tan\theta}{\rho} + \frac{3.84 M_o l \delta_t^{1/3} \rho^{2/3} (\sin\theta)^{-4/3}}{t\cos\theta} \tag{31}$$

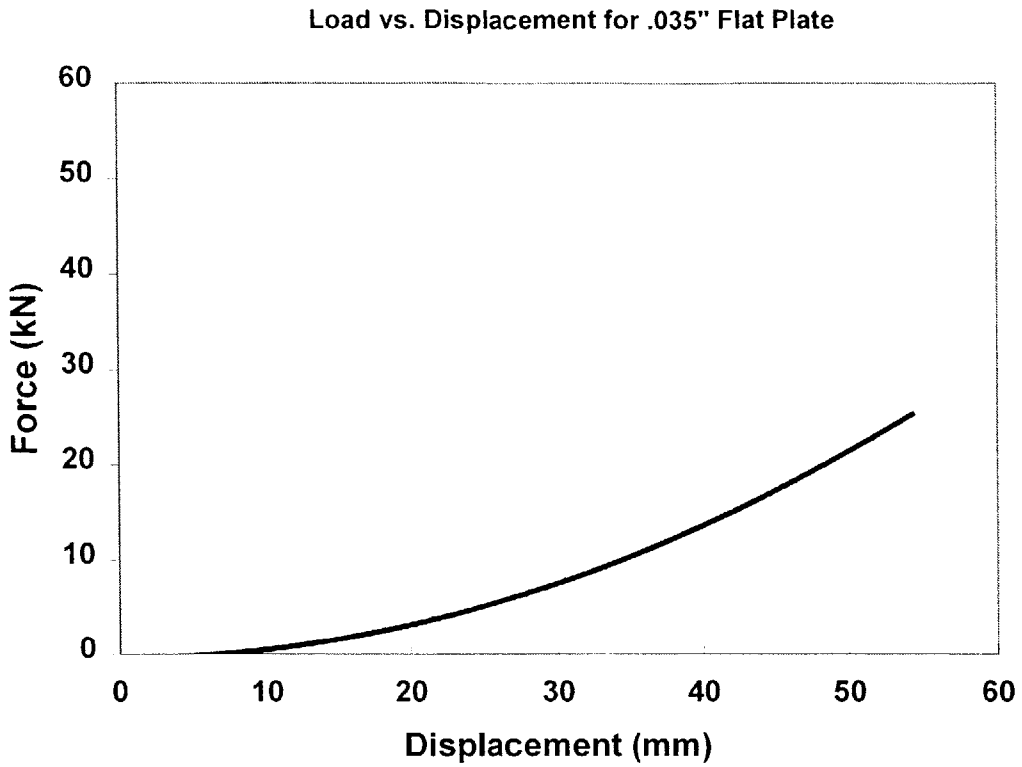

Figure 10: Approximate Theoretical Load Displacement Curve for Petalled Plate

Punch displacements, the measured radius of curvature, the experimental crack tip opening distance were all used in estimating punch force. Although a closed form expression for P vs. l was not developed for the load condition, forces were estimated using changes in total work over small increments of displacement.

$$dF \approx \frac{2}{d\delta}\left[\frac{4Ml^2\tan\theta}{\rho} + \frac{3.84M_o l\delta_t^{1/3}\rho^{2/3}(\sin\theta)^{-4/3}}{t\cos\theta}\right] \tag{32}$$

(Detailed computations can be reviewed in Appendix G.) In this case a piece-wise force-displacement curve for each petalled plate was generated using Wierzbicki's expressions and experimentally measured inputs. An example of a generated curve is shown in Figure 10.

Strain Field Development

In order to access the crack's behavior and growth characteristics, it is necessary to development a surrounding incremental strain field around. Given such strain field, one could then attempt to predict the crack's progress. In this case, the incremental strain is measured over a short interval, such that the crack progresses forward by one element. A stationary grid is used to map the movement of material points, as shown in Figure 11 below.

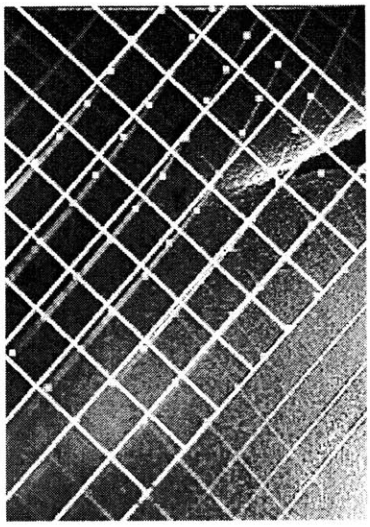

Frame 1: Time 30 sec

Frame Two: Time 45 sec

Figure 11: Incremental Strain Field Mapping

Assuming plane stress, the components of the strain tensor are:

$$\varepsilon_{11} = \frac{\partial u_x}{\partial x} \tag{33}$$

$$\varepsilon_{11} = \frac{\partial u_y}{\partial y} \tag{34}$$

$$\varepsilon_{12} = \frac{1}{2}\left(\frac{\partial u_x}{\partial y} + \frac{\partial u_y}{\partial x} \right) \tag{35}$$

Where u_x and u_y are components of the displacement vector.

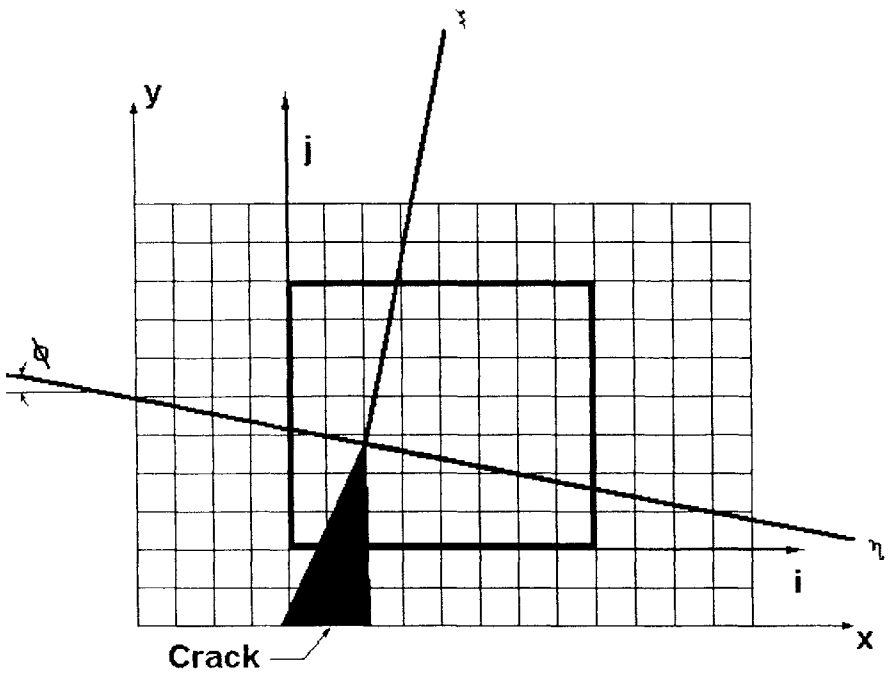

Figure 12: Incremental Strain Field Rotation

As shown in Figure 12 above, the strain field can then be rotated into alignment with the direction of crack growth by multiplying by the appropriate direction cosine. Although principal stresses are not know, the stress ratios (specifically, $\frac{\sigma_{11}}{\sigma_{22}}$ which governs necking) can be determined from ε_{11} and ε_{22} using the Von Mises yield condition and the associated flow rule.

$$\frac{d\varepsilon_{11}}{d\bar{\varepsilon}^p} = \frac{\sigma_{11}}{\bar{\sigma}} - \frac{1}{2}\frac{\sigma_{22}}{\bar{\sigma}} \tag{36}$$

$$\frac{d\varepsilon_{22}}{d\bar{\varepsilon}^p} = \frac{1}{2}\frac{\sigma_{11}}{\bar{\sigma}} - \frac{\sigma_{22}}{\bar{\sigma}} \tag{37}$$

Divide (36) by (37) and solve for $\frac{\sigma_{11}}{\sigma_{22}}$ in terms of $\frac{d\varepsilon_{11}}{d\varepsilon_{22}}$ to obtain:

$$\frac{\sigma_{11}}{\sigma_{22}} = \frac{\frac{d\varepsilon_{11}}{d\varepsilon_{22}} + \frac{1}{2}}{1 + \frac{1}{2}\frac{d\varepsilon_{11}}{d\varepsilon_{22}}} \tag{38}$$

Numerical Modeling

Preliminary Dishing Model in ABAQUS

ABAQUS was used to model the preliminary plate's loading condition. For convenience, a pressure loading condition (vice a displacement boundary condition) was selected as a first approximation. In this model, a uniform pressure was first distributed over the entire plate. This loading geometry resulted in dishing without reverse curvature and a necking fracture at the plate's clamped boundary. The uniform pressure, full radius loading analysis was not pursued further, since the load condition result in a realistic deformation mode.

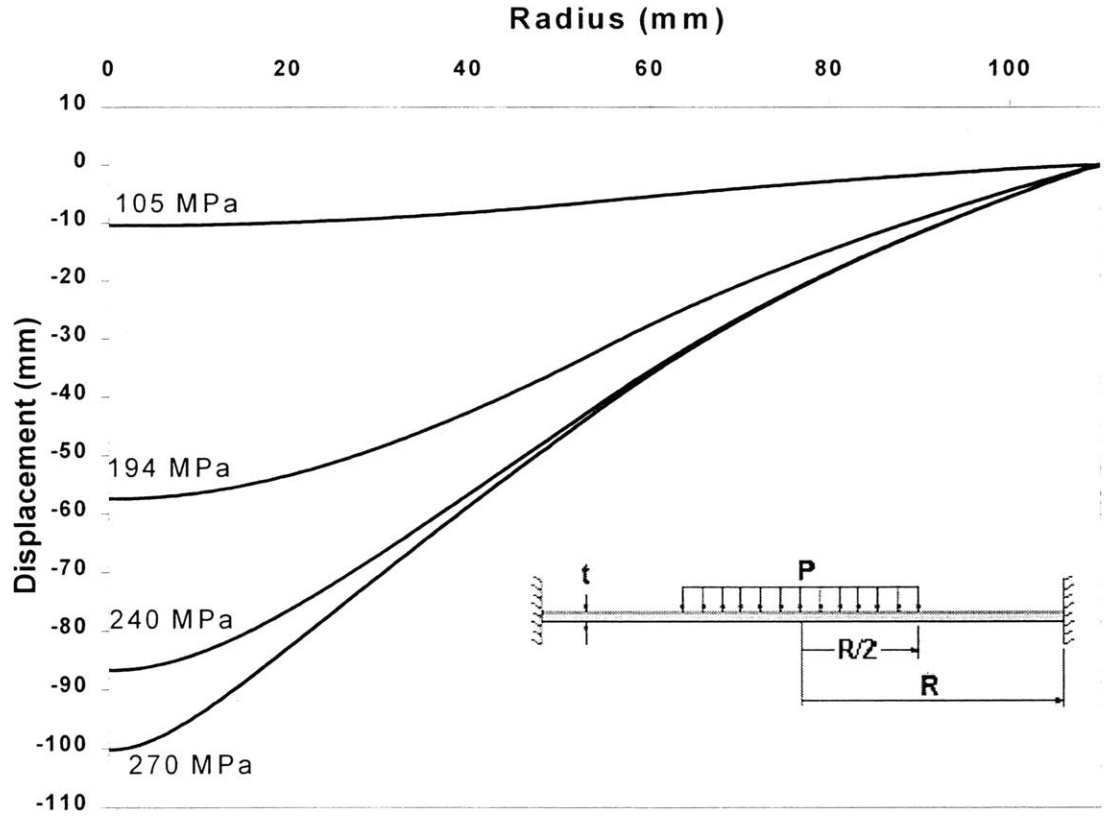

Figure 13: Displacement vs. Radius for Half-Radius Pressure Loading

Figures 14 and 15 show the displacements for the half radius pressure distribution. It was found that using a pressure distribution over half the plate's radius more closely modeled the conditions of hemispherical punch dishing.

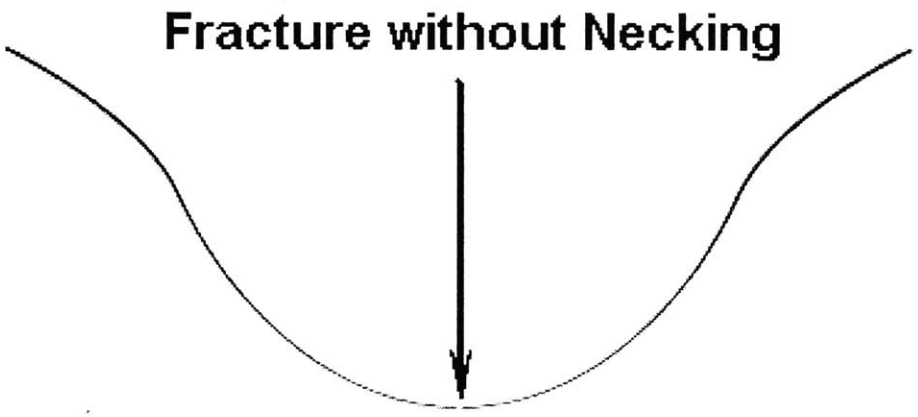

Figure 14: Sectional View of Deformed Plate at 240 MPa Pressure Amplitude

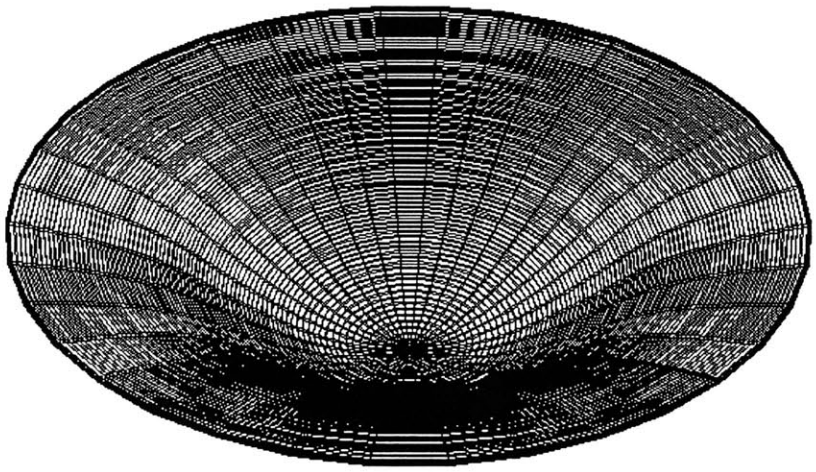

Figure 15: View of Deformed Plate at 240 MPa Pressure Amplitude

LS-DYNA Model

Towards the end of testing, a Finite Element model was created in LS-DYNA using the displacement boundary conditions of a rigid sphere, shown in Figure 16. Though the revised model moved further from the conditions of gas pressure loading (as in the preliminary simulation), it more accurately represented the quasi-static experiment. Three conditions were modeled: (1) the 75 mm radius sphere/ .055" plate, (2) 50 mm radius sphere/.045" plate, and (3) the 20 mm radius sphere/ .035" plate. Computational results were then compared with both the approximate analytical predictions (from Simonsen) and the experimental values. Data from this analysis can be found in the "Results and Discussion" section of this report. A sample LS-DYNA input file for theR=75mm/.055" plate test case can be found in Appendix H.

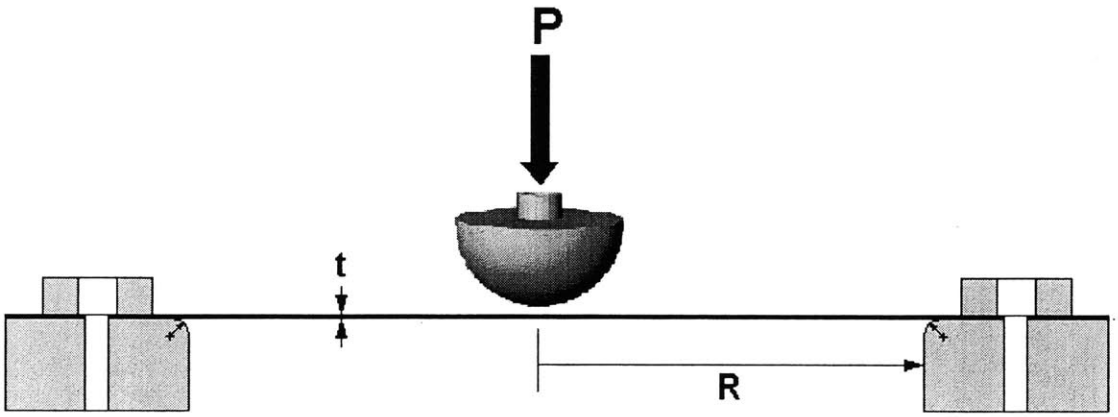

Figure 16: LS-DYNA Simulation with Rigid Body Sphere Boundary Condition

Design and Testing

Apparatus Design

A specialized fixture was fabricated for indentation testing of thin square sheets. Designed to work using a 200 KN load cell in a Universal Testing Machine, the fixture (shown below in Figure 17) can safely accept a central point load (P) up to the 200 KN machine limit. Edge fixity is achieved through the use of serrated bolting ring mating surfaces. Detailed size and material specifications for the fixture are shown in Figure 18. Further design explanations can be found in Appendix D.

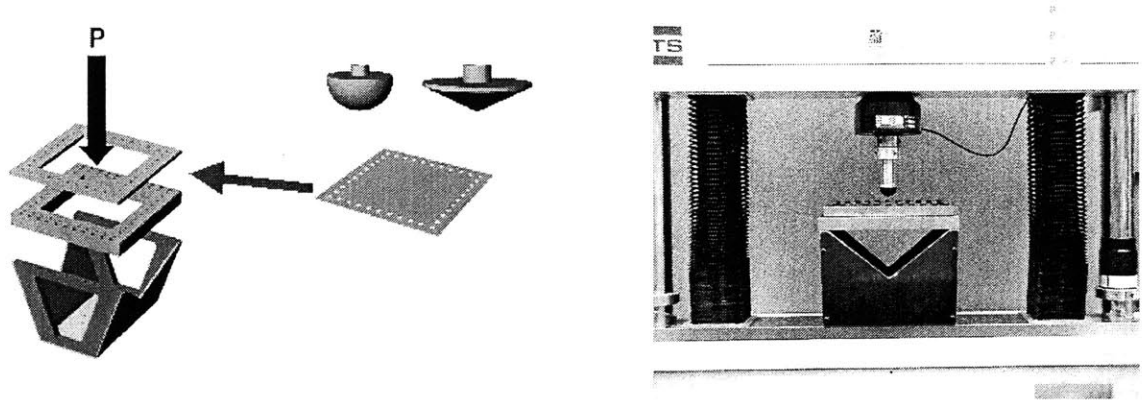

Figure 17: Notional Test Fixture and Completed Design

To create the dishing effect, three hemispherical indenters were used with radii of 20 mm, 50 mm, and 75 mm. Indenter speed (V) was set at a baseline of 10 mm/min. Indentation was continued through circumferential cracking until the instance at which radial fracture began. At that point, the dishing portion of the test was stopped. A 120° conical indenter was then used to simulate petalling from the flat plate condition for the same thickness.

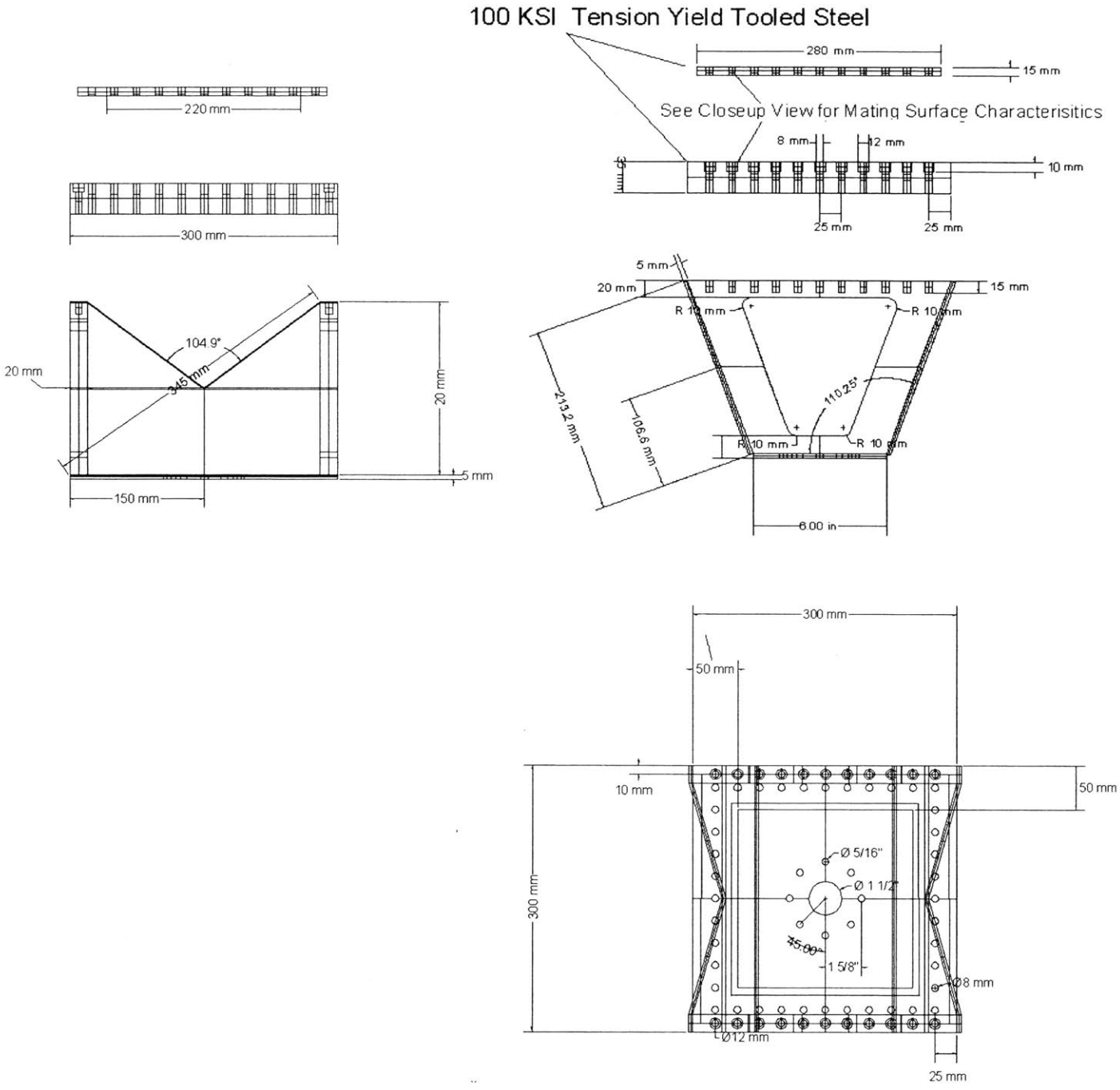

Figure 18: Detailed Fixture Specifications

Specimen Design

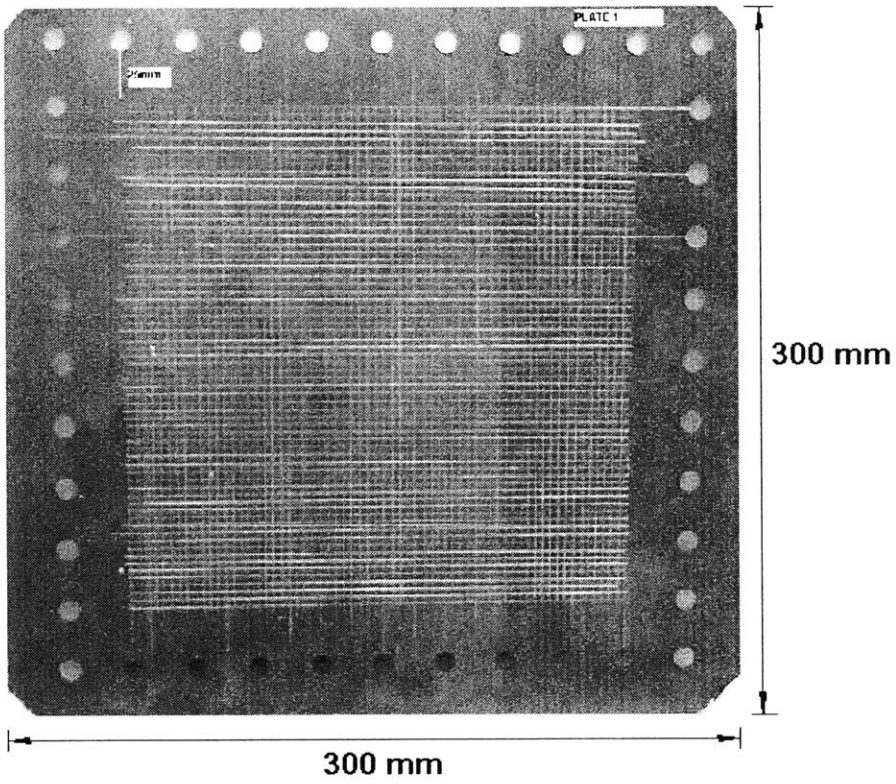

Figure 19: Test Plate

Figure 19 shows a representative test plate. Three plate thickness were tested (.035", .045", and .055"). The plate material has an average uniaxial tensile yield strength (σ_y) of 29,000 psi (200MPa), an average ultimate tensile strength (σ_u) of 46,000 psi (317 MPa), and a Rockwell Superficial Hardness of 72. Detailed material characteristics can be reviewed in Appendix E. The uncoated side of the plate is scribed with a 2.5 mm strain mesh (slightly larger than 2 plate thicknesses). During deformation, the horizontal and vertical local incremental strains are directly recorded using digital photography.

Testing

Table 1: Testing Matrix

Test Number		Spherical Indenter Radius			Conical Identer Angle	Precracks	Pre-cut Hole	Comments
		20 mm	50mm	75 mm	120°			
1	.035"	X				none		
2	.055"			X		none		
3	.045"		X			none		
4	.035"				X	none	22mm Dia.	
5	.045"				X	4 Cracks, 5mm	45 mm Dia.	
6	.045"		X		X	4 Cracks, 5mm	55 mm Dia.	Hole Post-Dish
7	.045"	X			X	none	10 mm Dia.	Hole Post-Dish
8	.035"				X	4 Cracks, 3mm	9.5 mm Dia.	
9	.045"				X	4 Cracks, 3mm	9.5 mm Dia.	
10	.055"				X	4 Cracks, 3mm	9.5 mm Dia.	
11	.035"				X	8 Cracks, 3mm	9.5 mm Dia.	
12	.035"				X	6 Cracks, 3mm	9.5 mm Dia.	
13	.035"				X	8 Cracks, 10mm	9.5 mm Dia.	
14	.035"				X	none	9.5 mm Dia.	
15	.035"				X	none	44.5 mm Dia.	

Table 1 shows the test matrix of the series of experiments performed with the Universal Testing Machine. Clearly, there were many testing variables to consider. With a finite number of test specimens, however, it was a goal of the study to develop a testing methodology and identify the most significant factors.

Tests 1 through 3 were spherical indentation tests, which were used to verify Simonsen's predictions. Tests 4 through 7 were used to determine the best approach given the limitations on time and equipment. In Test 4, a conical punch was used to indent a plate with a preformed hole. Later, Tests 14 and15 were used to observe to effect of hole size in this same loading condition. Test 5 was the first experiment in which the starter hole was pre-cracked in order to promote the petalling behavior. Tests 8, 9, and 10 also used pre-cracked holes to examine the effect of plate thickness. Tests 11 and 12 investigated the effect of increasing the number of pre-cracks, while Test 13 was used to observe the effect of increasing pre-crack length. Tests 4, 14 and 15 confirmed the effect of starter hole size.

Results and Discussion

Spherical Indentation

Figure 19 shows the experimental and approximate analytical results for spherical indentation testing. (Note, the analytical approximation is valid only up to Simonsen's failure prediction. Points beyond the maximum load are artifacts of the computation.)

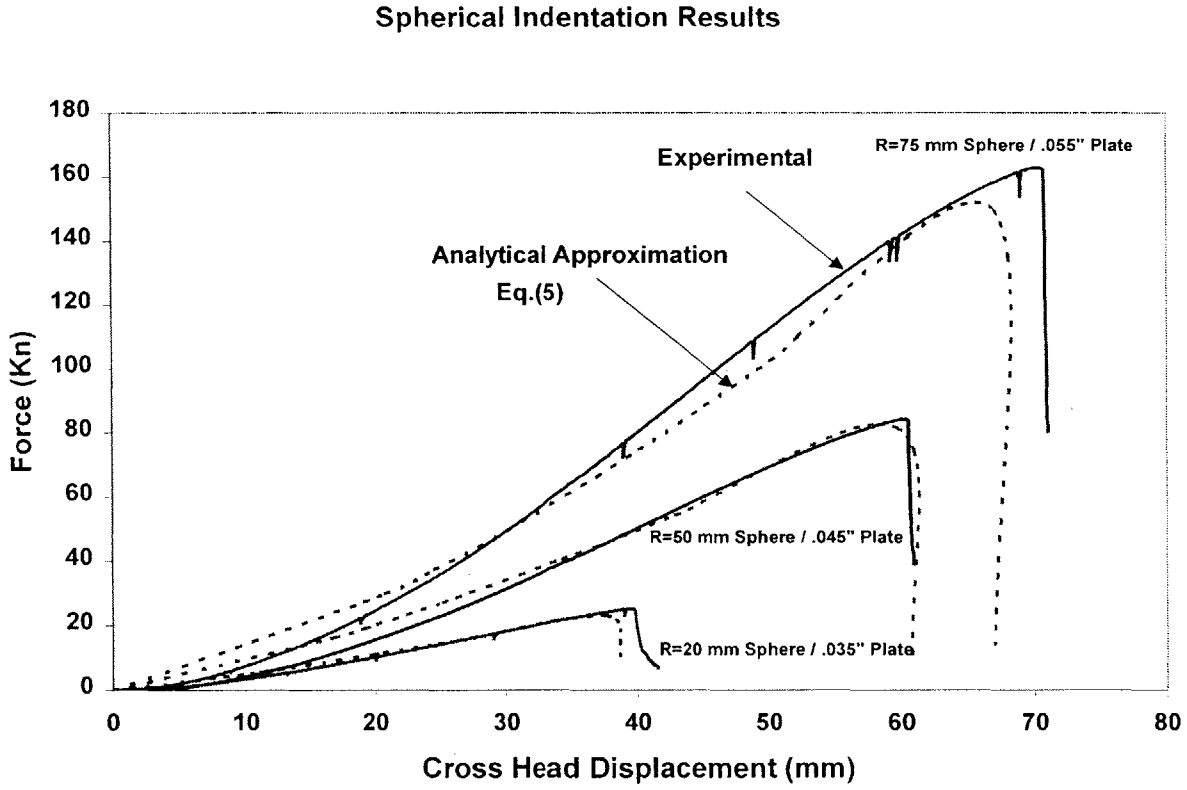

Figure 20: Approximate and Experimental Results for Spherical Indentation

Figures 21 through 23 on the following page, show results of the LS-DYNA numerical simulations for the same three load cases.

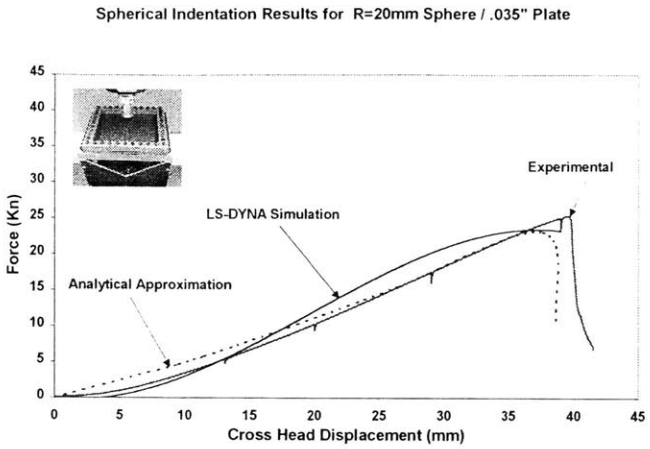

Figure 21: LS-DYNA Results for R=20 mm punch /.035" Plate

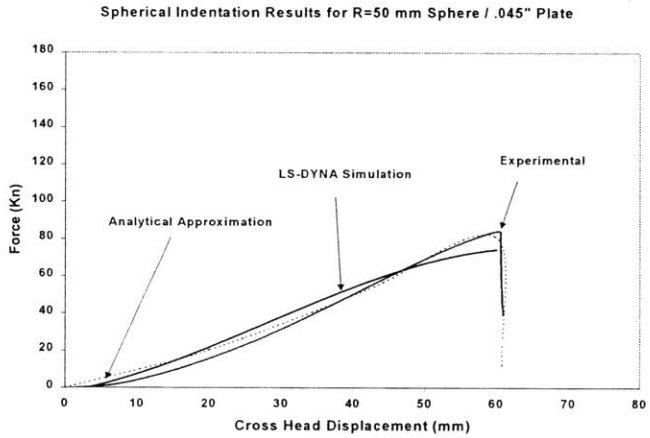

Figure 22: LS-DYNA Results for R=50 mm punch /.045" Plate

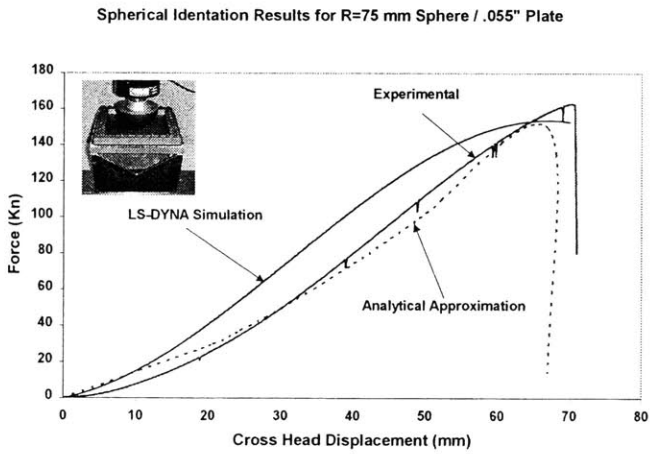

Figure 23: LS-DYNA Results for R=75 mm punch /.055" Plate

As in Simonsen's experiment, the experiments correlated to the analytical approximation within 5%. The preliminary LS-DYNA model (pictured in Figure 24) also resulted in good agreement, although the model requires further refinement for follow-on tests. This portion of testing validated the testing method and clearly proved that the new specimen test fixture functioned as designed.

During spherical indentation testing, it became clear that the specimen material was too ductile to carry out all tests as planned. Plastic deformations were quite large during dishing, and the shallow conical punches did not provide sufficient depth of stroke to continue petalling. Furthermore, the dishing failure always resulted in incomplete circumferential cracking (as in Figure 24 below). As a result of these two obstacles, the dishing and petalling phases were modeled in two entirely separate experiments.

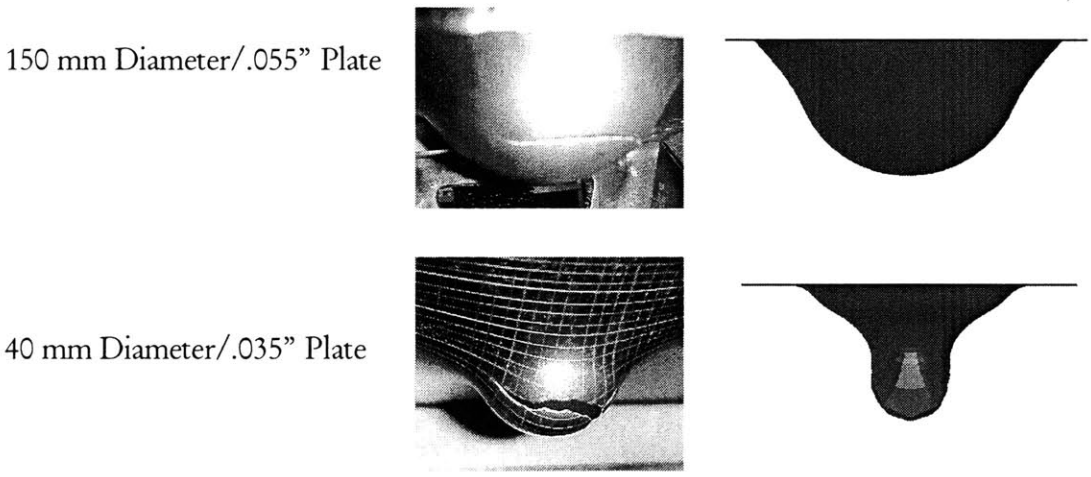

Figure 24: Experimental and LS-DYNA Spherical Dishing Deformations

Conical Indentation without Pre-cracks

Figure 25 shows the force-displacement relation observed during conical dishing. During this experiment, a constant plate thickness was tested while the starter hole was varied in size. The dashed line represents the analytical approximation derived earlier. The analytical approximation suggests that the force-displacement curve should be independent of hole size. This behavior was observed up to a displacement of about 20 mm. After that point, the 3 experiments diverge. Certainly the smaller hole size induced much earlier radial cracking due to much higher hoop stresses.

It is difficult to draw immediate conclusions, since each case's geometry, and consequently the material's load history, cannot be directly correlated. The analytical approximation, however, serves as a broad estimate of the material's general force-displacement behavior, but falls short in accounting for the problem's changing geometry.

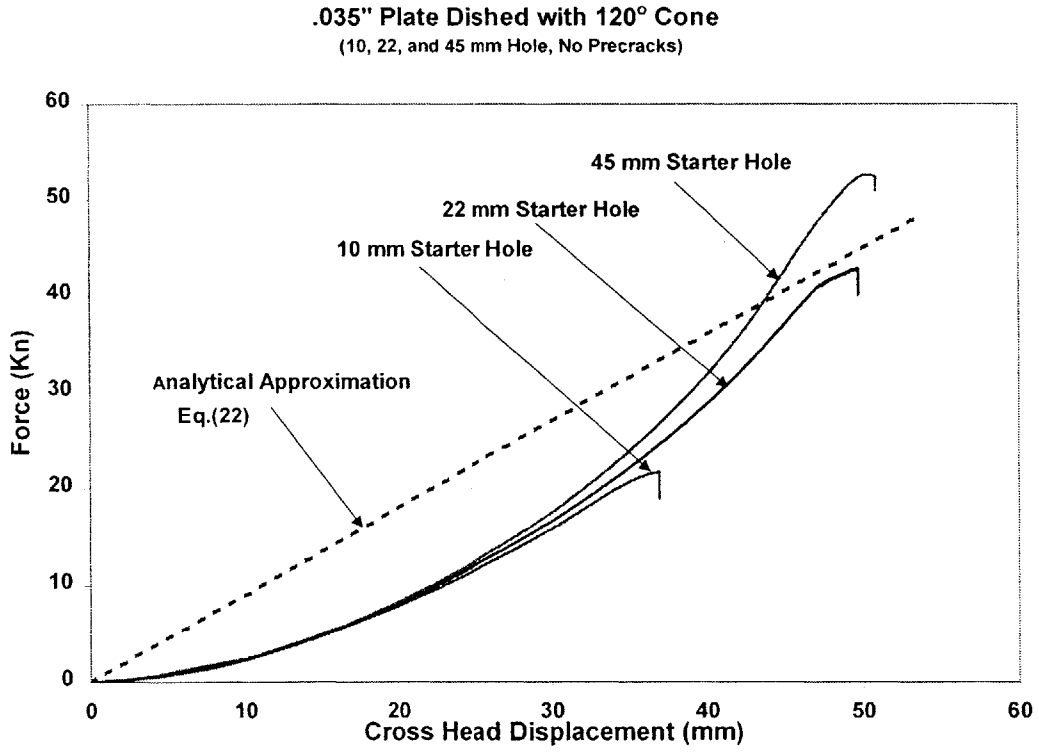

Figure 25: Conical Indentation Force-Displacement Curves (with Starter Hole)

Conical Indentation With Pre-cracks (Petalling)

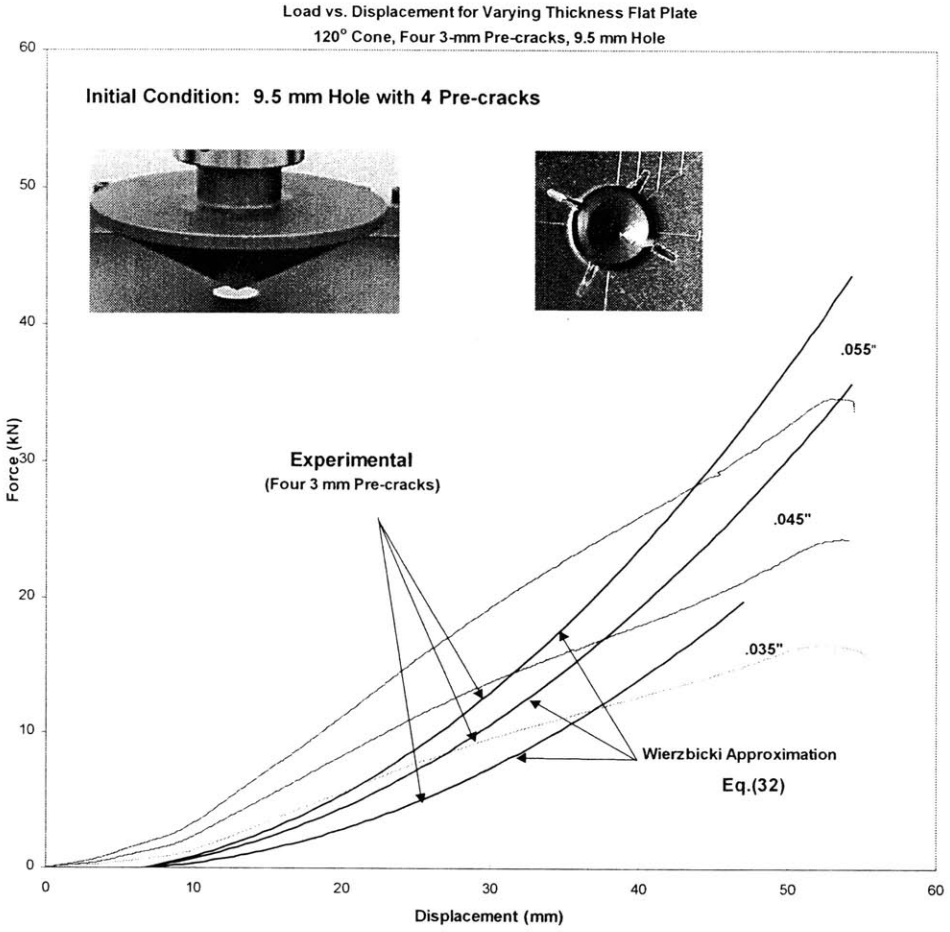

Figure 26: Conical Indentation Force-Displacement Curves (with Pre-cracks)

Figure 26 shows the results of the plate petalling experiment, which was conducted with a 9.5 mm starter hole and four, 3 mm pre-cracks. Figure 27 shows how the petalling test progressed.

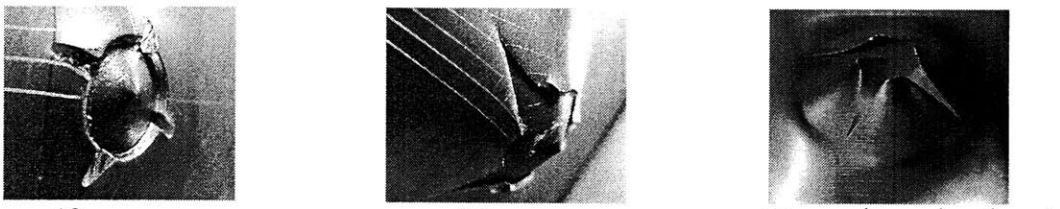

10 mm 25 mm 55 mm (completed test)

Figure 27: Petalling Test Punch Displacement Progression

The petalling test showed that the effect of plate thickness was approximately linear. In each experiment during the first 10 mm of displacement, the cone settled into the starter hole and propagated the pre-cracks. After that point, the petals began to form. From the pictures, one can see that very little curvature developed. Again, this was due to the shallow angle of the conical punches. Only 55 mm of punch displacement could be observed before the punch began to interfere with the fixture's boundary conditions, at which point the test had to be stopped.

Although, there appears to be disagreement between the analytical approximation and the observed force-displacement curves, the general trend and level of force correlate reasonably well. It is apparent that the artificiality of pre-cracking has some impact on the experiment. In the two experiments where natural radial cracks formed and petalling could be observed (Figure 28), the force-displacement curve closely resembled the behavior derived out of Wierzbicki's expressions Eq.(32).

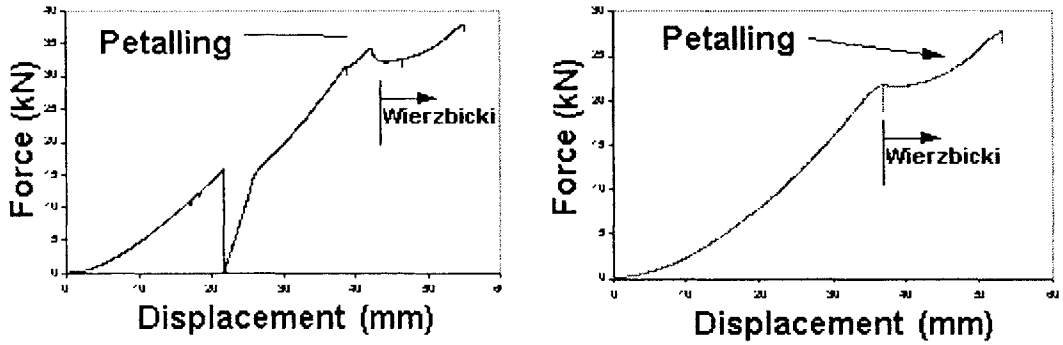

Pre-Dished and Cut Specimen Conical Dishing with Starter Hole

Figure 28: Force-Displacement Observations During Petalling

It is important to keep in mind that the dishing force is five to six times higher than the less critical petalling force. With the perspective that this approach is simply another available tool, this petalling approximation could certainly provide useful first-order estimates to a designer or post-explosion investigator.

Effect of Pre-crack Length

Figure 29 shows the effect of pre-crack length. Variation in the length of the starter crack produced little effect, other than lengthening the amount of time required for the cone to settle into full contact with the plate. The result was a small shift in the force – displacement curve. As displacement increased the effect was diminished. This behavior was expected, but required verification. The length of pre-crack, however, did affect the number of petals formed. The 3-mm pre-crack yielded four petals, while the 10-mm pre-crack yielded only four. This behavior agrees with Wierzbicki's prediction than some energy absorption minimum exists, tending to promote the formation of three to five petals.

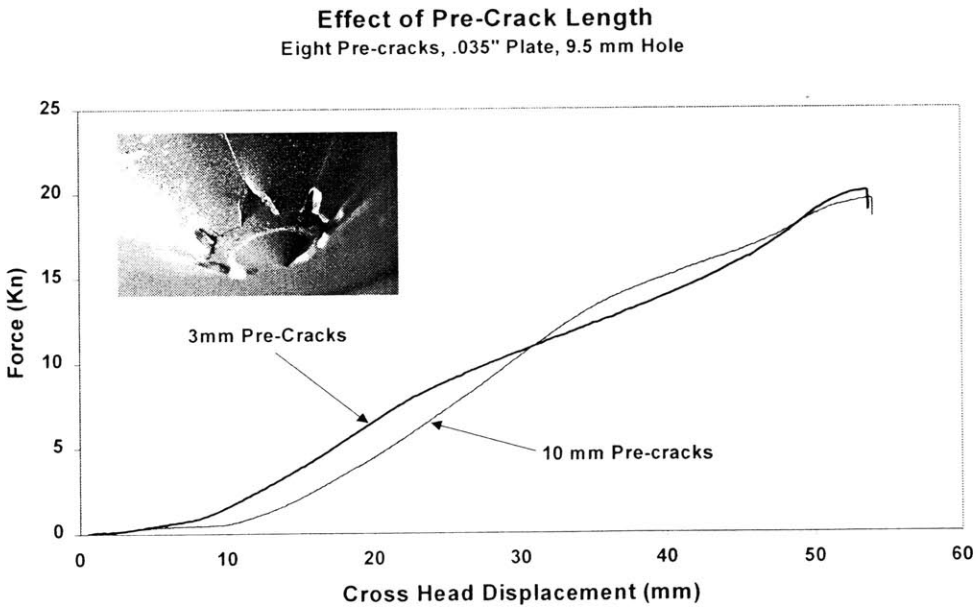

Figure 29: Effect of Pre-Crack Length on Force-Displacement Curve

Effect of Number of Pre-cracks

As shown in Figure 30, the number of pre-cracks had no significant effect of the overall force-displacement curve. Only four petals developed in each case, however. In both tests, all pre-cracks tended to start, but only four continued to grow. As in the previous examination of pre-crack length, this result also suggests that a petalling energy minimum exists, which is independent of the number of initial radial necks or cracks.

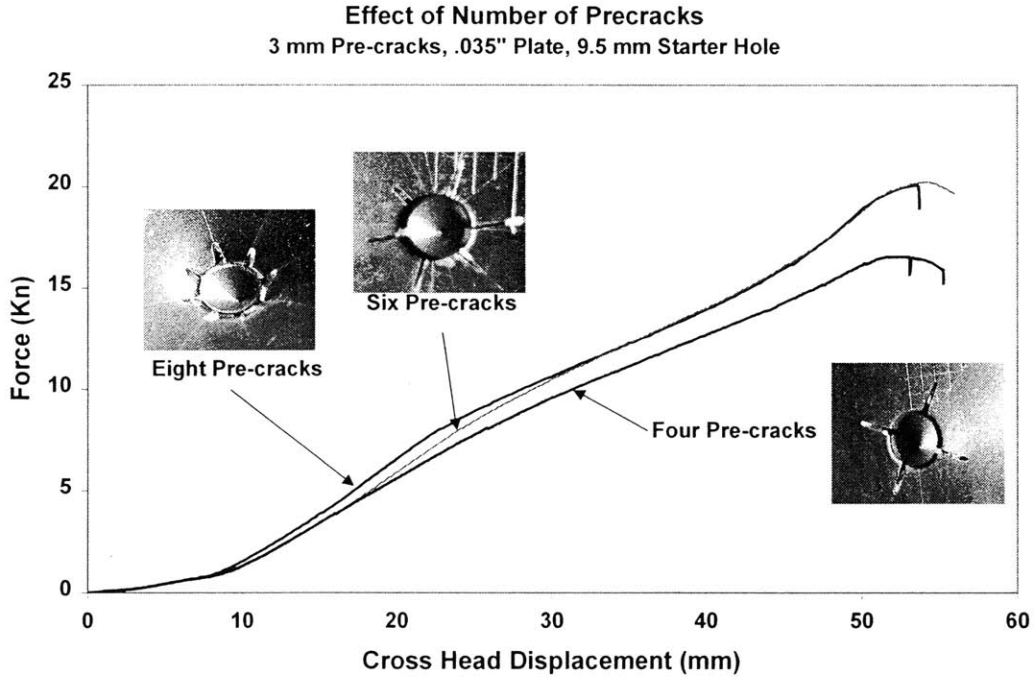

Figure 30: Effect of Number of Pre-Cracks on Force-Displacement Curve

Crack Displacement and Strain Field Examination

Figure 31 shows the increment of crack growth used while mapping the strain field around the crack tip. The crack was allowed to grow approximately 2.5 mm between frames. The white arrow gives a fixed point from which to visually reference the crack's advance. The mapping grid was laid out according to the method discussed in an earlier section.

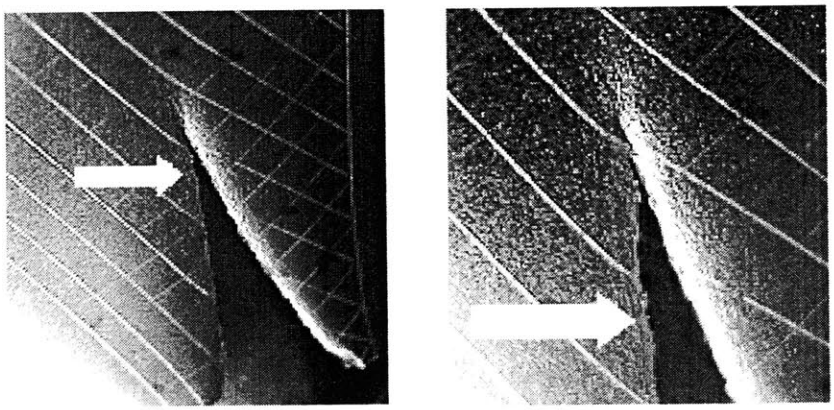

Frame 1 Frame 2

Figure 31: Crack Advance Increment

The displacement filed vectors are plotted relative to the crack tip. Examination of the displacement field shows that, at this instant in time, the membrane is rapidly stretching and thinning in the region in front of the crack.

Biaxial incremental strain values were computed for a small rectangular patch around the crack tip. Similarly, the principal stress ratio, $\frac{\sigma_{11}}{\sigma_{22}}$, was computed from Eq.(38) for each of the grid points, helping to identify regions where necking becomes critical. Figure 32 shows the measured displacement field in the postage stamp size area surrounding the crack tip. Figure 33 shows the measured incremental strain fields and Figure 34 shows the computed

$\frac{\sigma_{11}}{\sigma_{22}}$ field. A visual inspection of the displacement and strain fields suggests that necking occurs primarily directly ahead of the crack. This behavior was both expected and observed during the experiment.

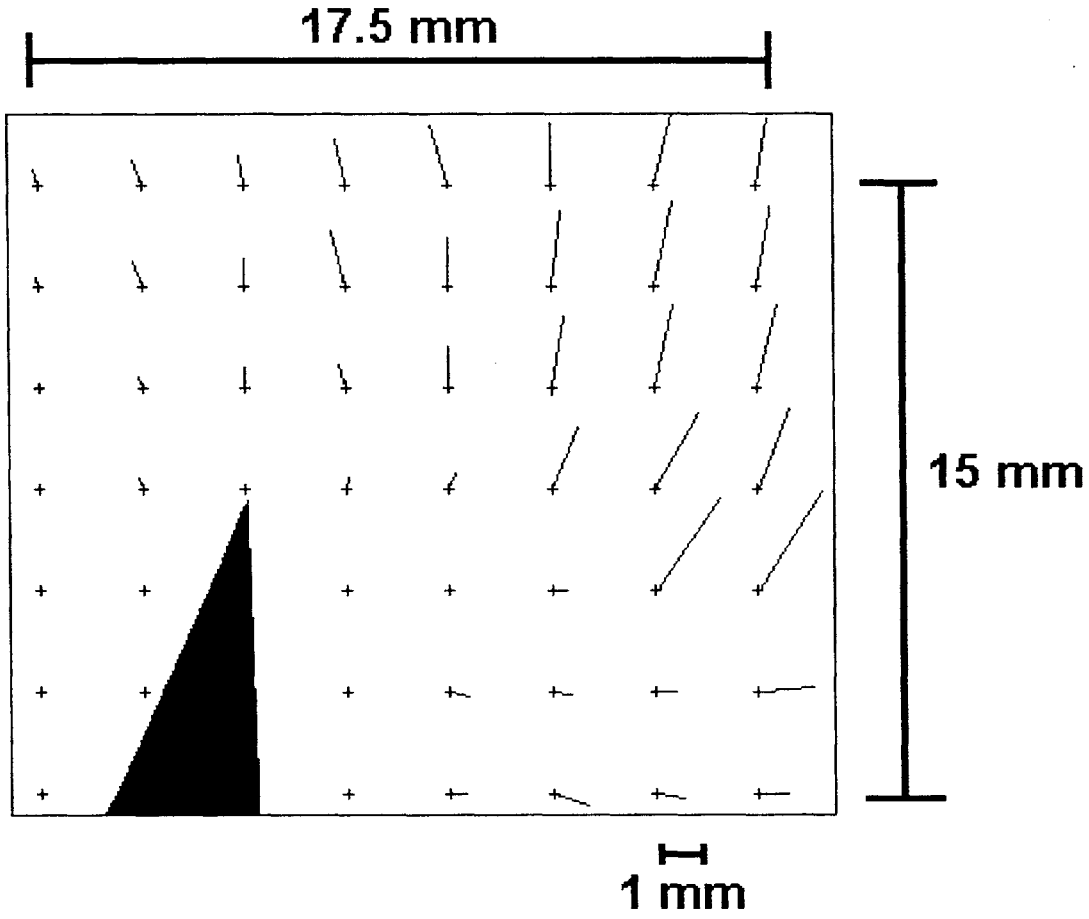

$$\delta u_{11} = \begin{pmatrix} -0.25 & -0.25 & -0.125 & -0.375 & 0 & 0 & 0.5 & 0.125 \\ -0.25 & -0.25 & 0 & -0.375 & 0 & 0.25 & 0.5 & 0.25 \\ 0 & -0.25 & 0 & -0.25 & 0 & 0.5 & 0.5 & 0.75 \\ 0 & 0 & 0 & 0.125 & 0.25 & 0.5 & 1.125 & 0.875 \\ 0 & 0 & 0 & 0 & 0.25 & 0.5 & 1.875 & 1.5 \\ 0 & 0 & 0 & 0 & 0.5 & 0.5 & 0.75 & 1.5 \\ 0 & 0 & 0 & 0 & 0.5 & 1 & 0.5 & 1 \end{pmatrix} \text{mm} \quad \delta u_{22} = \begin{pmatrix} 0.5 & 0.75 & 0.875 & 1 & 1.25 & 1.25 & 1.5 & 1.5 \\ 0.25 & 0.75 & 0.875 & 1.125 & 1.25 & 1.75 & 2 & 2 \\ 0 & 0.25 & 0.625 & 0.625 & 1.25 & 2 & 2 & 2.125 \\ 0 & -0.25 & 0 & 0.25 & 0.375 & 1.625 & 2 & 2 \\ 0 & 0 & 0 & 0 & 0 & 0 & 2.25 & 2.375 \\ 0 & 0 & 0 & 0 & -0.25 & -0.125 & 0 & 0.125 \\ 0 & 0 & 0 & 0 & 0 & -0.25 & -0.125 & 0 \end{pmatrix} \text{mm}$$

Figure 32: Crack Advance Incremental Displacement Field

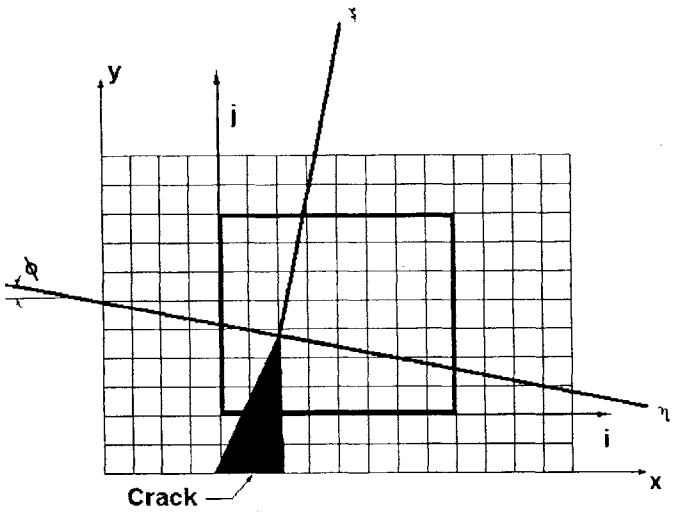

$$\delta e_{\eta\eta} = \begin{pmatrix} 0.393 & 0.491 & 0.54 & 0.589 & 0.687 & 0.687 & 0.785 & 0.785 \\ 0.196 & 0.491 & 0.54 & 0.638 & 0.687 & 0.883 & 0.982 & 0.982 \\ 0.196 & 0.294 & 0.442 & 0.442 & 1.669 & 0.982 & 0.982 & 1.031 \\ 0.196 & 0.109 & 0.218 & 0.327 & 0.382 & 0.927 & 0.982 & 0.982 \\ 0 & 0 & 0.164 & 0.218 & 0.218 & 0.218 & 1.08 & 1.129 \\ 0 & 0 & 0 & 0 & 0.098 & 0.147 & 0.196 & 0.245 \\ 0 & 0 & 0 & 0 & 0 & 0.123 & 0.184 & 0.245 \end{pmatrix}$$

$$\delta e_{\xi\xi} = \begin{pmatrix} 0.407 & 0.509 & 0.56 & 0.611 & 0.713 & 0.713 & 0.815 & 0.815 \\ 0.204 & 0.509 & 0.56 & 0.662 & 0.713 & 0.917 & 1.019 & 1.019 \\ 0.204 & 0.306 & 0.458 & 0.458 & 1.732 & 1.019 & 1.019 & 1.07 \\ 0.204 & 0.113 & 0.226 & 0.34 & 0.396 & 0.962 & 1.019 & 1.019 \\ 0 & 0 & 0.17 & 0.226 & 0.226 & 0.226 & 1.121 & 1.172 \\ 0 & 0 & 0 & 0 & 0.102 & 0.153 & 0.204 & 0.255 \\ 0 & 0 & 0 & 0 & 0 & 0.127 & 0.191 & 0.255 \end{pmatrix}$$

$$\delta e_{\xi\eta} = \begin{pmatrix} 0.294 & 0.294 & 0.344 & 0.294 & 0.344 & 0.442 & 0.589 & 0.515 \\ 0.245 & 0.294 & 0.368 & 0.344 & 0.442 & 0.589 & 0.687 & 0.638 \\ 0.207 & 0.213 & 0.319 & 0.27 & 0.933 & 0.687 & 0.687 & 0.761 \\ 0.221 & 0.164 & 0.218 & 0.3 & 0.354 & 0.682 & 0.864 & 0.787 \\ 0 & 0 & 0.164 & 0.218 & 0.273 & 0.327 & 1.066 & 0.987 \\ 0 & 0 & 0 & 0 & 0.258 & 0.288 & 0.368 & 0.537 \\ 0 & 0 & 0 & 0 & 0 & 0.429 & 0.337 & 0.491 \end{pmatrix}$$

Figure 33: Resultant Strain Increment Fields

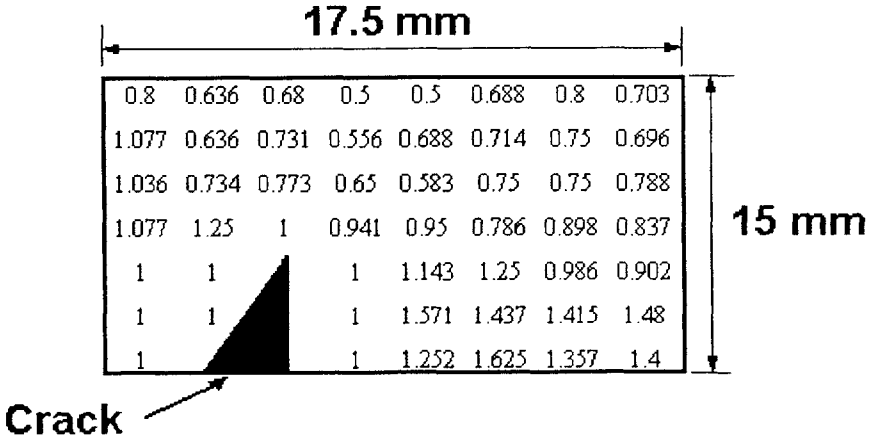

Figure 34: Resultant Principal Stress Ratio Field

Conclusions and Recommendations

Conclusions

This study has investigated using simple, inexpensive quasi-static tearing tests to gain insight into the complex dynamic problem of explosions. It has been shown that these tests can successfully reproduce plate deformations similar in nature to those found after large-scale explosions. It was also shown that the forces, displacements, and energy dissipation in the plate-dishing phase can be accurately approximated by Simonsen's approach (within 5%). Although this series of experiments was not able to generate spiraled petals, Wierzbicki's calculation of petalling work appeared to provide reasonably good (within 20%) estimates of energy dissipation during the second phase of deformation. The conical punch test, however, requires a revised mechanical design in order to better model the flat plate petalling and post-dish petalling cases.

An approach to developing fracture criterion was also presented by measuring incremental strains around the crack tip. Subsequently, the local stress ratios governing material necking were computed. With that information in hand, crack growth can be predicted in the next increment. This approach could result in a revised crack growth criterion, which might then be used to improve existing hydrodynamically coupled finite element simulations.

Recommendations

- The punch tests should explore a wider range of penetrator geometries. Punch variation may introduce more curvature into the resulting petals, helping to capture more of the dynamic effects. Pyramid or volute shapes might be considered. Certainly, narrower cone angles should be tried in order to increase the punch displacement and extend observation time.

- Future analytical work should attempt to more closely link the quasi-static test results with characteristics of the dynamic problem. To do so may require dynamic testing, which could be accomplished at government blast testing facilities.

- Future numerical simulations should apply new punch geometries and include new plate structures (sandwiches, foam, etc...) which might potentially be considered for ship hull reinforcement. Future numerical simulations should also attempt to more completely capture the dynamic aspects of an explosion.

- The potential improvement in crack growth criterion could result in a tremendous advance in the understanding of crack propagation due to intense blast pressures. This avenue should be explored more fully in order to update current prediction codes.

- Other areas of application for this research should be investigated. Certainly pipeline explosions (as in the natural gas industry), internal aircraft explosions, and pressure vessel explosions are just of few items for consideration

Bibliography

[1] Rajendran, R. and K. Narasimhan (2000) "Damage Prediction of Clamped Circular Plates Subjected to Contact Underwater Explosion", International Journal of Impact Engineering Vol. 25, pp. 373-386.

[2] Simonsen, Bo Cerup and Lars Peder Lauridsen. (2000) "Energy Absorption and Ductile Failure in Metal Sheets Under Lateral Indentation by a Sphere", International Journal of Impact Engineering Vol. 24, pp.1017-1039.

[3] Wierzbicki, Tomasz and G.N. Nurick (1996) "Large Deformation of Thin Plates under Localised Impulsive Loading", Engineering Fracture Mechanics, Vol. 20, No. 1, pp. 159-167.

[4] Wierzbicki, Tomasz (1999) "Petalling of Plates Under Explosive and Impact Loading", International Journal of Impact Engineering Vol. 22, pp.935-954.

[5] Wierzbicki, Tomasz and P. Thomas (1993) "Closed Form Solution for Wedge cutting Force Through Thin Metal Sheets", International Journal of Mechanical Sciences, Vol. 35, No. 3/4, pp. 209-229.

[6] Nurick, G.N. and G.C. Shave (1996) "The Deformation and Tearing of Thin Square Plates subjected to Impulsive Loads - An Experimental Study ", Engineering Fracture Mechanics, Vol. 18, No. 1, pp. 99-116.

[7] Nurick G.N., M.E. Gelman, and N.S. Marshall (1996) "Tearing of Blast Loaded Plates with Clamped Boundary Conditions", Engineering Fracture Mechanics, Vol. 18, No. 7, pp. 803-827.

[8] Taylor, G.I. (1948) "The Formation and Enlargement of a Circular Hole in a Thin Plastic Sheet", Quarterly Journal of Mechanics and Applied Mathematics, Vol. 1, pp. 103-124

[9] McClintock, F.A. and Z.M. Zheng (1993) "Ductile Fracture Before Localized Necking in a Strip under Tension", International Journal of Fracture Vol. 64, pp.191-200.

[10] Cole, Robert H. (1948), "Underwater Explosions", Princeton University Press.

[11] G.I. Taylor (1948) "The Pressure and Impulse of Submarine Explosion Waves on Plates", "The Scientic Papers of Sir Geoffrey Ingram Taylor", Vol. 3, No. 31, pp 287-303.

[12] Nazeer M.M., M Afzal Khan, and Atheer Naheem(2000), "Analysis of Conical Tool Perforation of Ductile Metal Sheets" International Journal of Mechanical Sciences, Vol. 42, pp. 1391-1403.

[13] Atkins, A.G., M. Afzal Khan, and J.H. Liu, "Necking and Radial Cracking Around Perforations in Thin Sheets at Normal Incidence", International Journal of Impact Engineering Vol. 21 No. 7, pp. 521-539.

[14] Arndt, S., S. Swillo, and A.G. Atkins (2001), Multiple Necks Around Biaxially Loaded Holes in Sheets" International Journal of Mechanical Sciences, Vol. 43 pp. 245-263.

[15] Jones, Norman and C. Jones (2001),"Inelastic Failure of fully Clamped Beams and Circular Plates under Impact Loading" Journal of Mechanical Engineering Science, Vol. 216 Part C, pp. 133-149.

[16] Snelling, William A. (1946) "Direct Explosion Test for Welded Armor and Ship Plate: Prime and Welded Plate Tests", Ship Structure Committee Report 4.

[17] Shames, Irving H. (1989) "Introduction to Solid Mechanics", Prentice-Hall.

[18] Kalpakjain, Serope (1995) "Manufacturing Engineering and Technology", Addison-Wesley.

[19] Hughes, Owen B (1988) "Ship Structural Design", The Society of Naval Architects and Marine Engineers.

Appendices

Appendix A: Introductory Material

Since the inception of the warship, designers have sought means to make combatant vessels more damage resistant. Only since World War II, however, has there been significant effort to compile and analyze detailed reports of vessel battle damage. In the subsequent post war years, much analysis was conducted in the areas of hull armor, resistance to mine attack, and torpedo side-protection. As might be expected, the systems that were ultimately developed to enhance survivability, incurred substantial weight, space, and performance penalties. As the years have passed, the damage database has deteriorated. Since the late 1940's, the U.S Navy has relied largely on full-scale tests or "SINKEX's" to demonstrate battle damage effects. There have been only a handful of wartime incidents demonstrating the realistic damage absorbing and recovery capabilities of modern warships. In that time, threat weapons (mines, missiles, and torpedoes) have been improved markedly. In contrast to their World War II predecessors, state of the art weapons are extremely likely carry out a successful attack and inflict extraordinary damage with a high degree of accuracy.

As seen more recently in the case of the U.S.S. Cole, tremendous hull damage can be suffered during unconventional close aboard explosions. Figure A1 shows the 20-ft by 40-ft amidships hole torn in the ship's port side by a waterline explosion.

Inspection of the picture shows that the explosion created a spherical bulge, or dishing, in the ship' hull, prior to tearing into numerous petals. Though officially unconfirmed, it has been suggested that the attack was carried out using between 400 and 700 lbs. of C-4 military explosive. Unofficial standoff distance estimates range from on-contact to 10 feet.

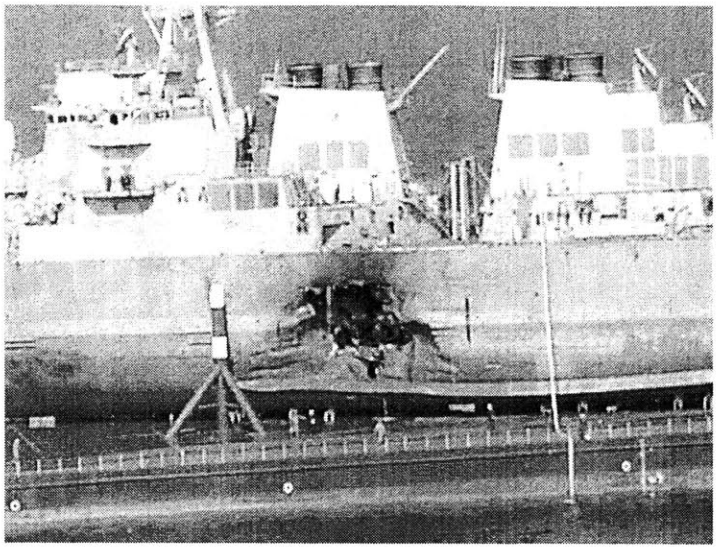

Figure A1: USS Cole Port Side Damage

In this instance, a majority of the damage occurred below the waterline. Figure 2 clearly shows the above-waterline tearing. From Figure A2, the characteristic petal formations can be identified, as well as the upper deck hard point at which crack propagation is arrested. Hull panels at this location on a typical naval combatant ship are usually constructed of either mild steel (MTS-45) or HY-80, and they can vary between .375" and .5" in thickness.

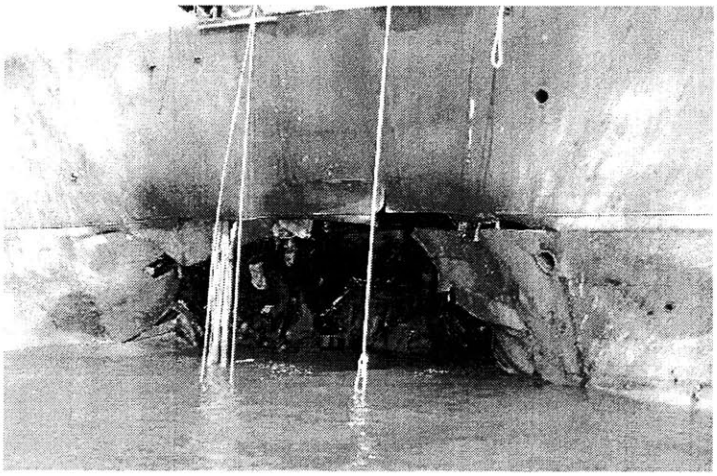

Figure A2: Close Up View of Above Waterline Damage

Appendix B: Additional Background

Holing prediction for metal plate has been a topic of study since the early 1900's. The research is rooted in a 1912 study done by Bertram Hopkinson, which examined the resistance of naval plating against artillery shell penetration. In that case, the deformed

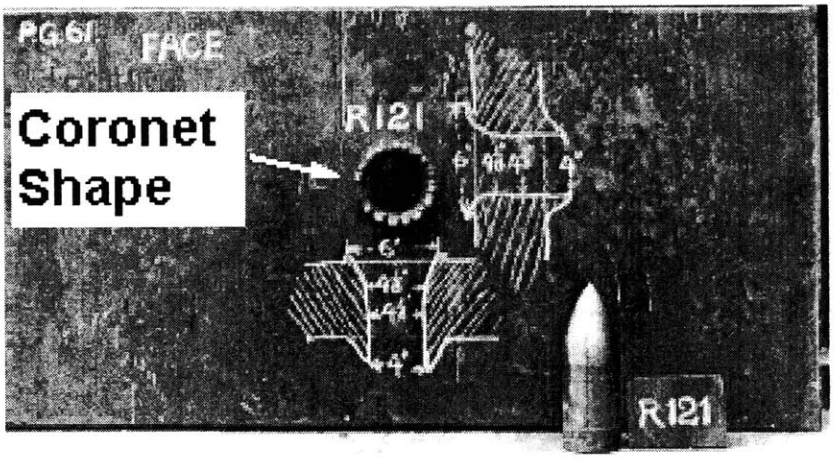

Figure B1: Hopkinson's 1912 Armor Plate

plating, shown in Figure B1, developed a coronet-shaped pattern with radial cracks and necking at the petal edges. Since that time there have been countless experiments investigating armor effectiveness. Until the past two decades, the vast majority of plate holing and deformation studies have focused on the impact and associated damage of ballistic particles. The most notable and comprehensive exception is the 1940's work of Sir G.I Taylor (1948) who examined the nature of submerged blast waves and their effects on thin plates. Taylor's work in the area of submerged explosions was continued by Robert Cole (1948) in the text, Underwater Explosions. Together, these two researchers provide much of the technical underpinning for current blast damage prediction methods.

Explosive deformation and holing studies in naval vessels, largely classified, have been empirical derivations based on years of accrued data. An undisclosed solution developed by ONR, predicts a minimum and maximum expected hole radius in naval panels for a given set of panel parameters. This engineering tool was the result of hundreds of live fire tests, and is one of the most commonly used methods used by U.S. Navy designers in estimating expected battle damage due to close proximity explosions. This solution suggests the following general relationship:

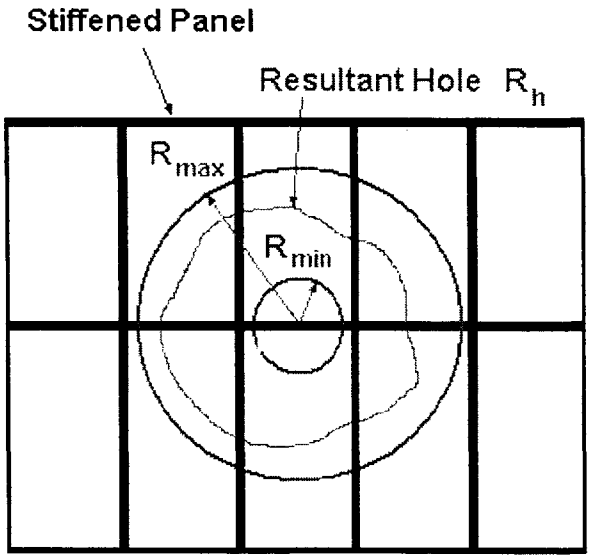

Figure B2: Current Panel Damage Formulation

$$R_{Min} \leq R_h \leq R_{Max} = f(G,T,M)$$

R_h = Resultant Hole Size

R_{min} = Minimum Predicted Hole Size

R_{max} = Maximum Predicted Hole Size

G = Panel Geometry

T = Plate Thickness

M = Material Properties

Other problems, however, lend themselves to the study of panels under explosive loading. Wierzbicki and Thomas (1993), by examining plate cutting behavior, were able to related the geometry of the deformed plating geometry to the mechanical and frictional work done in a vessel grounding, thereby predicting damage. Later, Wierzbicki (1996) and Nurick (1996), investigated the response of clamped thin sheets when subjected to on-contact charges. Wierzbicki (1999) subsequently proposed that the kinematics of the cutting process, shown in Figure B3, were very similar to both those of the explosive petalling and ballistic penetrator problem.

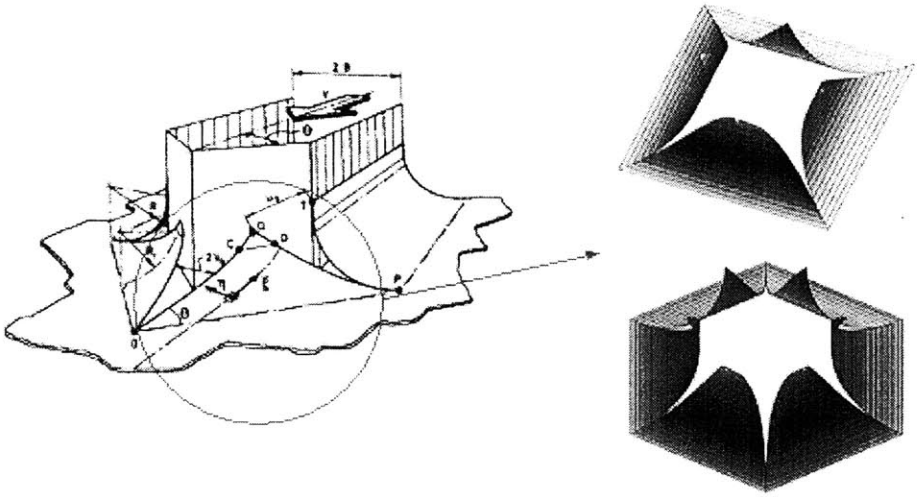

Figure B3: Cutting and Petalling Geometric Similarities

Along similar lines, Atkins (1998) observed the necking and radial crack formation in ductile materials when perforated by both spherical and conical penetrators. Using a hydraulic bulger, he later analyzed thin sheet necking around biaxially loaded holes (1999). Simonsen (2000), built upon this work, using spherical indenters to analyze force-displacement relationship in clamped mild steel plates. Again, these studies were targeted at making damage prediction for vessel collisions and ballistic penetrators. Nevertheless, these

experiments closely model thin sheet behavior during the dishing, disking, and pre-petalling phases of an explosion.

To date, there has been little effort to correlate the results of quasi-static indenter experiments to the damage observed both in live fire explosive tests and in combat. With that goal in mind, this research is deemed both relevant and unique.

Appendix C: Problem Statement Details

Currently, U.S. Navy surface ships are built using a damaged length design standard equivalent to 15% Length Between Perpendiculars (LBP). This rule for damaged length is based on both past operating experience and on the damage expected from a given threat weapon. As illustrated in Figure C1, accurately determining the opening size is crucial in determining compartment layout, equipment placement, and bulkhead spacing. In a poorly designed 500-ft ship, for instance, a 15% damage length (75ft) could result in total loss of propulsion. By the same token, over designing a ship using excessive damage length results in increased structural weight, higher cost, and decreased performance.

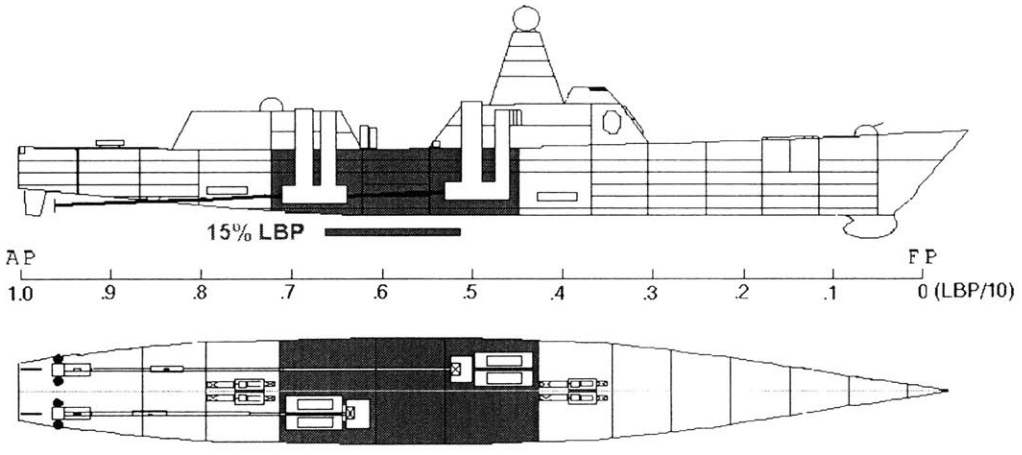

Figure C1: Surface Ship 15% LBP Damage Length

Damage prediction methods can be extraordinarily complex. The most modern techniques use machine codes, which couple explosive mechanics with the concurrent hydrodynamic effects. These codes, however, are both expensive and time consuming. Furthermore, the accuracy of their output is not yet fully validated. Other than scaled live

fire tests, no reliable prediction tool exists which can quickly and accurately estimate damage. An analytical method which uses inputs such as charge size, standoff distance, material could prove useful both to ship and weapon designers.

Appendix D: Fixture Design Supplemental

A significant amount of design work was required to ensure that the mechanism (1) did not fail under the expected test loads and (2) was adaptable for use in the Universal Testing Machine (UTM) belonging to the MIT Impact and Crashworthiness Laboratory.

As shown in the drawings, the fixture horizontally holds a 300 mm x 300 mm square thin sheet while an indenter or punch is lowered. The clamped dimensions, shown in Figure D1, are 220 mm x 220 mm. The specimens maximum dimensions were selected based on several criteria. First, the specimen needed to be large enough to easily observe the resultant deformations, yet small enough to fit within the UTM. Further, it was desirable to have a portable, light-weight test fixture (in this case 75 lbs. was designated as an upper weight limit). Lastly, steel sheet stock is normally manufactured in 4 ft x 8 ft sheets. A 300 mm square sample allows 32 specimens to be taken from a single sheet with minimal waste.

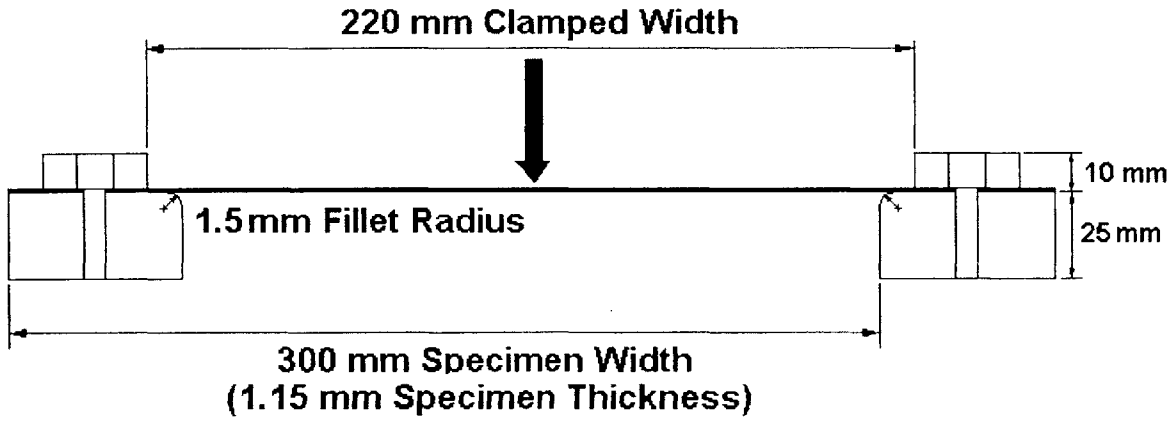

Figure D1: Clamped Specimen Cross Section

Since the test specimen represents a single clamped panel, the specimen needed to be geometrically similar to existing naval panels. Frame spacing within a mid-sized combatant is generally near 8 ft, with the panels being nearly square (or slightly rectangular). At thicknesses of 1/2" to 3/8", a panel width-to-thickness ratio (w/t) of 200 can be reasonably assumed. In order to maintain this ratio, three specimen thicknesses (.89mm, 1.14 mm, and 1.40 mm) were selected from available mild steel stock.

The body of the fixture is machined from mild steel (45ksi Yield Strength). Member thicknesses were selected to prevent yield during normal testing and to minimize weight. Note that the fixture narrows to 6" at its base to transfer force directly to the load bearing beam in the UTM. Thin lateral bracing panels were used to prevent fixture racking during testing. The fixture mounts to the UTM through a series of threaded holes in its baseplate.

The upper and lower bolting rings are used to hold the specimen in place. These rings are machined from A2 Air Hardened Steel (108 ksi Yield Strength). This grade of steel was selected to satisfy fixity requirements. Firm edge fixity is required in order to make boundary condition assumptions. Past experiment have shown that simple bolting flanges do not provide sufficient clamping restraint. Typically a drawbead can be used to overcome this problem. When testing thick or high strength materials, however, it becomes difficult to form the specimen around a drawbead. For this reason (and since the fixture is intended to test a wide range of materials and thickness), a serrated mating surface was used to provide fixity.

In order to ensure sufficient tooth hardness and clamping force, an estimate of material strength was made using Slip Line Fracture Mechanics. The analysis showed that the mating surfaces must have a yield strength at least 50% higher than that of the test specimen. The estimates are summarized in Figures D2 and D3.

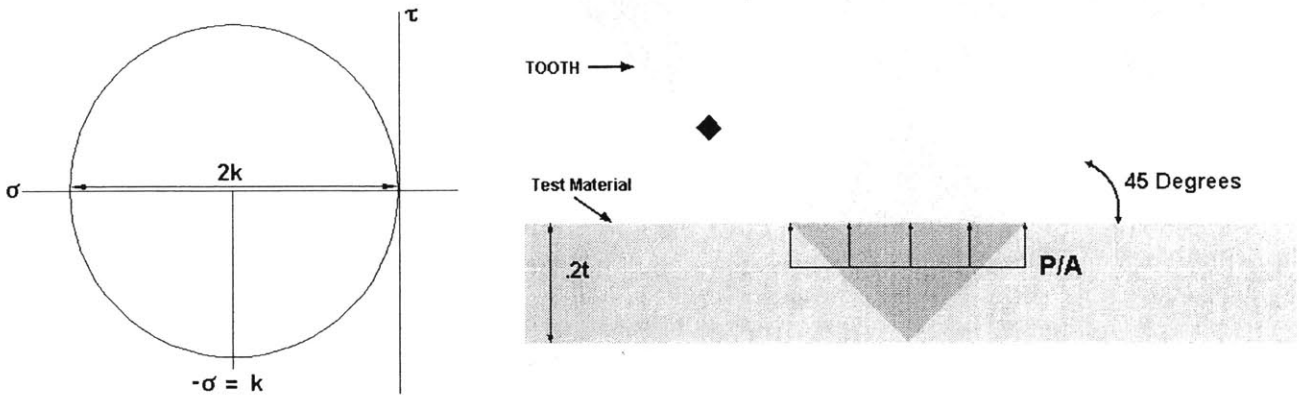

Figure D2: Mohr Circle For Tooth Element Tooth

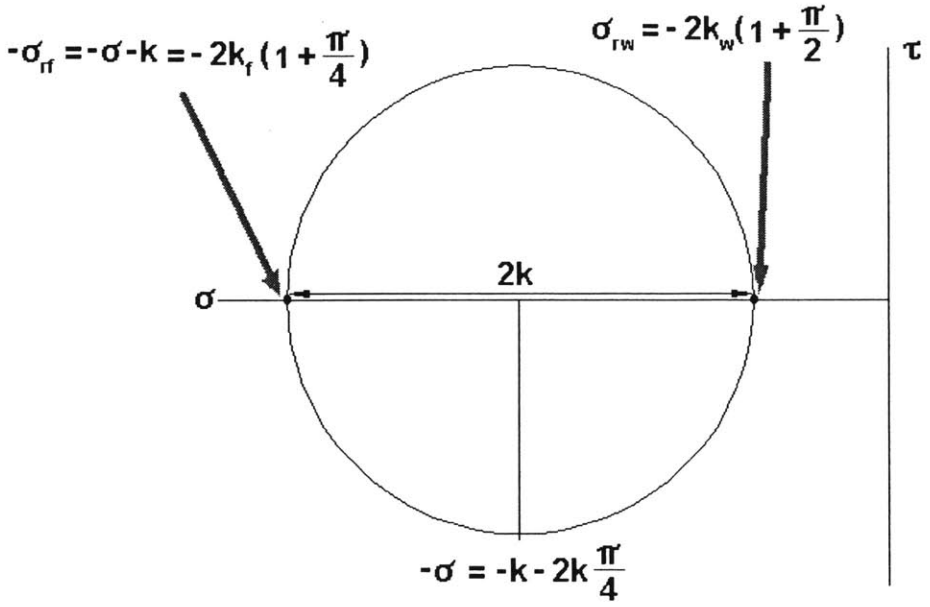

Figure D3: Mohr Circle For 45-Degree Rotation Tooth Element

$$\sigma_{rf} = \sigma_{rw} \tag{D1}$$

$$k_f(1+\frac{\pi}{4}) = k_w(1+\frac{\pi}{2}) \tag{D2}$$

$$\frac{k_f}{k_w} = \frac{1+\frac{\pi}{2}}{1+\frac{\pi}{4}} = 1.44 \qquad \text{(Ratio of Base Plate Yield to Test Material Yield)} \tag{D3}$$

Estimate of Frame Sizes and Stresses Induced During Indentation Testing

Cross Beam Dimensions:

$h \equiv 25.4\,mm \qquad b := 50\,mm \qquad L := 300\,mm$

Expected Load and Material Characteristics:

$P := 105000\,N \qquad P = 2.36 \times 10^{4}\,lbf$

$Y := 108000\,psi \qquad Y = 7.446 \times 10^{8}\,Pa$

Assuming a Rigid Test Specimen and a
Simply Supported Beam with a Concentated Central Load:

$M := \frac{L}{2} \cdot \frac{P}{4} \qquad c := \frac{h}{2} \qquad I := b \cdot \frac{h^3}{12}$

$\sigma_{beam} := M \cdot \frac{c}{I} \qquad \sigma_{beam} = 7.324 \times 10^{8}\,Pa$

Safety Factor:

$$\frac{Y}{\sigma_{beam}} = 1.017$$

...or distibuting load along ther beam, gives the same result for the maximum developed stress:

$w := \frac{P}{4L} \qquad M := \frac{1}{2} \cdot w \cdot L^2$

$\sigma_{beam} := M \cdot \frac{c}{I} \qquad \sigma_{beam} = 7.324 \times 10^{8}\,Pa$

Safety Factor:

$$\frac{Y}{\sigma_{beam}} = 1.017$$

Using the exact solution for sinusoidally loaded, simply supported plate:

$$F_D := \frac{P}{\pi^2} \qquad M := F_D \cdot \frac{L}{2}$$

$$\sigma_{beam} := M \cdot \frac{c}{I} \qquad \sigma_{beam} = 2.968 \times 10^8\ Pa$$

Safety Factor:

$$\frac{Y}{\sigma_{beam}} = 2.509$$

Compressive Load on Legs:

$$Y_{leg} := 45000 \cdot psi$$

$$t_{leg} := 20 \cdot mm \qquad w_{leg} := 49.3 \cdot mm \qquad A_{leg} := 2 \cdot \left(2 \cdot t_{leg} \cdot w_{leg}\right)$$

$$\sigma_{leg} := \frac{P}{A_{leg}} \qquad \sigma_{leg} = 2.662 \times 10^7\ Pa$$

$$\frac{Y_{leg}}{\sigma_{leg}} = 11.654$$

Appendix E: Uniaxial Testing

The mild steel plate material was tested Uni.-axially in tension according to ASTM standards. The .035" and .045" were tested in 1999 in concert with a separate project. The .055" thickness was tested specifically for this research. All specimens were tested in the X and Y direction to verify that the material behaved isotropically.

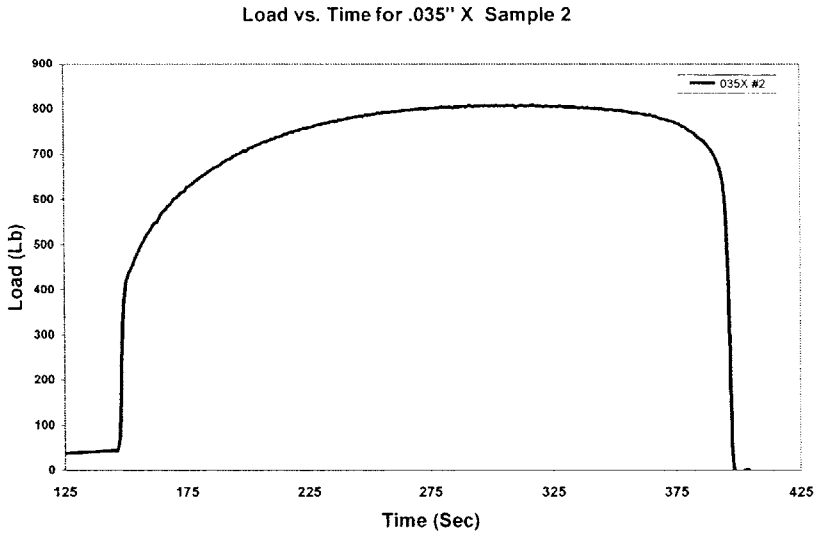

Figure E1: Representative Load vs. Time Curve

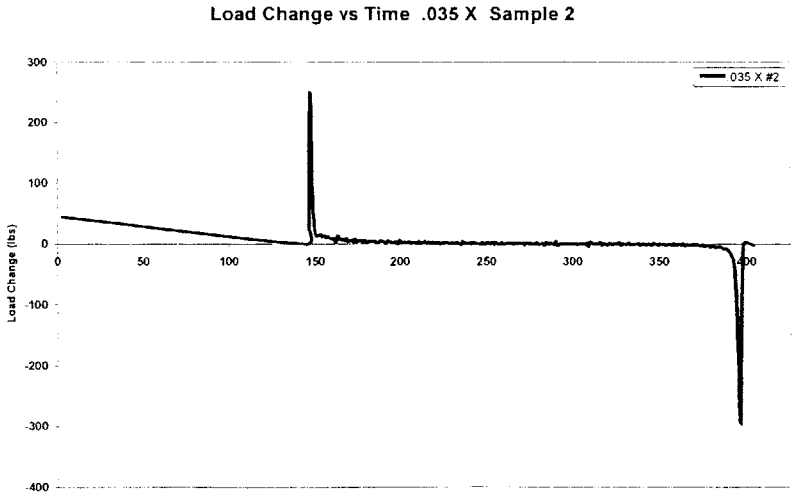

Figure E2: Representative Load Change vs. Time Curve

During the uni-axial testing, all of the thin strip specimens displayed stable fracture, consequently the precise load at fracture was not readily apparent. By plotting the change in load vs. time for each specimen, a "knuckle" in the load vs. Time plot was clearly identified, which indicated the onset of fracture. Figures E1 and E2 illustrate this approach. Figures E3 and E4, respectively, show a representative uni-axial specimen and a close-up view of the fracture.

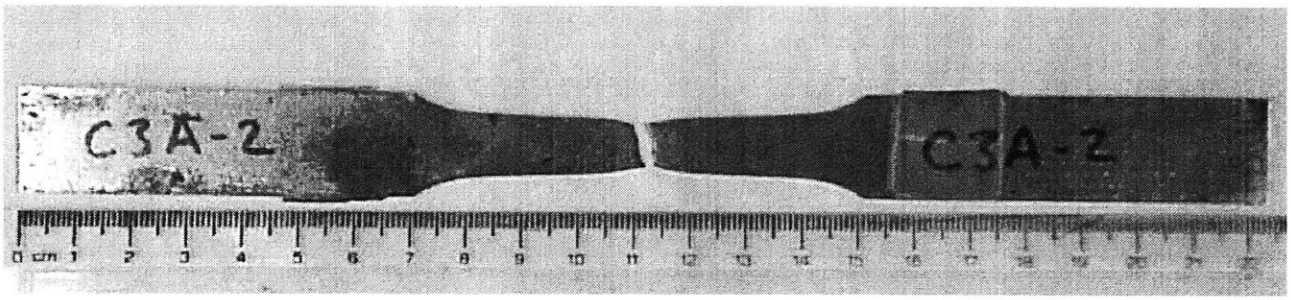

Figure E3: Final .035" Uni-axial Specimen

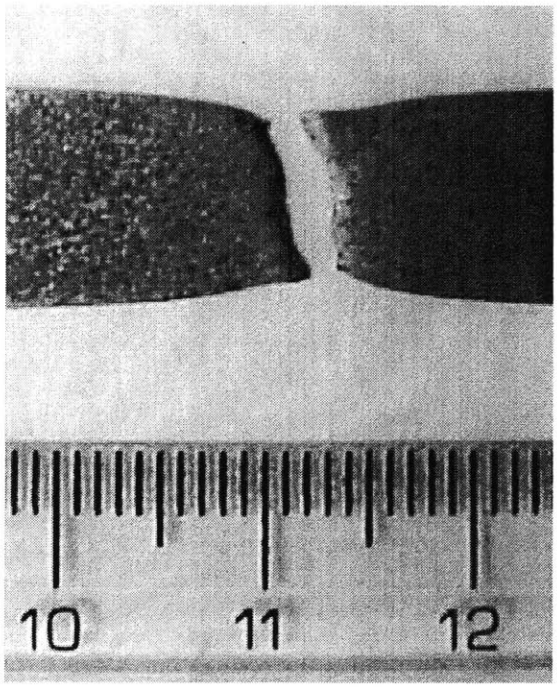

Figure E4: Final .035" Specimen Fracture Closeup

The final dimensions of each specimen's cross section were measured in order to determine the true stress and strain of the specimen at fracture. This data point was vital in constructing the true stress-strain curve for the finite element simulation. Due to necking, the specimen's highest true fracture stress and strain were achieved in the middle, where the fracture initiated. Figure E5 shows the approximate final geometry for the necked specimens.

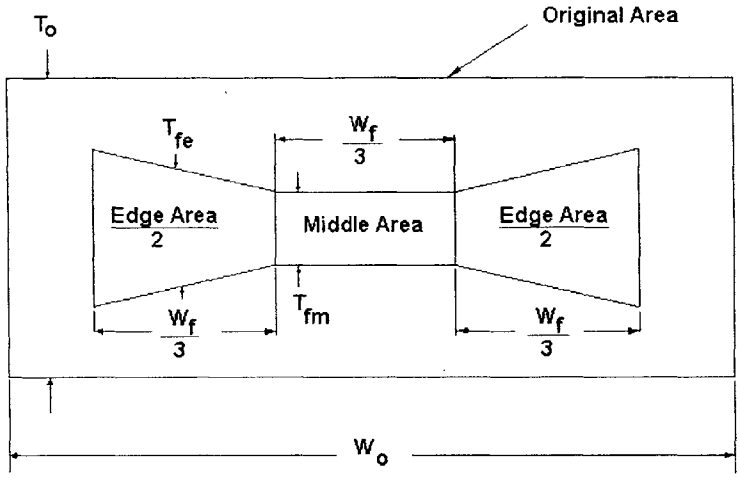

Figure E5: Approximate Necked Specimen Geometry

Reduction in Squared Thickness (RST) and true fracture strain for the thin strips were computed in accordance with McClintock and Zheng (1993),

$$RST = 1 - (t_f / t_o)^2 \tag{E1}$$

$$\varepsilon_f = -\ln(1 - RST) \tag{E2}$$

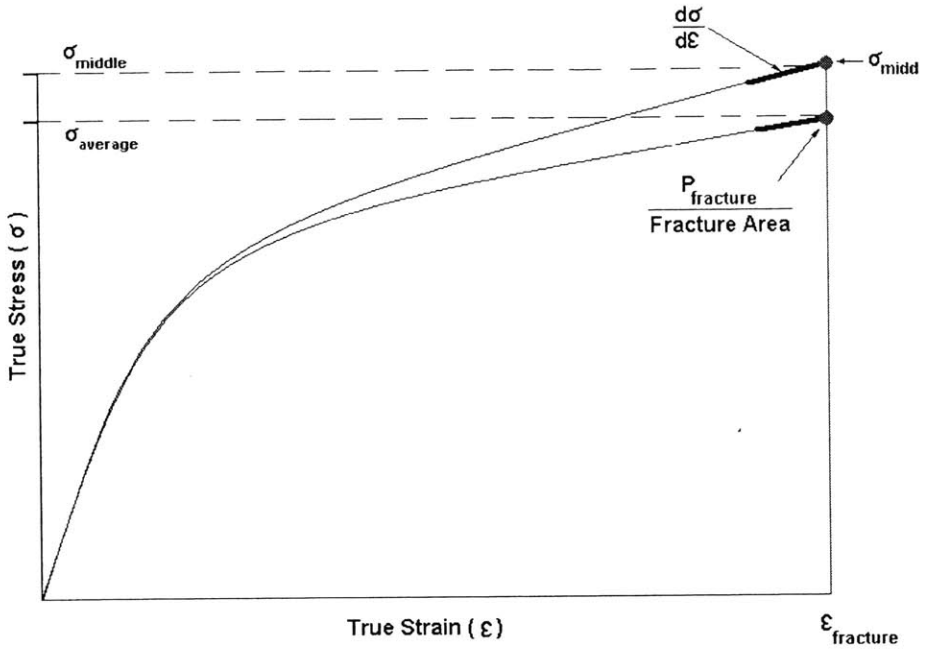

Figure E6: Representative True Stress vs. Strain Curve for Uniaxial Test

Some formulation was required to compute σ_{middle} (σ_m) :

$$\sigma_e = \sigma_m - (\varepsilon_m - \varepsilon_e)\frac{d\sigma}{d\varepsilon} \tag{E3}$$

$$P_{fracture} = A_m\sigma_m + A_e\sigma_e \tag{E4}$$

Where substituting (E3) into (E4) yields,

$$P_{fracture} = A_m\sigma_m + A_e(\sigma_m - (\varepsilon_m - \varepsilon_e)\frac{d\sigma}{d\varepsilon}) \tag{E5}$$

and solving (E5) for $\sigma_{m,}$

$$\sigma_m = \frac{P_{fracture} + A_e(\varepsilon_m - \varepsilon_e)\frac{d\sigma}{d\varepsilon}}{A_m + A_e} \tag{E6}$$

Table E1: Edge and Middle Thickness at Fracture for Uniaxial Tests

Measured Data			
Sample	**W_o (mm)**	**T_o (mm)**	**W_f (mm)**
.035 X #1	12.83	0.89	8.62
.035 X #2	12.83	0.89	8.70
.035 Y #1	12.78	0.89	8.40
.035 Y #2	12.78	0.89	8.21
.045 X #1	12.79	1.14	7.85
.045 X #2	12.83	1.14	8.03
.045 Y #1	12.80	1.14	7.24
.045 Y #2	12.81	1.14	7.46
.055 X #1	12.79	1.40	6.81
.055 X #2	12.83	1.40	6.90
.055 Y #1	12.80	1.40	6.88
.055 Y #2	12.81	1.40	6.87
Sample	**$T_{Left\ Edge}$ (mm)**	**T_{Middle} (mm)**	**$T_{Right\ Edge}$ (mm)**
.035 X #1	0.36	0.30	0.40
.035 X #2	0.38	0.32	0.42
.035 Y #1	0.39	0.29	0.40
.035 Y #2	0.42	0.28	0.43
.045 X #1	0.56	0.47	0.56
.045 X #2	0.58	0.45	0.57
.045 Y #1	0.56	0.45	0.55
.045 Y #2	0.55	0.45	0.55
.055 X #1	0.65	0.57	0.62
.055 X #2	0.64	0.58	0.64
.055 Y #1	0.63	0.56	0.63
.055 Y #2	0.64	0.57	0.62

Table E2: Right and Left Edge Fracture Strain for Uniaxial Tests

Right Edge			
Sample	RST	Right Edge Fracture Strain	Fracture Area (mm^2)
.035 X #1	0.8364	1.8102	1.0344
.035 X #2	0.8177	1.7021	1.1020
.035 Y #1	0.8080	1.6501	1.0920
.035 Y #2	0.7773	1.5019	1.1494
.045 X #1	0.7587	1.4217	1.4653
.045 X #2	0.7412	1.3515	1.5525
.045 Y #1	0.7587	1.4217	1.3515
.045 Y #2	0.7672	1.4577	1.3677
.055 X #1	0.7844	1.5345	1.4755
.055 X #2	0.7844	1.5345	1.4755
.055 Y #1	0.7975	1.5970	1.4448
.055 Y #2	0.7975	1.5970	1.4448

Left Edge			
Sample	RST	Left Edge Fracture Strain	Fracture Area (mm^2)
.035 X #1	0.7980	1.5995	1.1493
.035 X #2	0.7773	1.5019	1.2180
.035 Y #1	0.7980	1.5995	1.1200
.035 Y #2	0.7666	1.4549	1.1768
.045 X #1	0.7587	1.4217	1.4653
.045 X #2	0.7500	1.3863	1.5257
.045 Y #1	0.7672	1.4577	1.3273
.045 Y #2	0.7672	1.4577	1.3677
.055 X #1	0.8039	1.6290	1.4074
.055 X #2	0.7910	1.5655	1.4720
.055 Y #1	0.7975	1.5970	1.4448
.055 Y #2	0.8039	1.6290	1.4198

Table E3: Middle Fracture Strain for Uniaxial Tests

Middle			
Sample	RST	Fracture Strain	Area Middle (A_M) (mm^2)
.035 X #1	0.8864	2.1749	0.8620
.035 X #2	0.8707	2.0458	0.9280
.035 Y #1	0.8938	2.2427	0.8120
.035 Y #2	0.9010	2.3129	0.7663
.045 X #1	0.8300	1.7721	1.2298
.045 X #2	0.8442	1.8591	1.2045
.045 Y #1	0.8442	1.8591	1.0860
.045 Y #2	0.8442	1.8591	1.1190
.055 X #1	0.8342	1.7972	1.2939
.055 X #2	0.8284	1.7624	1.3340
.055 Y #1	0.8400	1.8326	1.2843
.055 Y #2	0.8342	1.7972	1.3053

Table E4: Estimation of Average Uniaxial Fracture Stress

Computed Values			
Sample	Edge Fracture Strain ($Epsilon_E$)	Total Edge Area (A_E)	dSigma/dEpsilon
.035 X #1	1.705	2.1837	300
.035 X #2	1.602	2.3200	300
.035 Y #1	1.625	2.2120	300
.035 Y #2	1.478	2.3262	300
.045 X #1	1.422	2.9307	300
.045 X #2	1.369	3.0782	300
.045 Y #1	1.440	2.6788	300
.045 Y #2	1.458	2.7353	300
.055 X #1	1.582	2.8829	300
.055 X #2	1.550	2.9475	300
.055 Y #1	1.597	2.8896	300
.055 Y #2	1.613	2.8646	300
Sample	Fracture Load (lb)	Average Fracture stress (MPA)	Fracture Stress Middle (MPA)
.035 X #1	697.78	1019.08	1120.18
.035 X #2	696.04	953.24	1048.34
.035 Y #1	674.84	992.66	1128.25
.035 Y #2	673.49	968.76	1157.07
.045 X #1	923.38	987.23	1061.28
.045 X #2	925.15	960.91	1066.60
.045 Y #1	924.08	1091.83	1181.34
.045 Y #2	921.48	1063.46	1148.91
.055 X #1	923.38	983.38	1027.98
.055 X #2	925.15	961.17	1005.04
.055 Y #1	924.08	984.82	1033.75
.055 Y #2	921.48	982.98	1020.94

Table E5: .035" Uniaxial Sample Test Data

.035" Thickness X Direction

file name: c2x-1.dat
description: 0.035" sheet metal, "X" direction
test date: 11/9/1999
test mach.; Instron 1331
specimen #: C2X-1
area: 0.0176
thickness: 0.0350
width: 0.5035

pretest notes
data acquisition = 300 msec, 22 bits
channel 1 = strain, 10%/v
channel 2 = load, 562 lbs/v
sampling rate = 0.5 sec
load rate = 0.2 in/min
first data point = zero load, second data point = zero strain

C2X-1	test notes
yeild stress:	23,300
ult. stress:	46,294
break point:	inside gage area

file name: c2x-2.dat
description: 0.035" sheet metal, "X" direction
test date: 11/9/1999
test mach.; Instron 1331
specimen #: C2X-2
area: 0.0176
thickness: 0.0350
width: 0.5030

pretest notes
data acquisition = 300 msec, 22 bits
channel 1 = strain, 10%/v
channel 2 = load, 562 lbs/v
sampling rate = 0.5 sec
load rate = 0.2 in/min
first data point = zero load, second data point = zero strain

C2X-2	test notes
yeild stress:	23,300
ult. stress:	45,903
break point:	inside gage area

.035 Thickness Y Direction

file name: c2y-1.dat
description: 0.035" sheet metal, "Y" direction
test date: 11/9/1999
test mach.; Instron 1331
specimen #: C2Y-1
area: 0.0176
thickness: 0.0350
width: 0.5040

pretest notes
data acquisition = 300 msec, 22 bits
channel 1 = strain, 10%/v
channel 2 = load, 562 lbs/v
sampling rate = 0.5 sec
load rate = 0.2 in/min
first data point = zero load, second data point = zero strain

C2Y-1	test notes
yeild stress:	25,100
ult. stress:	45,176
break point:	inside gage area

file name: c2y-2.dat
description: 0.035" sheet metal, "Y" direction
test date: 11/9/1999
test mach.; Instron 1331
specimen #: C2Y-2
area: 0.0177
thickness: 0.0350
width: 0.5045

pretest notes
data acquisition = 300 msec, 22 bits
channel 1 = strain, 10%/v
channel 2 = load, 562 lbs/v
sampling rate = 0.5 sec
load rate = 0.2 in/min
first data point = zero load, second data point = zero strain

C2Y-2	test notes
yeild stress:	25,100
ult. stress:	45,146
break point:	inside gage area

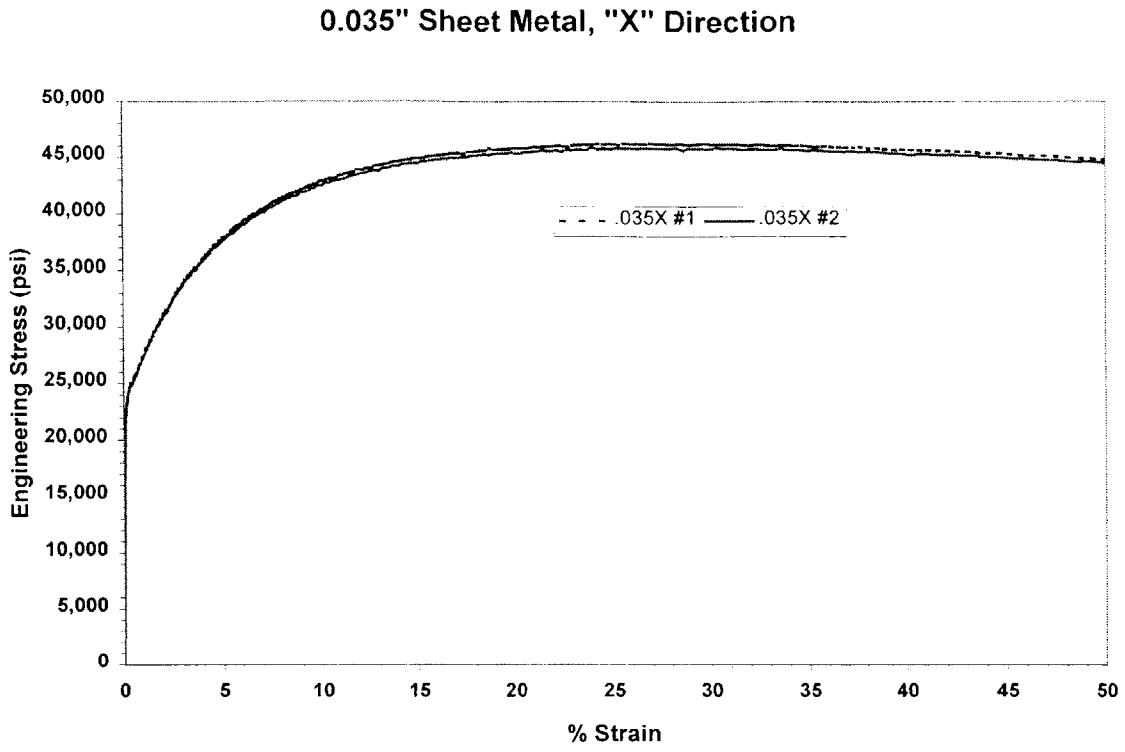

Figure E7: Engineering Stress vs. Strain Curve for .035" X Uniaxial Test

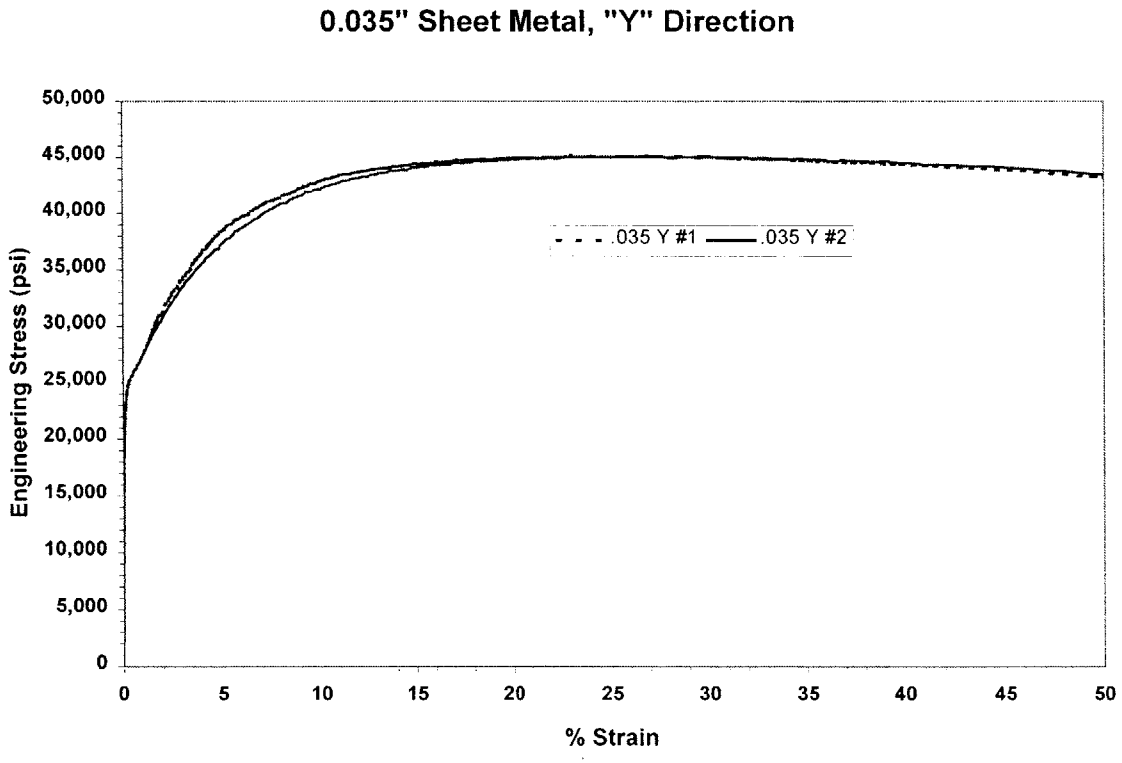

Figure E8: Engineering Stress vs. Strain Curve for .035" Y Uniaxial Test

Table E6: .045" Uniaxial Sample Test Data

.045" Thickness X Direction

file name: c3x-1.dat
description: 0.045" sheet metal, "X" direction
test date: 11/9/1999
test mach.; Instron 1331
specimen #: C3X-1
area: 0.0227
thickness: 0.0450
width: 0.5050

pretest notes
data acquisition = 300 msec, 22 bits
channel 1 = strain: 10%/v
channel 2 = load: 562 lbs/v
sampling rate = 0.5 sec
load rate = 0.2 in/min
first data point = zero load, second data point = zero strain

C3X-1	test notes
yeild stress:	28,600
ult. stress:	47,776
break point:	inside gage area

file name: c3x-2.dat
description: 0.045" sheet metal, "X" direction
test date: 11/9/1999
test mach.; Instron 1331
specimen #: C3X-2
area: 0.0227
thickness: 0.0450
width: 0.5050

pretest notes
data acquisition = 300 msec, 22 bits
channel 1 = strain: 10%/v
channel 2 = load: 562 lbs/v
sampling rate = 0.5 sec
load rate = 0.2 in/min
first data point = zero load, second data point = zero strain

C3X-2	test notes
yeild stress:	28,600
ult. stress:	47,688
break point:	inside gage area

.045" Thickness Y Direction

file name: c3y-1.dat
description: 0.045" sheet metal, "Y" direction
test date: 11/9/1999
test mach.; Instron 1331
specimen #: C3Y-1
area: 0.0226
thickness: 0.0450
width: 0.5030

pretest notes
data acquisition = 300 msec, 22 bits
channel 1 = strain: 10%/v
channel 2 = load: 562 lbs/v
sampling rate = 0.5 sec
load rate = 0.2 in/min
first data point = zero load, second data point = zero strain

C3Y-1	test notes
yeild stress:	30,000
ult. stress:	46,948
break point:	inside gage area

file name: c3y-2.dat
description: 0.045" sheet metal, "Y" direction
test date: 11/9/1999
test mach.; Instron 1331
specimen #: C3Y-2
area: 0.0226
thickness: 0.0450
width: 0.5030

pretest notes
data acquisition = 300 msec, 22 bits
channel 1 = strain: 10%/v
channel 2 = load: 562 lbs/v
sampling rate = 0.5 sec
load rate = 0.2 in/min
first data point = zero load, second data point = zero strain

C3Y-2	test notes
yeild stress:	30,000
ult. stress:	46,999
break point:	inside gage area

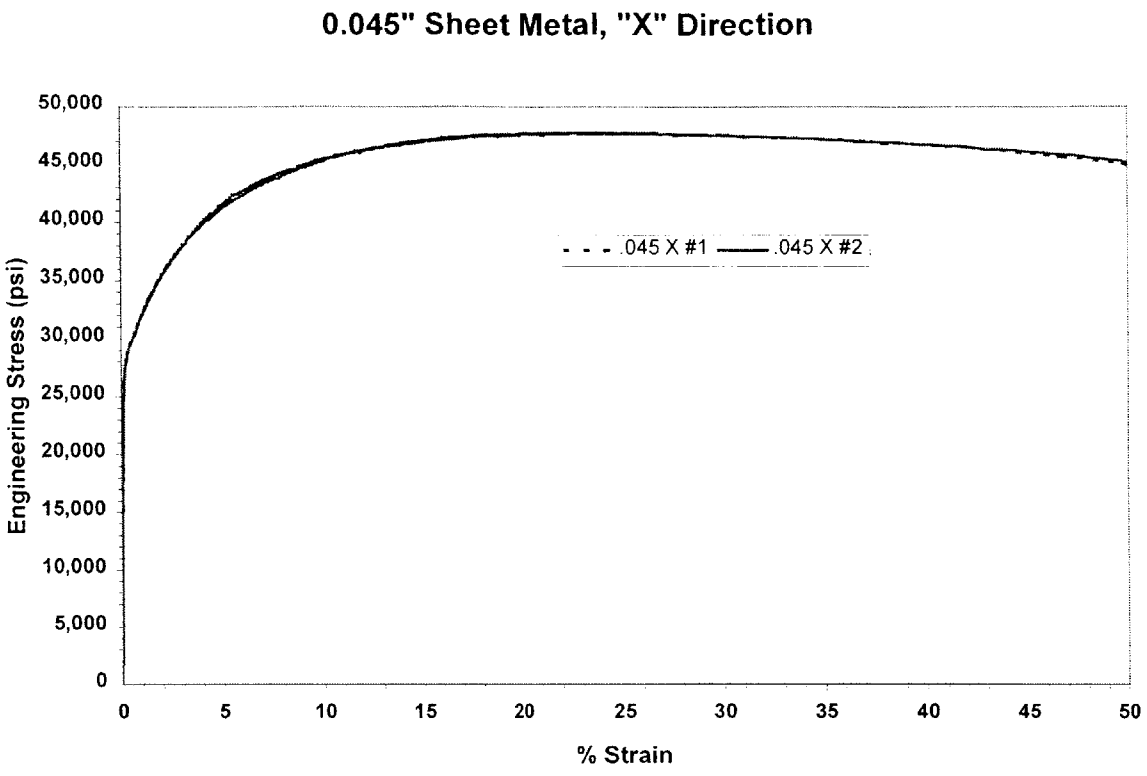

Figure E9: Engineering Stress vs. Strain Curve for .045" X Uniaxial Test

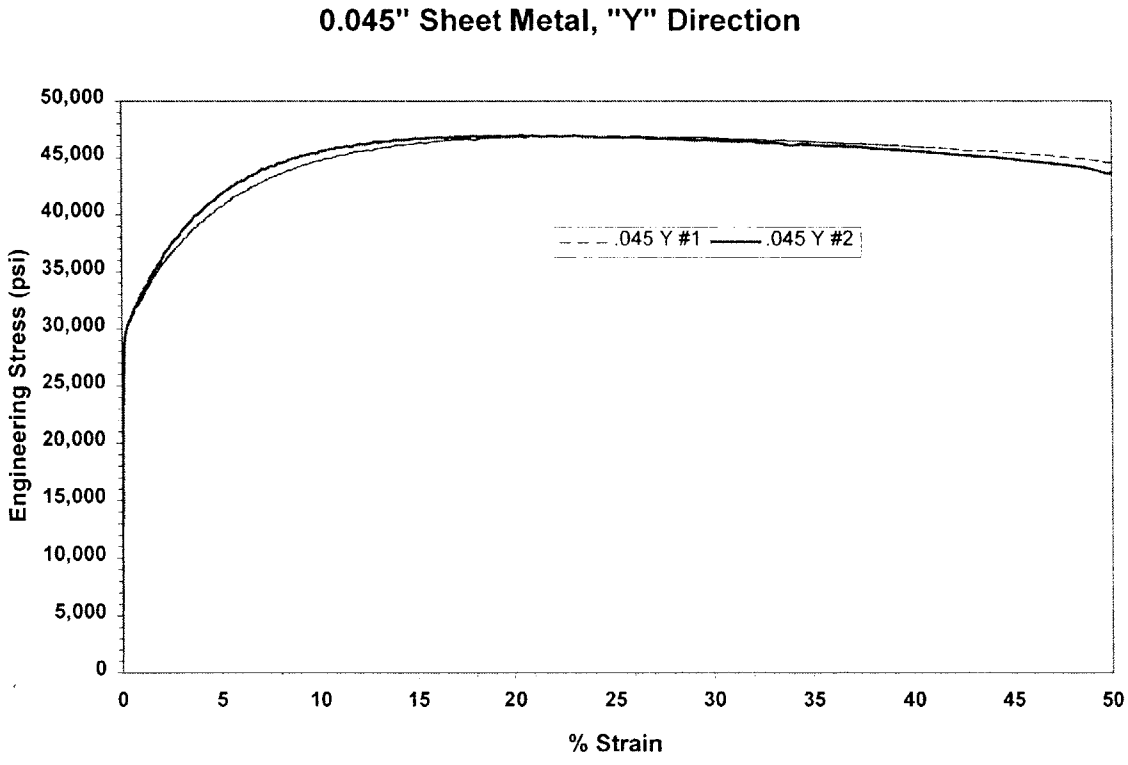

Figure E10: Engineering Stress vs. Strain Curve for .045" Y Uniaxial Test

Table E7: .055" Uniaxial Sample Test Data

.055" Thickness X Direction

file name: c4x-1.dat
description: 0.055" sheet metal, "X" direction
test date: 6/22/2002
test mach.; UTS
specimen #: C3X-1
area: 0.0278
thickness: 0.0550
width: 0.5050

pretest notes
data acquisition = 300 msec, 22 bits
channel 1 = strain: 10%/v
channel 2 = load: 562 lbs/v
sampling rate = 0.5 sec
load rate = 0.2 in/min
first data point = zero load, second data point = zero strain

C3X-1	test notes
yeild stress:	28,800
ult. stress:	48,202
break point:	inside gage area

file name: c4x-2.dat
description: 0.055" sheet metal, "X" direction
test date: 6/22/2002
test mach.; UTS
specimen #: C3X-2
area: 0.0278
thickness: 0.0550
width: 0.5050

pretest notes
data acquisition = 300 msec, 22 bits
channel 1 = strain: 10%/v
channel 2 = load: 562 lbs/v
sampling rate = 0.5 sec
load rate = 0.2 in/min
first data point = zero load, second data point = zero strain

C3X-2	test notes
yeild stress:	28,900
ult. stress:	48,321
break point:	inside gage area

.055" Thickness Y Direction

file name: C4Y-1.dat
description: 0.055" sheet metal, "Y" direction
test date: 6/22/2002
test mach.; UTS
specimen #: C4Y-1
area: 0.0277
thickness: 0.0550
width: 0.5040

pretest notes
data acquisition = 300 msec, 22 bits
channel 1 = strain: 10%/v
channel 2 = load: 562 lbs/v
sampling rate = 0.5 sec
load rate = 0.2 in/min
first data point = zero load, second data point = zero strain

C4Y-1	test notes
yeild stress:	30,100
ult. stress:	47,129
break point:	inside gage area

file name: C4Y-2.dat
description: 0.055" sheet metal, "Y" direction
test date: 6/22/2002
test mach.; UTS
specimen #: C4Y-2
area: 0.0277
thickness: 0.0550
width: 0.5040

pretest notes
data acquisition = 300 msec, 22 bits
channel 1 = strain: 10%/v
channel 2 = load: 562 lbs/v
sampling rate = 0.5 sec
load rate = 0.2 in/min
first data point = zero load, second data point = zero strain

C4Y-2	test notes
yeild stress:	30,215
ult. stress:	47,111
break point:	inside gage area

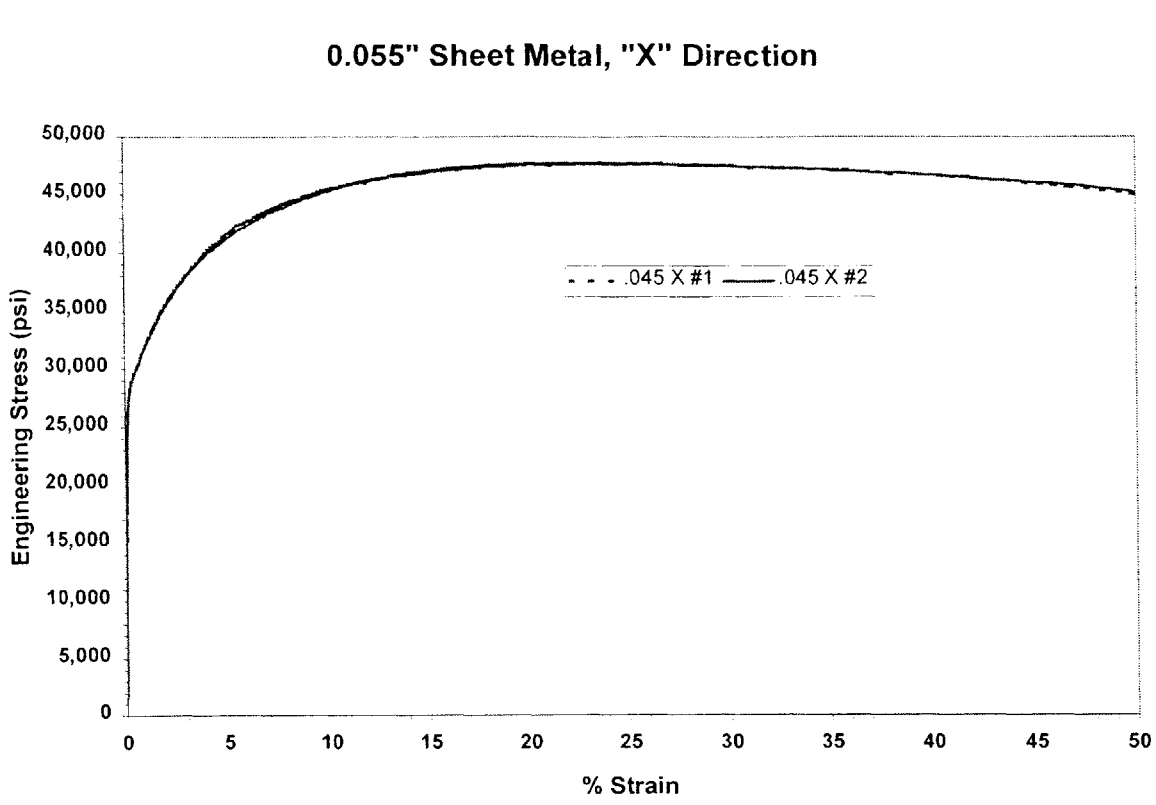

Figure E11: Engineering Stress vs. Strain Curve for .055" Uniaxial Test

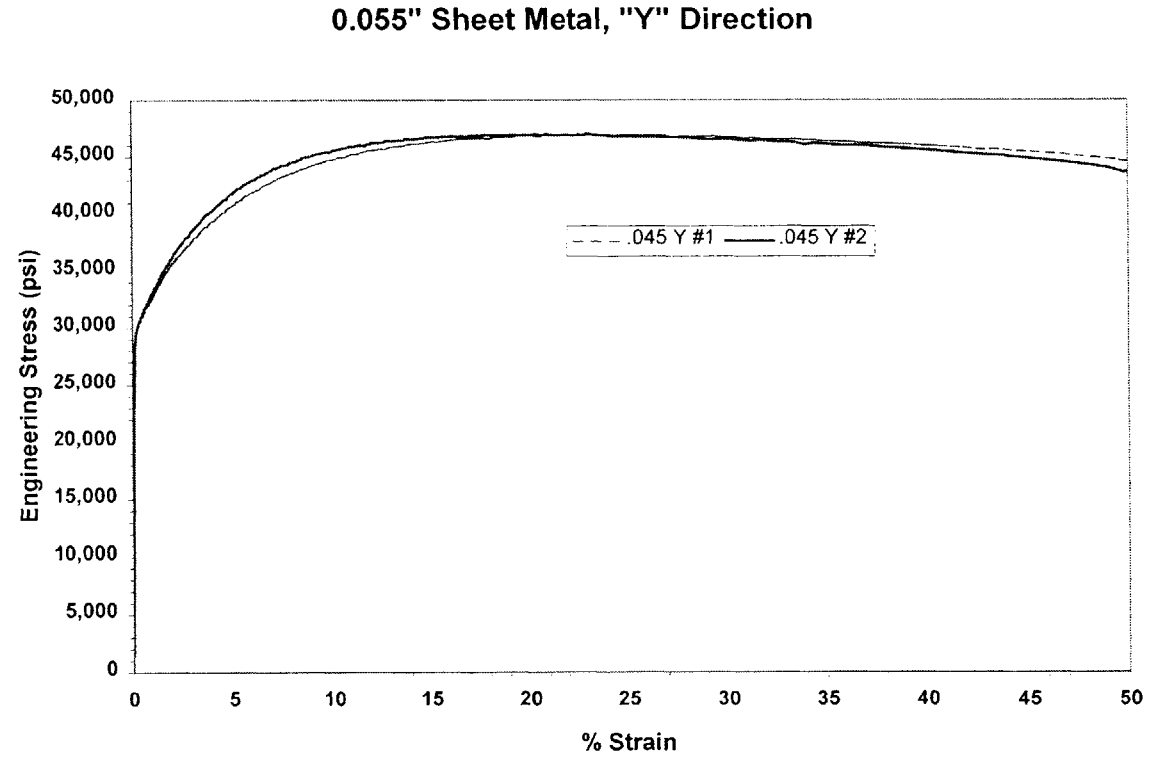

Figure E12: Engineering Stress vs. Strain Curve for .055" Uniaxial Test

Appendix F: Analytic Solution Worksheet

.035" Thickness using 20 mm Radius Punch

Entering Arguments for Analytic Solution

Work Hardening Exponent and Coefficient:

$n := .22$ $C_o := 460 \cdot 10^6 \cdot Pa$

Material Yield and Ultimate Strength $\sigma_y := 23300\,psi$ $\sigma_u := 46100\,psi$

Plate Thickness $t_o := .035 \cdot in$

Plate Clamped Radius $R := 110 \cdot mm$

Punch Radius $R_b \equiv 20 \cdot mm$

Compute Failure Parameters

$\psi_{c\_fail} := (.957 + .399 \cdot n) \cdot rad$ $\psi_{c\_fail} = 1.045$

$\delta_{fail} := 1.41 \cdot n^{.33} \cdot R^{.48} \cdot R_b^{.52}$ $\delta_{fail} = 38.781mm$

Compute Stresses

Flow Stress $\sigma_o := \frac{(\sigma_y + \sigma_u)}{2}$ $\sigma_o = 2.392 \times 10^8\,Pa$

Generalized Membrane Stress $N_o := 2 \cdot \sigma_o \cdot \frac{t_o}{\sqrt{3}}$ $N_o = 2.456 \times 10^5 \frac{N}{m}$

Plate Predictions at Failure

$R := 110$

$$P_{fail} := \left[2 \cdot \pi \cdot N_o \cdot R_b \left(\sin\left(\psi_{c\_fail} \right) \right)^2 \right] \qquad P_{fail} = 2.308 \times 10^4 \text{ N}$$

$$R_{c\_fail} := R_b \cdot \sin\left(\psi_{c\_fail} \right) \qquad Rcf := \frac{R_{c\_fail}}{mm}$$

$r_f := Rcf .. R$

$$w_{fail}(r_f) := \left[\frac{P_{fail} \cdot \ln\left[\frac{\left[r_f + \left[\sqrt{(r_f)^2 - \left(\sin\left(\psi_{c\_fail} \right) \right)^4} \right] \right]}{\left[R + \left[\sqrt{(R)^2 - \left(\sin\left(\psi_{c\_fail} \right) \right)^4} \right] \right]} \right]}{2 \cdot \pi \cdot N_o} \right] \Bigg/ mm$$

Establish Load Range in 5000 N Increments, Up to the Predicted Failure Load:

Load:

$i := 1 .. 7$

$$P := \begin{pmatrix} 0 \\ \frac{P_{fail}}{5 \cdot N} \\ \frac{P_{fail}}{4 \cdot N} \\ \frac{P_{fail}}{3 \cdot N} \\ \frac{P_{fail}}{2 \cdot N} \\ \frac{2 \cdot P_{fail}}{3 \cdot N} \\ \frac{P_{fail}}{N} \end{pmatrix} \cdot N$$

$P_0 := 0 \cdot N$

$$P_1 := \frac{P_{fail}}{5} \qquad P_1 = 4.616 \times 10^3 \text{ N}$$

$$P_2 := \frac{P_{fail}}{4} \qquad P_2 = 5.771 \times 10^3 \text{ N}$$

$$P_3 := \frac{P_{fail}}{3} \qquad P_3 = 7.694 \times 10^3 \text{ N}$$

$$P_4 := \frac{P_{fail}}{2} \qquad P_4 = 1.154 \times 10^4 \text{ N}$$

$$P_5 := \frac{2P_{fail}}{3} \qquad P_5 = 1.539 \times 10^4 \text{ N}$$

Wrapping Angle

$$\psi_i := \operatorname{asin}\left(\sqrt{\frac{P}{2\cdot\pi\cdot N_o\cdot R_b}}\right)$$

$$\psi_i = \begin{pmatrix} 0 \\ 22.753 \\ 25.62 \\ 29.954 \\ 37.699 \\ 44.92 \\ 59.861 \end{pmatrix} \text{deg}$$

$$\psi 0 := \operatorname{asin}\left(\sqrt{\frac{P_0}{2\cdot\pi\cdot N_o\cdot R_b}}\right) \qquad \psi 1 := \operatorname{asin}\left(\sqrt{\frac{P_1}{2\cdot\pi\cdot N_o\cdot R_b}}\right)$$

$$\psi 2 := \operatorname{asin}\left(\sqrt{\frac{P_2}{2\cdot\pi\cdot N_o\cdot R_b}}\right) \qquad \psi 3 := \operatorname{asin}\left(\sqrt{\frac{P_3}{2\cdot\pi\cdot N_o\cdot R_b}}\right)$$

$$\psi 4 := \operatorname{asin}\left(\sqrt{\frac{P_4}{2\cdot\pi\cdot N_o\cdot R_b}}\right) \qquad \psi 5 := \operatorname{asin}\left(\sqrt{\frac{P_5}{2\cdot\pi\cdot N_o\cdot R_b}}\right)$$

$$\psi 6 := \operatorname{asin}\left(\sqrt{\frac{P_{fail}}{2\cdot\pi\cdot N_o\cdot R_b}}\right)$$

Strain Components

$$\varepsilon_{rr} := \ln\left(\frac{1}{\cos(\psi_i)}\right) \qquad \varepsilon_{tt} := -\varepsilon_{rr}$$

$$\varepsilon_{rr} = \begin{pmatrix} 0 \\ 0.081 \\ 0.103 \\ 0.143 \\ 0.234 \\ 0.345 \\ 0.689 \end{pmatrix} \qquad \varepsilon_{tt} = \begin{pmatrix} 0 \\ -0.081 \\ -0.103 \\ -0.143 \\ -0.234 \\ -0.345 \\ -0.689 \end{pmatrix}$$

Deformed Plate Thickness $t := t_o \cdot \cos(\psi_i)$

True Material Stress:

$$\sigma_{rr} := C_o \cdot \left(-\ln\left(\cos(\psi_i)\right)\right)^n$$

$$\sigma_{rr} = \begin{pmatrix} 0 \\ 2.646 \times 10^8 \\ 2.793 \times 10^8 \\ 3 \times 10^8 \\ 3.342 \times 10^8 \\ 3.64 \times 10^8 \\ 4.238 \times 10^8 \end{pmatrix} \text{Pa}$$

Strain Components

$$\varepsilon_{rr} := \ln\left(\frac{1}{\cos(\psi_i)}\right) \qquad \varepsilon_{tt} := -\varepsilon_{rr}$$

$$\varepsilon_{rr} = \begin{pmatrix} 0 \\ 0.081 \\ 0.103 \\ 0.143 \\ 0.234 \\ 0.345 \\ 0.689 \end{pmatrix} \qquad \varepsilon_{tt} = \begin{pmatrix} 0 \\ -0.081 \\ -0.103 \\ -0.143 \\ -0.234 \\ -0.345 \\ -0.689 \end{pmatrix}$$

Deformed Plate Thickness $t := t_o \cdot \cos(\psi_i)$

True Material Stress:

$$\sigma_{rr} := C_o \cdot \left(-\ln\left(\cos(\psi_i)\right)\right)^n$$

$$\sigma_{rr} = \begin{pmatrix} 0 \\ 2.646 \times 10^8 \\ 2.793 \times 10^8 \\ 3 \times 10^8 \\ 3.342 \times 10^8 \\ 3.64 \times 10^8 \\ 4.238 \times 10^8 \end{pmatrix} \text{Pa}$$

Solve for Shape of plate, valid for $R_c < r < R$

$R := 110$

$$P = \begin{pmatrix} 0 \\ 4.616 \\ 5.771 \\ 7.694 \\ 11.541 \\ 15.388 \\ 23.082 \end{pmatrix} N \cdot 10^3 \qquad \psi_i = \begin{pmatrix} 0 \\ 0.397 \\ 0.447 \\ 0.523 \\ 0.658 \\ 0.784 \\ 1.045 \end{pmatrix} \qquad \psi_i = \begin{pmatrix} 0 \\ 22.753 \\ 25.62 \\ 29.954 \\ 37.699 \\ 44.92 \\ 59.861 \end{pmatrix} deg$$

$$Rc0 := R_b \cdot \frac{\sin(\psi 0)}{mm} \qquad Rc0 = 0$$

$$Rc1 := R_b \cdot \frac{\sin(\psi 1)}{mm} \qquad Rc1 = 7.735$$

$$Rc2 := R_b \cdot \frac{\sin(\psi 2)}{mm} \qquad Rc2 = 8.648$$

$$Rc3 := R_b \cdot \frac{\sin(\psi 3)}{mm} \qquad Rc3 = 9.986$$

$$Rc4 := R_b \cdot \frac{\sin(\psi 4)}{mm} \qquad Rc4 = 12.23$$

$$Rc5 := R_b \cdot \frac{\sin(\psi 5)}{mm} \qquad Rc5 = 14.122$$

Computation of Plate Shape at Several Loads

$P_1 = 4.616 \times 10^3$ N

$r := Rc1 .. 110$

$$w1(r) := \frac{\left[P_1 \cdot \ln\left[\frac{\left[r + \left[\sqrt{(r)^2 - (\sin(\psi 1))^4} \right] \right]}{\left[R + \left[\sqrt{(R)^2 - (\sin(\psi 1))^4} \right] \right]} \right] \right]}{2 \cdot \pi \cdot N_o} \cdot mm$$

$P_2 = 5.771 \times 10^3$ N

$r2 := Rc2 .. 110$

$$w2(r2) := \frac{\left[P_2 \cdot \ln\left[\frac{\left[r2 + \left[\sqrt{(r2)^2 - (\sin(\psi 2))^4} \right] \right]}{\left[R + \left[\sqrt{(R)^2 - (\sin(\psi 2))^4} \right] \right]} \right] \right]}{2 \cdot \pi \cdot N_o} \cdot mm$$

$P_3 = 7.694 \times 10^3$ N

$r3 := Rc3 .. 110$

$$w3(r3) := \frac{\left[P_3 \cdot \ln\left[\frac{\left[r3 + \left[\sqrt{(r3)^2 - (\sin(\psi 3))^4} \right] \right]}{\left[R + \left[\sqrt{(R)^2 - (\sin(\psi 3))^4} \right] \right]} \right] \right]}{2 \cdot \pi \cdot N_o} \cdot mm$$

$P_4 = 1.154 \times 10^4$ N

$r4 := Rc4 .. 110$

$$w4(r4) := \frac{\left[P_4 \cdot \ln\left[\frac{\left[r4 + \left[\sqrt{(r4)^2 - (\sin(\psi 4))^4} \right] \right]}{\left[R + \left[\sqrt{(R)^2 - (\sin(\psi 4))^4} \right] \right]} \right] \right]}{2 \cdot \pi \cdot N_o} \cdot mm$$

$P_5 = 1.539 \times 10^4$ N

$r5 := Rc5 .. 110$

$$w5(r5) := \frac{\left[P_5 \cdot \ln\left[\frac{\left[r5 + \left[\sqrt{(r5)^2 - (\sin(\psi 5))^4} \right] \right]}{\left[R + \left[\sqrt{(R)^2 - (\sin(\psi 5))^4} \right] \right]} \right] \right]}{2 \cdot \pi \cdot N_o} \cdot mm$$

Plot of Analytic Solution for Plate Shape Up to Failure (Valid for r > R_c):

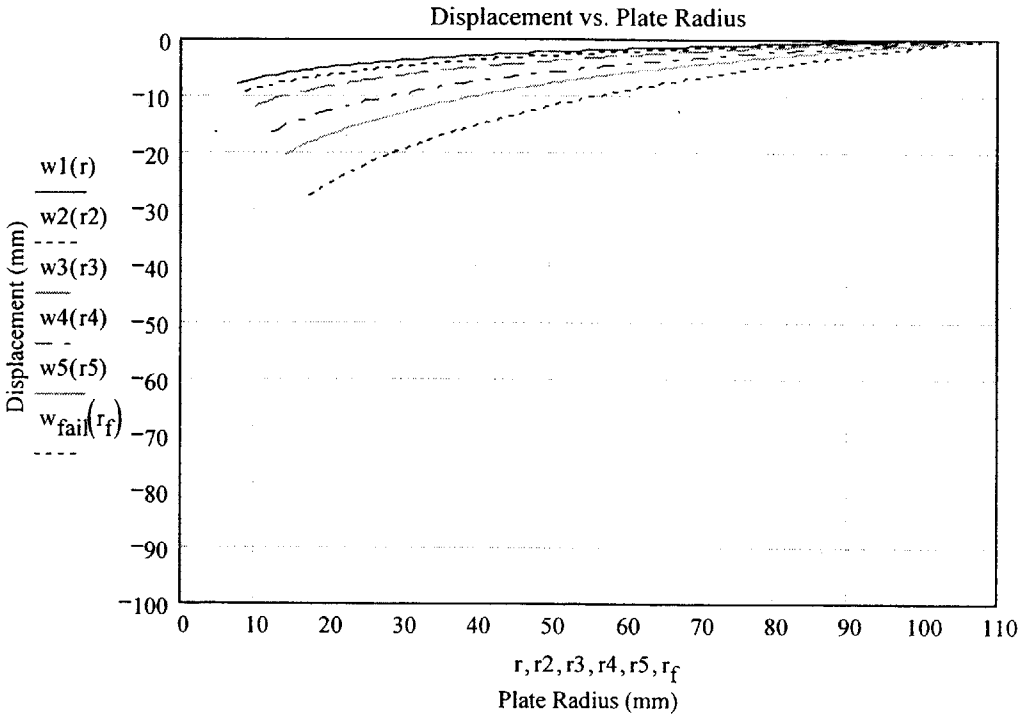

PUNCH SIZE: $R_b = 20\text{mm}$

$$P = \begin{pmatrix} 0 \\ 4.616 \\ 5.771 \\ 7.694 \\ 11.541 \\ 15.388 \\ 23.082 \end{pmatrix} \text{N} \cdot 10^3 \qquad R_c = \begin{pmatrix} 0 \\ 7.735 \\ 8.648 \\ 9.986 \\ 12.23 \\ 14.122 \\ 17.296 \end{pmatrix} \text{mm}$$

$P_{fail} = 2.308 \times 10^4\ \text{N}$ $\qquad R_{c\_fail} = 17.296\text{mm}$

Plot the Force vs. Displacement Relation:

Displacement at Point C:

$$\delta_i := \begin{pmatrix} 0 \\ w1(Rc1) \\ w2(Rc2) \\ w3(Rc3) \\ w4(Rc4) \\ w5(Rc5) \\ w_{fail}(Rcf) \end{pmatrix}$$

$$\delta_{plot} := R_b \cdot \frac{\left(1 - \cos\left(\psi_i\right)\right)}{mm} - \delta_i$$

Total Punch Displacement:

$$\delta_{plot} = \begin{pmatrix} 0 \\ 9.499 \\ 11.477 \\ 14.635 \\ 20.605 \\ 26.311 \\ 37.637 \end{pmatrix}$$

$$\delta_{max} := \text{trunc}\left[R_b \cdot \frac{\left(1 - \cos\left(\psi 6\right)\right)}{mm} - w_{fail}(Rcf)\right]$$

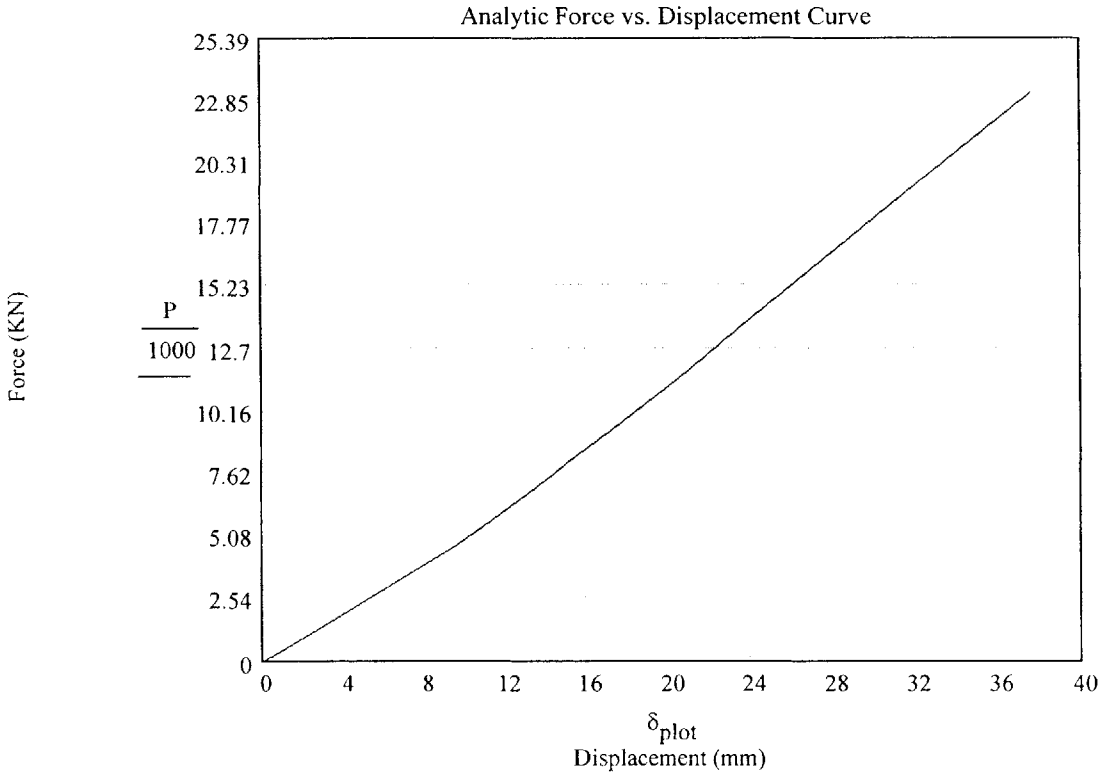

Analytic Solution for P vs Displacement During Conical Punching Before Fracture

$\theta := 30 \cdot deg$

$$P_{cone}(\delta_{cone}) := \pi \cdot C_o \cdot \delta_{cone} \cdot t_o \cdot \frac{\tan(\theta)^{2 \cdot n}}{2^n}$$

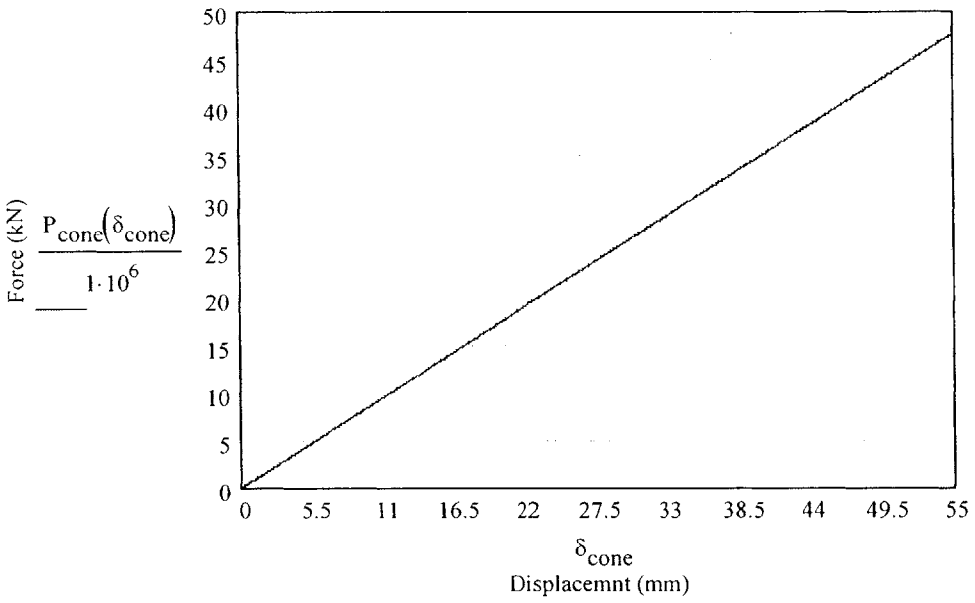

.045" Thickness using 50 mm Radius Punch

Entering Arguments for Analytic Solution

Work Hardening Exponent and Coefficient:

$n := .22$ $C_o := 460 \cdot 10^6 \cdot Pa$

Material Yield and Ultimate Strength $\sigma_y := 28600\,psi$ $\sigma_u := 47600\,psi$

Plate Thickness $t_o := .045 \cdot in$

Plate Clamped Radius $R := 110 \cdot mm$

Punch Radius $R_b \equiv 50 \cdot mm$

Compute Failure Parameters

$\psi_{c\_fail} := (.957 + .399 \cdot n) \cdot rad$ $\psi_{c\_fail} = 1.045$

$\delta_{fail} := 1.41 \cdot n^{.33} \cdot R^{.48} \cdot R_b^{.52}$ $\delta_{fail} = 62.453mm$

Compute Stresses

Flow Stress $\sigma_o := \frac{(\sigma_y + \sigma_u)}{2}$ $\sigma_o = 2.627 \times 10^8\,Pa$

Generalized Membrane Stress $N_o := 2 \cdot \sigma_o \cdot \frac{t_o}{\sqrt{3}}$ $N_o = 3.467 \times 10^5\,\frac{N}{m}$

Plate Predictions at Failure

$R := 110$

$$P_{fail} := \left[2 \cdot \pi \cdot N_o \cdot R_b \left(\sin\left(\psi_{c\_fail} \right) \right)^2 \right] \qquad P_{fail} = 8.146 \times 10^4 \text{ N}$$

$$R_{c\_fail} := R_b \cdot \sin\left(\psi_{c\_fail} \right) \qquad Rcf := \frac{R_{c\_fail}}{mm}$$

$r_f := Rcf .. R$

$$w_{fail}(r_f) := \frac{\left[P_{fail} \cdot \ln\left[\frac{\left[r_f + \left[\sqrt{(r_f)^2 - \left(\sin\left(\psi_{c\_fail} \right) \right)^4} \right] \right]}{\left[R + \left[\sqrt{(R)^2 - \left(\sin\left(\psi_{c\_fail} \right) \right)^4} \right] \right]} \right] \right]}{2 \cdot \pi \cdot N_o}}{mm}$$

Establish Load Range in 5000 N Increments, Up to the Predicted Failure Load:

Load:

$i := 1 .. 7$

$$P := \begin{pmatrix} 0 \\ \frac{P_{fail}}{5 \cdot N} \\ \frac{P_{fail}}{4 \cdot N} \\ \frac{P_{fail}}{3 \cdot N} \\ \frac{P_{fail}}{2 \cdot N} \\ \frac{2 \cdot P_{fail}}{3 \cdot N} \\ \frac{P_{fail}}{N} \end{pmatrix} \cdot N$$

$P_0 := 0 \cdot N$

$P_1 := \frac{P_{fail}}{5}$ $\qquad P_1 = 1.629 \times 10^4 \text{ N}$

$P_2 := \frac{P_{fail}}{4}$ $\qquad P_2 = 2.037 \times 10^4 \text{ N}$

$P_3 := \frac{P_{fail}}{3}$ $\qquad P_3 = 2.715 \times 10^4 \text{ N}$

$P_4 := \frac{P_{fail}}{2}$ $\qquad P_4 = 4.073 \times 10^4 \text{ N}$

$P_5 := \frac{2P_{fail}}{3}$ $\qquad P_5 = 5.431 \times 10^4 \text{ N}$

Wrapping Angle

$$\psi_i := \operatorname{asin}\left(\sqrt{\frac{P}{2\cdot\pi\cdot N_o\cdot R_b}}\right)$$

$$\psi_i = \begin{pmatrix} 0 \\ 22.753 \\ 25.62 \\ 29.954 \\ 37.699 \\ 44.92 \\ 59.861 \end{pmatrix} \text{deg}$$

$$\psi 0 := \operatorname{asin}\left(\sqrt{\frac{P_0}{2\cdot\pi\cdot N_o\cdot R_b}}\right) \qquad \psi 1 := \operatorname{asin}\left(\sqrt{\frac{P_1}{2\cdot\pi\cdot N_o\cdot R_b}}\right)$$

$$\psi 2 := \operatorname{asin}\left(\sqrt{\frac{P_2}{2\cdot\pi\cdot N_o\cdot R_b}}\right) \qquad \psi 3 := \operatorname{asin}\left(\sqrt{\frac{P_3}{2\cdot\pi\cdot N_o\cdot R_b}}\right)$$

$$\psi 4 := \operatorname{asin}\left(\sqrt{\frac{P_4}{2\cdot\pi\cdot N_o\cdot R_b}}\right) \qquad \psi 5 := \operatorname{asin}\left(\sqrt{\frac{P_5}{2\cdot\pi\cdot N_o\cdot R_b}}\right)$$

$$\psi 6 := \operatorname{asin}\left(\sqrt{\frac{P_{fail}}{2\cdot\pi\cdot N_o\cdot R_b}}\right)$$

Strain Components

$$\varepsilon_{rr} := \ln\left(\frac{1}{\cos(\psi_i)}\right) \qquad \varepsilon_{tt} := -\varepsilon_{rr}$$

$$\varepsilon_{rr} = \begin{pmatrix} 0 \\ 0.081 \\ 0.103 \\ 0.143 \\ 0.234 \\ 0.345 \\ 0.689 \end{pmatrix} \qquad \varepsilon_{tt} = \begin{pmatrix} 0 \\ -0.081 \\ -0.103 \\ -0.143 \\ -0.234 \\ -0.345 \\ -0.689 \end{pmatrix}$$

Deformed Plate Thickness $t := t_o \cdot \cos(\psi_i)$

True Material Stress:

$$\sigma_{rr} := C_o \cdot \left(-\ln\left(\cos(\psi_i)\right)\right)^n$$

$$\sigma_{rr} = \begin{pmatrix} 0 \\ 2.646 \times 10^8 \\ 2.793 \times 10^8 \\ 3 \times 10^8 \\ 3.342 \times 10^8 \\ 3.64 \times 10^8 \\ 4.238 \times 10^8 \end{pmatrix} \text{Pa}$$

To Find the Maximum Punch Displacement:

$R := 110 \cdot mm$

Find the Amplitude:

$$a := \ln\left[\frac{\left[\left[\left[\frac{R}{R_b} + \left[\sqrt{\left(\frac{R}{R_b}\right)^2 - \left(\sin(\psi_i)\right)^4}\right]\right]\right]\right]}{\sin(\psi_i)\cdot\left(1 + \cos(\psi_i)\right)}\right]$$

Solve for Maximum Displacement using Geometric Relations

$$\delta_{max} := -R_b\cdot\left[1 - \cos(\psi_i) + a\cdot\left(\sin(\psi_i)\right)^2\right]$$

Find Radius of Contact Wrapping Point C:

$$R_c := R_b\cdot\sin(\psi_i) \qquad R_c = \begin{pmatrix} 0 \\ 19.338 \\ 21.62 \\ 24.965 \\ 30.576 \\ 35.306 \\ 43.241 \end{pmatrix} mm$$

Solve for Shape of plate, valid for $R_c < r < R$

$R := 110$

$$P = \begin{pmatrix} 0 \\ 16.292 \\ 20.365 \\ 27.154 \\ 40.731 \\ 54.308 \\ 81.462 \end{pmatrix} N \cdot 10^3 \qquad \psi_i = \begin{pmatrix} 0 \\ 0.397 \\ 0.447 \\ 0.523 \\ 0.658 \\ 0.784 \\ 1.045 \end{pmatrix} \qquad \psi_i = \begin{pmatrix} 0 \\ 22.753 \\ 25.62 \\ 29.954 \\ 37.699 \\ 44.92 \\ 59.861 \end{pmatrix} deg$$

$Rc0 := R_b \cdot \frac{\sin(\psi 0)}{mm}$ $\quad Rc0 = 0$

$Rc1 := R_b \cdot \frac{\sin(\psi 1)}{mm}$ $\quad Rc1 = 19.338$

$Rc2 := R_b \cdot \frac{\sin(\psi 2)}{mm}$ $\quad Rc2 = 21.62$

$Rc3 := R_b \cdot \frac{\sin(\psi 3)}{mm}$ $\quad Rc3 = 24.965$

$Rc4 := R_b \cdot \frac{\sin(\psi 4)}{mm}$ $\quad Rc4 = 30.576$

$Rc5 := R_b \cdot \frac{\sin(\psi 5)}{mm}$ $\quad Rc5 = 35.306$

Computation of Plate Shape at Several Loads

$P_1 = 1.629\times 10^4\ N$

$r := Rc1..110$

$$w1(r) := \frac{\left[P_1\cdot\ln\left[\frac{\left[r+\left[\sqrt{(r)^2-(\sin(\psi 1))^4}\right]\right]}{\left[R+\left[\sqrt{(R)^2-(\sin(\psi 1))^4}\right]\right]}\right]\right]}{2\cdot\pi\cdot N_o}\cdot mm$$

$P_2 = 2.037\times 10^4\ N$

$r2 := Rc2..110$

$$w2(r2) := \frac{\left[P_2\cdot\ln\left[\frac{\left[r2+\left[\sqrt{(r2)^2-(\sin(\psi 2))^4}\right]\right]}{\left[R+\left[\sqrt{(R)^2-(\sin(\psi 2))^4}\right]\right]}\right]\right]}{2\cdot\pi\cdot N_o}\cdot mm$$

$P_3 = 2.715\times 10^4\ N$

$r3 := Rc3..110$

$$w3(r3) := \frac{\left[P_3\cdot\ln\left[\frac{\left[r3+\left[\sqrt{(r3)^2-(\sin(\psi 3))^4}\right]\right]}{\left[R+\left[\sqrt{(R)^2-(\sin(\psi 3))^4}\right]\right]}\right]\right]}{2\cdot\pi\cdot N_o}\cdot mm$$

$P_4 = 4.073\times 10^4\ N$

$r4 := Rc4..110$

$$w4(r4) := \frac{\left[P_4\cdot\ln\left[\frac{\left[r4+\left[\sqrt{(r4)^2-(\sin(\psi 4))^4}\right]\right]}{\left[R+\left[\sqrt{(R)^2-(\sin(\psi 4))^4}\right]\right]}\right]\right]}{2\cdot\pi\cdot N_o}\cdot mm$$

$P_5 = 5.431\times 10^4\ N$

$r5 := Rc5..110$

$$w5(r5) := \frac{\left[P_5\cdot\ln\left[\frac{\left[r5+\left[\sqrt{(r5)^2-(\sin(\psi 5))^4}\right]\right]}{\left[R+\left[\sqrt{(R)^2-(\sin(\psi 5))^4}\right]\right]}\right]\right]}{2\cdot\pi\cdot N_o}\cdot mm$$

Plot of Analytic Solution for Plate Shape Up to Failure (Valid for r > R_c):

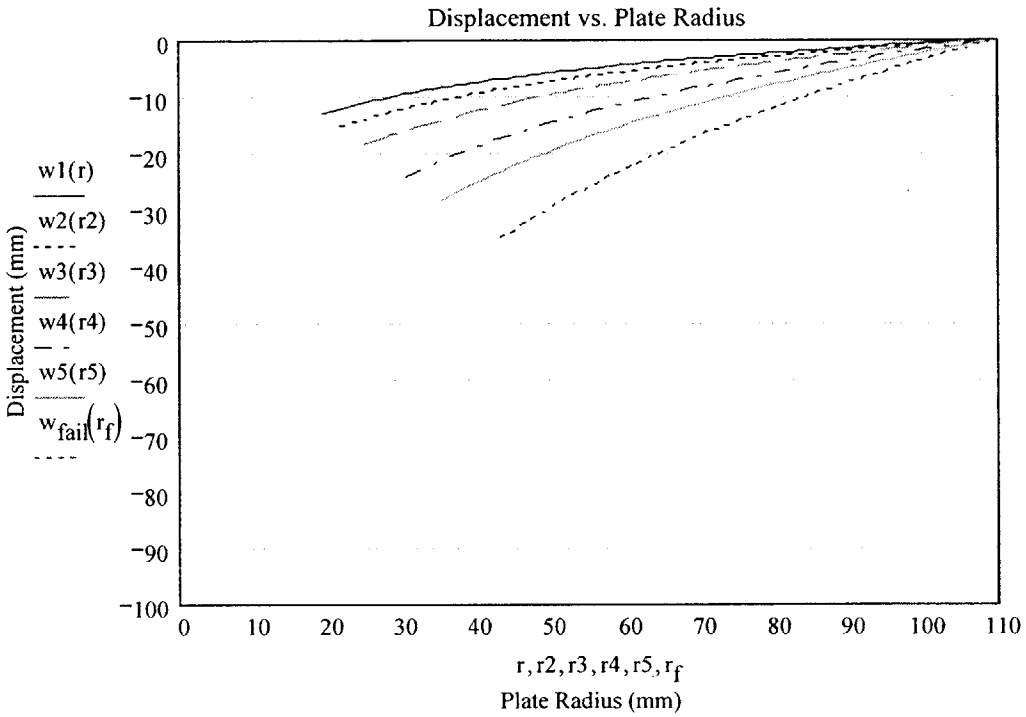

PUNCH SIZE: $R_b = 50\text{mm}$

$$P = \begin{pmatrix} 0 \\ 16.292 \\ 20.365 \\ 27.154 \\ 40.731 \\ 54.308 \\ 81.462 \end{pmatrix} \text{N} \cdot 10^3 \qquad R_c = \begin{pmatrix} 0 \\ 19.338 \\ 21.62 \\ 24.965 \\ 30.576 \\ 35.306 \\ 43.241 \end{pmatrix} \text{mm}$$

$P_{fail} = 8.146 \times 10^4\ \text{N}$ $\qquad R_{c\_fail} = 43.241\text{mm}$

Plot the Force vs. Displacement Relation:

Displacement at Point C:

$$\delta_i := \begin{pmatrix} 0 \\ w1(Rc1) \\ w2(Rc2) \\ w3(Rc3) \\ w4(Rc4) \\ w5(Rc5) \\ w_{fail}(Rcf) \end{pmatrix}$$

$$\delta_{plot} := R_b \cdot \frac{\left(1 - \cos\left(\psi_i\right)\right)}{mm} - \delta_i$$

Total Punch Displacement:

$$\delta_{plot} = \begin{pmatrix} 0 \\ 16.893 \\ 20.125 \\ 25.165 \\ 34.377 \\ 42.928 \\ 59.814 \end{pmatrix}$$

$$\delta_{max} := \text{trunc}\left[R_b \cdot \frac{\left(1 - \cos\left(\psi 6\right)\right)}{mm} - w_{fail}(Rcf)\right]$$

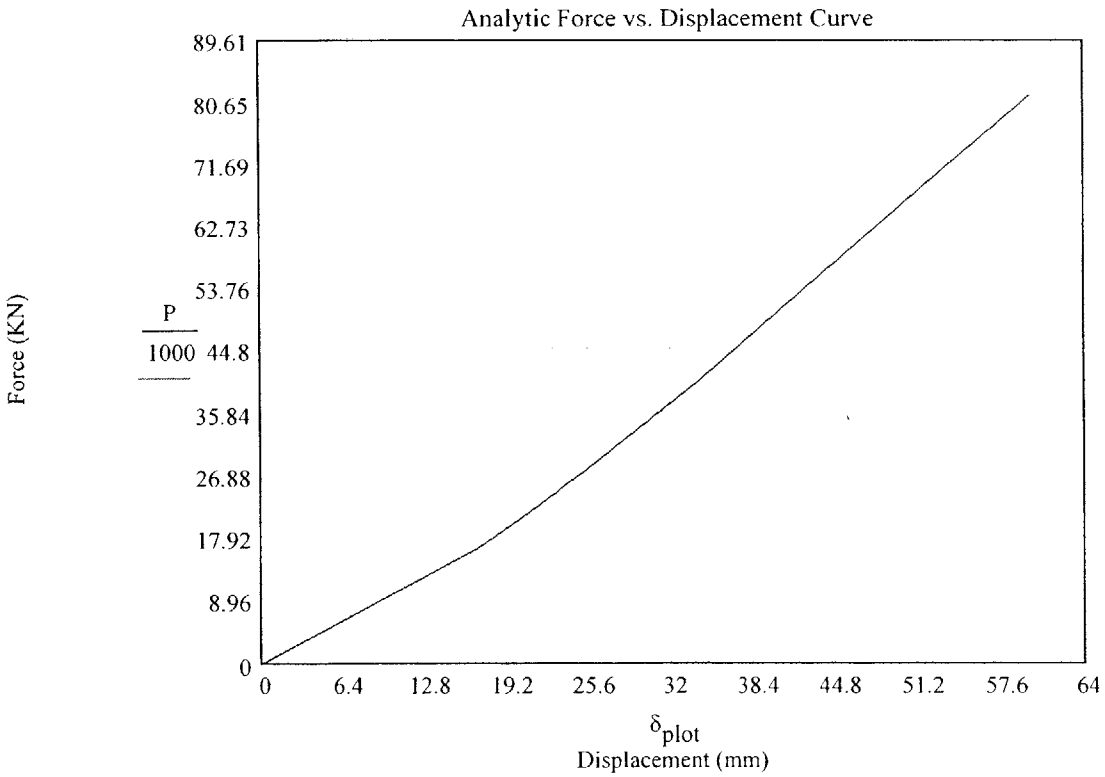

Analytic Solution for P vs Displacement During Conical Punching Before Fracture

$\theta := 30 \cdot deg$

$$P_{cone}(\delta_{cone}) := \pi \cdot C_o \cdot \delta_{cone} \cdot t_o \cdot \frac{\tan(\theta)^{2 \cdot n}}{2^n}$$

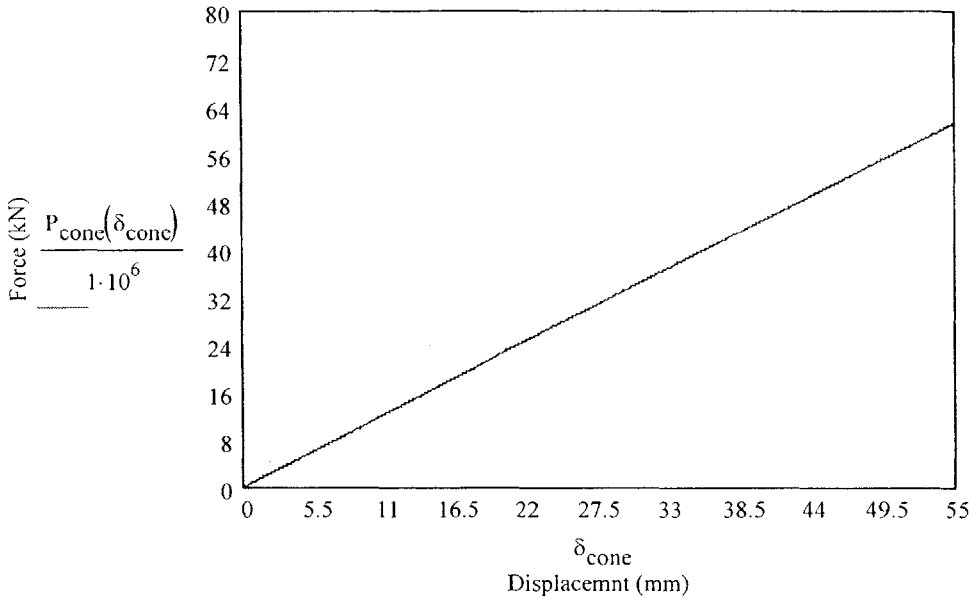

.055" Thickness using 75 mm Radius Punch

Entering Arguments for Analytic Solution

Work Hardening Exponent and Coefficient:

$n := .22$ $C_o := 460 \cdot 10^6 \cdot Pa$

Material Yield and Ultimate Strength $\sigma_y := 28600\,psi$ $\sigma_u := 47600\,psi$

Plate Thickness $t_o := .055 \cdot in$

Plate Clamped Radius $R := 110 \cdot mm$

Punch Radius $R_b \equiv 75 \cdot mm$

Compute Failure Parameters

$\psi_{c\_fail} := (.957 + .399 \cdot n) \cdot rad$ $\psi_{c\_fail} = 1.045$

$\delta_{fail} := 1.41 \cdot n^{.33} \cdot R^{.48} \cdot R_b^{.52}$ $\delta_{fail} = 77.111mm$

Compute Stresses

Flow Stress $\sigma_o := \frac{(\sigma_y + \sigma_u)}{2}$ $\sigma_o = 2.627 \times 10^8\,Pa$

Generalized Membrane Stress $N_o := 2 \cdot \sigma_o \cdot \frac{t_o}{\sqrt{3}}$ $N_o = 4.238 \times 10^5 \frac{N}{m}$

Plate Predictions at Failure

$R := 110$

$$P_{fail} := \left[2 \cdot \pi \cdot N_o \cdot R_b \left(\sin\left(\psi_{c\_fail} \right) \right)^2 \right] \qquad P_{fail} = 1.493 \times 10^5 \text{ N}$$

$$R_{c\_fail} := R_b \cdot \sin\left(\psi_{c\_fail} \right) \qquad Rcf := \frac{R_{c\_fail}}{mm}$$

$r_f := Rcf .. R$

$$w_{fail}(r_f) := \frac{\left[P_{fail} \cdot \ln\left[\frac{\left[r_f + \left[\sqrt{(r_f)^2 - \left(\sin\left(\psi_{c\_fail} \right) \right)^4} \right] \right]}{\left[R + \left[\sqrt{(R)^2 - \left(\sin\left(\psi_{c\_fail} \right) \right)^4} \right] \right]} \right] \right]}{2 \cdot \pi \cdot N_o} \Bigg]}{mm}$$

Establish Load Range in 5000 N Increments, Up to the Predicted Failure Load:

Load:

$i := 1 .. 7$

$$P := \begin{pmatrix} 0 \\ \frac{P_{fail}}{5 \cdot N} \\ \frac{P_{fail}}{4 \cdot N} \\ \frac{P_{fail}}{3 \cdot N} \\ \frac{P_{fail}}{2 \cdot N} \\ \frac{2 \cdot P_{fail}}{3 \cdot N} \\ \frac{P_{fail}}{N} \end{pmatrix} \cdot N$$

$P_0 := 0 \cdot N$

$$P_1 := \frac{P_{fail}}{5} \qquad P_1 = 2.987 \times 10^4 \text{ N}$$

$$P_2 := \frac{P_{fail}}{4} \qquad P_2 = 3.734 \times 10^4 \text{ N}$$

$$P_3 := \frac{P_{fail}}{3} \qquad P_3 = 4.978 \times 10^4 \text{ N}$$

$$P_4 := \frac{P_{fail}}{2} \qquad P_4 = 7.467 \times 10^4 \text{ N}$$

$$P_5 := \frac{2P_{fail}}{3} \qquad P_5 = 9.956 \times 10^4 \text{ N}$$

Wrapping Angle

$$\psi_i := \operatorname{asin}\left(\sqrt{\frac{P}{2\cdot\pi\cdot N_o\cdot R_b}}\right)$$

$$\psi_i = \begin{pmatrix} 0 \\ 22.753 \\ 25.62 \\ 29.954 \\ 37.699 \\ 44.92 \\ 59.861 \end{pmatrix} \text{deg}$$

$$\psi 0 := \operatorname{asin}\left(\sqrt{\frac{P_0}{2\cdot\pi\cdot N_o\cdot R_b}}\right) \qquad \psi 1 := \operatorname{asin}\left(\sqrt{\frac{P_1}{2\cdot\pi\cdot N_o\cdot R_b}}\right)$$

$$\psi 2 := \operatorname{asin}\left(\sqrt{\frac{P_2}{2\cdot\pi\cdot N_o\cdot R_b}}\right) \qquad \psi 3 := \operatorname{asin}\left(\sqrt{\frac{P_3}{2\cdot\pi\cdot N_o\cdot R_b}}\right)$$

$$\psi 4 := \operatorname{asin}\left(\sqrt{\frac{P_4}{2\cdot\pi\cdot N_o\cdot R_b}}\right) \qquad \psi 5 := \operatorname{asin}\left(\sqrt{\frac{P_5}{2\cdot\pi\cdot N_o\cdot R_b}}\right)$$

$$\psi 6 := \operatorname{asin}\left(\sqrt{\frac{P_{fail}}{2\cdot\pi\cdot N_o\cdot R_b}}\right)$$

Strain Components

$$\varepsilon_{rr} := \ln\left(\frac{1}{\cos(\psi_i)}\right) \qquad \varepsilon_{tt} := -\varepsilon_{rr}$$

$$\varepsilon_{rr} = \begin{pmatrix} 0 \\ 0.081 \\ 0.103 \\ 0.143 \\ 0.234 \\ 0.345 \\ 0.689 \end{pmatrix} \qquad \varepsilon_{tt} = \begin{pmatrix} 0 \\ -0.081 \\ -0.103 \\ -0.143 \\ -0.234 \\ -0.345 \\ -0.689 \end{pmatrix}$$

Deformed Plate Thickness $t := t_o \cdot \cos(\psi_i)$

True Material Stress:

$$\sigma_{rr} := C_o \cdot \left(-\ln\left(\cos(\psi_i)\right)\right)^n$$

$$\sigma_{rr} = \begin{pmatrix} 0 \\ 2.646 \times 10^8 \\ 2.793 \times 10^8 \\ 3 \times 10^8 \\ 3.342 \times 10^8 \\ 3.64 \times 10^8 \\ 4.238 \times 10^8 \end{pmatrix} \text{Pa}$$

To Find the Maximum Punch Displacement:

$R := 110 \cdot mm$

Find the Amplitude:

$$a := \ln\left[\frac{\left[\left[\frac{R}{R_b} + \left[\sqrt{\left(\frac{R}{R_b}\right)^2 - \left(\sin(\psi_i)\right)^4}\right]\right]\right]}{\sin(\psi_i)\cdot\left(1 + \cos(\psi_i)\right)}\right]$$

Solve for Maximum Displacement using Geometric Relations

$$\delta_{max} := -R_b\cdot\left[1 - \cos(\psi_i) + a\cdot\left(\sin(\psi_i)\right)^2\right]$$

Find Radius of Contact Wrapping Point C:

$$R_c := R_b\cdot\sin(\psi_i) \qquad R_c = \begin{pmatrix} 0 \\ 29.007 \\ 32.431 \\ 37.448 \\ 45.864 \\ 52.959 \\ 64.861 \end{pmatrix} mm$$

Solve for Shape of plate, valid for $R_c < r < R$

$R := 110$

$$P = \begin{pmatrix} 0 \\ 29.869 \\ 37.337 \\ 49.782 \\ 74.673 \\ 99.565 \\ 149.347 \end{pmatrix} N \cdot 10^3 \qquad \psi_i = \begin{pmatrix} 0 \\ 0.397 \\ 0.447 \\ 0.523 \\ 0.658 \\ 0.784 \\ 1.045 \end{pmatrix} \qquad \psi_i = \begin{pmatrix} 0 \\ 22.753 \\ 25.62 \\ 29.954 \\ 37.699 \\ 44.92 \\ 59.861 \end{pmatrix} deg$$

$Rc0 := R_b \cdot \frac{\sin(\psi 0)}{mm}$ $\quad Rc0 = 0$

$Rc1 := R_b \cdot \frac{\sin(\psi 1)}{mm}$ $\quad Rc1 = 29.007$

$Rc2 := R_b \cdot \frac{\sin(\psi 2)}{mm}$ $\quad Rc2 = 32.431$

$Rc3 := R_b \cdot \frac{\sin(\psi 3)}{mm}$ $\quad Rc3 = 37.448$

$Rc4 := R_b \cdot \frac{\sin(\psi 4)}{mm}$ $\quad Rc4 = 45.864$

$Rc5 := R_b \cdot \frac{\sin(\psi 5)}{mm}$ $\quad Rc5 = 52.959$

Computation of Plate Shape at Several Loads

$P_1 = 2.987 \times 10^4\ N$

$r := Rc1 .. 110$

$$w1(r) := \frac{\left[P_1 \cdot \ln\left[\frac{\left[r + \left[\sqrt{(r)^2 - (\sin(\psi 1))^4} \right] \right]}{\left[R + \left[\sqrt{(R)^2 - (\sin(\psi 1))^4} \right] \right]} \right] \right]}{2 \cdot \pi \cdot N_o} \cdot mm$$

$P_2 = 3.734 \times 10^4\ N$

$r2 := Rc2 .. 110$

$$w2(r2) := \frac{\left[P_2 \cdot \ln\left[\frac{\left[r2 + \left[\sqrt{(r2)^2 - (\sin(\psi 2))^4} \right] \right]}{\left[R + \left[\sqrt{(R)^2 - (\sin(\psi 2))^4} \right] \right]} \right] \right]}{2 \cdot \pi \cdot N_o} \cdot mm$$

$P_3 = 4.978 \times 10^4\ N$

$r3 := Rc3 .. 110$

$$w3(r3) := \frac{\left[P_3 \cdot \ln\left[\frac{\left[r3 + \left[\sqrt{(r3)^2 - (\sin(\psi 3))^4} \right] \right]}{\left[R + \left[\sqrt{(R)^2 - (\sin(\psi 3))^4} \right] \right]} \right] \right]}{2 \cdot \pi \cdot N_o} \cdot mm$$

$P_4 = 7.467 \times 10^4\ N$

$r4 := Rc4 .. 110$

$$w4(r4) := \frac{\left[P_4 \cdot \ln\left[\frac{\left[r4 + \left[\sqrt{(r4)^2 - (\sin(\psi 4))^4} \right] \right]}{\left[R + \left[\sqrt{(R)^2 - (\sin(\psi 4))^4} \right] \right]} \right] \right]}{2 \cdot \pi \cdot N_o} \cdot mm$$

$P_5 = 9.956 \times 10^4\ N$

$r5 := Rc5 .. 110$

$$w5(r5) := \frac{\left[P_5 \cdot \ln\left[\frac{\left[r5 + \left[\sqrt{(r5)^2 - (\sin(\psi 5))^4} \right] \right]}{\left[R + \left[\sqrt{(R)^2 - (\sin(\psi 5))^4} \right] \right]} \right] \right]}{2 \cdot \pi \cdot N_o} \cdot mm$$

Plot of Analytic Solution for Plate Shape Up to Failure (Valid for r > R_c):

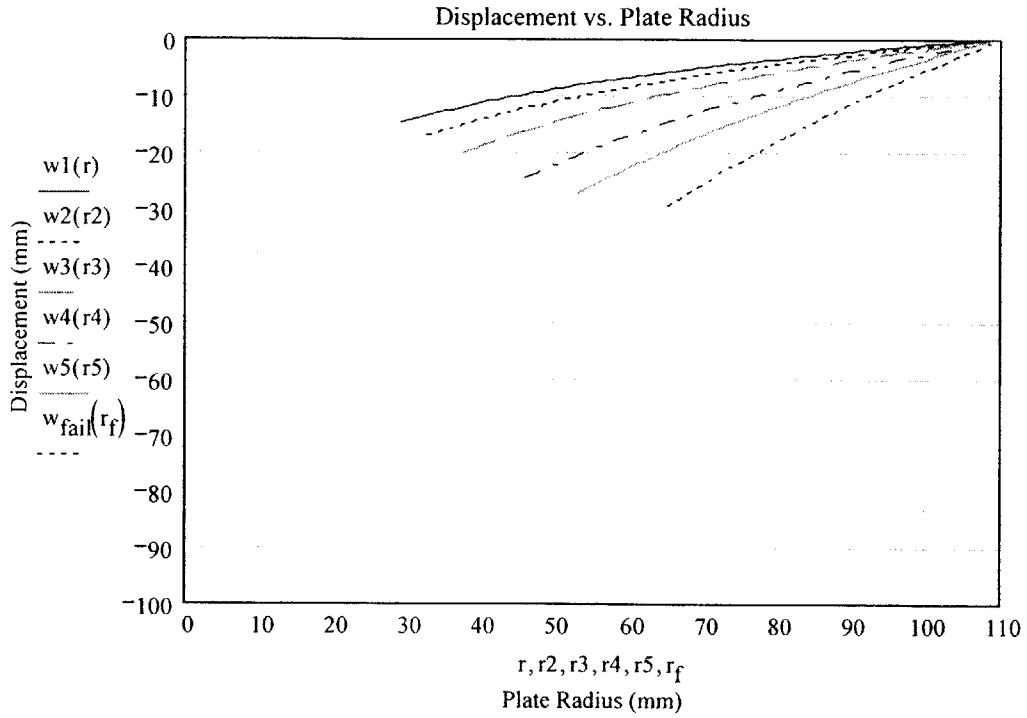

PUNCH SIZE: $R_b = 75\text{mm}$

$$P = \begin{pmatrix} 0 \\ 29.869 \\ 37.337 \\ 49.782 \\ 74.673 \\ 99.565 \\ 149.347 \end{pmatrix} \text{N} \cdot 10^3 \qquad R_c = \begin{pmatrix} 0 \\ 29.007 \\ 32.431 \\ 37.448 \\ 45.864 \\ 52.959 \\ 64.861 \end{pmatrix} \text{mm}$$

$P_{fail} = 1.493 \times 10^5\ \text{N}$ $\qquad R_{c\_fail} = 64.861\text{mm}$

Plot the Force vs. Displacement Relation:

Displacement at Point C:

$$\delta_i := \begin{pmatrix} 0 \\ w1(Rc1) \\ w2(Rc2) \\ w3(Rc3) \\ w4(Rc4) \\ w5(Rc5) \\ w_{fail}(Rcf) \end{pmatrix}$$

$$\delta_{plot} := R_b \cdot \frac{\left(1 - \cos\left(\psi_i\right)\right)}{mm} - \delta_i$$

Total Punch Displacement:

$$\delta_{plot} = \begin{pmatrix} 0 \\ 20.79 \\ 24.502 \\ 30.165 \\ 40.193 \\ 49.228 \\ 66.974 \end{pmatrix}$$

$$\delta_{max} := \text{trunc}\left[R_b \cdot \frac{\left(1 - \cos\left(\psi 6\right)\right)}{mm} - w_{fail}(Rcf)\right]$$

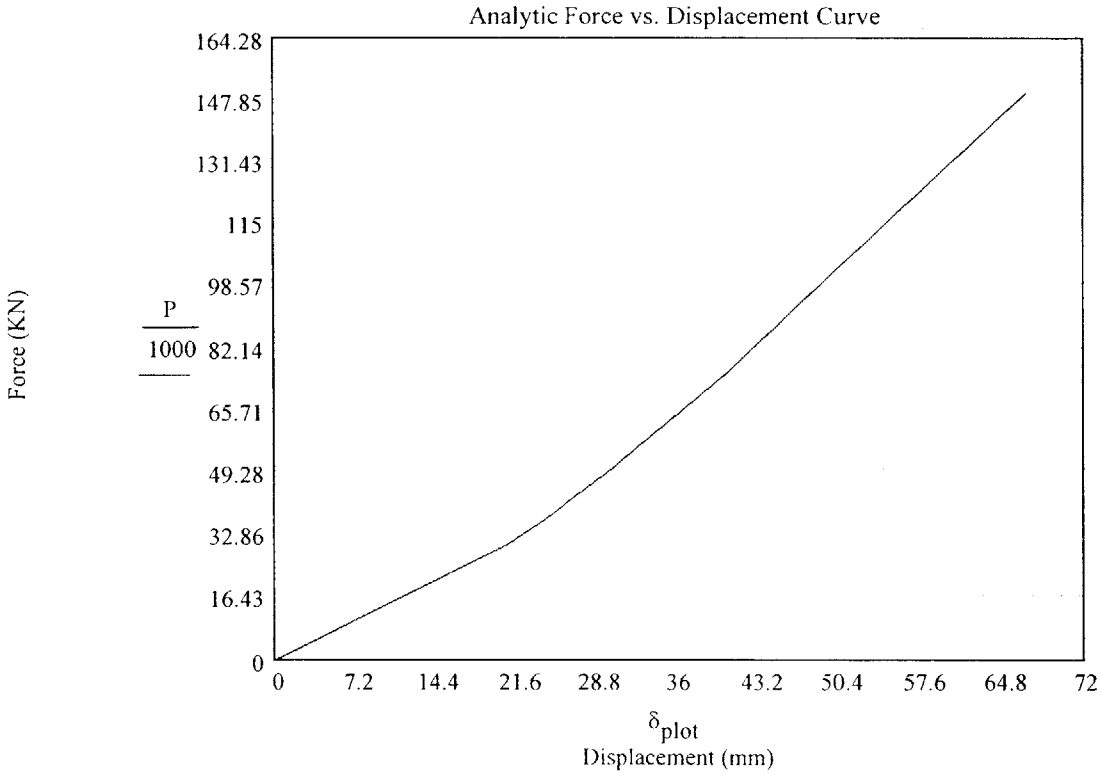

Analytic Solution for P vs Displacement During Conical Punching Before Fracture

$\theta := 30 \cdot deg$

$$P_{cone}(\delta_{cone}) := \pi \cdot C_o \cdot \delta_{cone} \cdot t_o \cdot \frac{\tan(\theta)^{2 \cdot n}}{2^n}$$

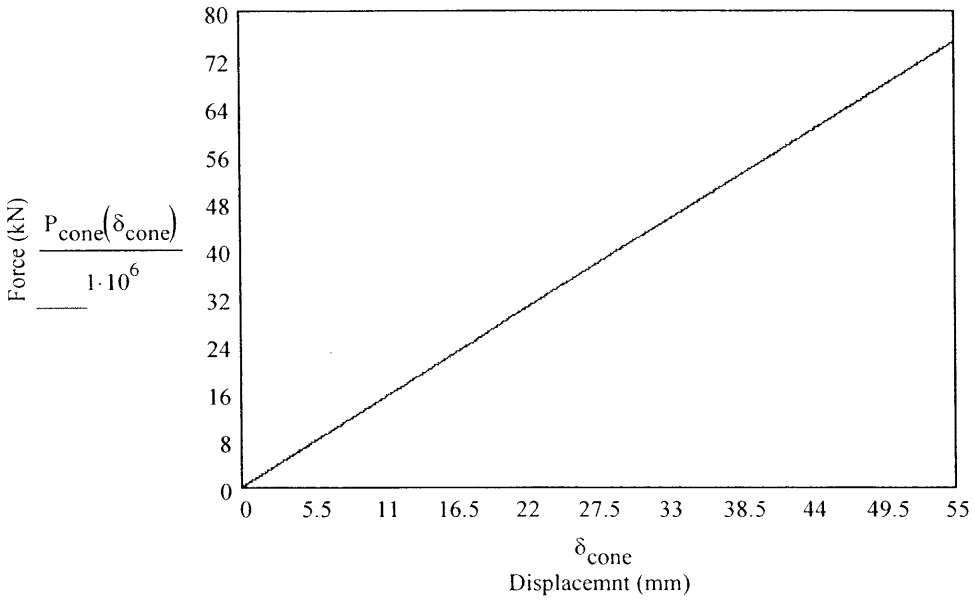

Appendix G: Petalling Work Approximations

Petalling Work Computation for .035" Sheet with 9.5mm Starter Hole and Four 3-mm Precracks

Material Properties

$\sigma_y \equiv 23300\,psi \qquad \sigma_u \equiv 45900\,psi \qquad \sigma_o := \frac{(\sigma_y + \sigma_u)}{2}$

Number of Petals

$N_p := 4$

Crack Length

$a_0 \equiv 0 \cdot mm$

$a_1 \equiv 10 \cdot mm \qquad a_5 \equiv 50 \cdot mm$

$a_2 \equiv 20 \cdot mm \qquad a_6 \equiv 60 \cdot mm$

$a_3 \equiv 30 \cdot mm \qquad a_7 \equiv 65 \cdot mm$

$a_4 \equiv 40 \cdot mm \qquad a_8 \equiv 70 \cdot mm$

Petal Semi-Angle

$\theta := \frac{360}{2N_p} \cdot deg$

Moment Amplification Factor (Flat Plate)

$\eta \equiv 1$

Plate Thickness

$t \equiv .035 \cdot in$

Petal Root Length

$b_0 := a_0 \cdot \sin(\theta)$

$b_1 := a_1 \cdot \sin(\theta) \qquad b_5 := a_5 \cdot \sin(\theta)$

$b_2 := a_2 \cdot \sin(\theta) \qquad b_6 := a_6 \cdot \sin(\theta)$

$b_3 := a_3 \cdot \sin(\theta) \qquad b_7 := a_7 \cdot \sin(\theta)$

$b_4 := a_4 \cdot \sin(\theta) \qquad b_8 := a_8 \cdot \sin(\theta)$

Measured radius of Curvature

$\rho := 150 \cdot mm$

Bending Moment

$$M_{o0} := \frac{2\sigma_o \cdot t^2 \cdot b_0}{4}$$

$$M_{o1} := \frac{2\sigma_o \cdot t^2 \cdot b_1}{4} \qquad M_{o5} := \frac{2\sigma_o \cdot t^2 \cdot b_5}{4}$$

$$M_{o2} := \frac{2\sigma_o \cdot t^2 \cdot b_2}{4} \qquad M_{o6} := \frac{2\sigma_o \cdot t^2 \cdot b_6}{4}$$

$$M_{o3} := \frac{2\sigma_o \cdot t^2 \cdot b_3}{4} \qquad M_{o7} := \frac{2\sigma_o \cdot t^2 \cdot b_7}{4}$$

$$M_{o4} := \frac{2\sigma_o \cdot t^2 \cdot b_4}{4} \qquad M_{o8} := \frac{2\sigma_o \cdot t^2 \cdot b_8}{4}$$

Starter Hole Radius

$r_o := 4.75 \cdot mm$

Cone Punch Horizontal Angle

$\phi := 30 \cdot deg$

Punch Vertical Speed

$V_p := 10 \cdot \frac{mm}{min}$

Petal Perpendicular Length

$l_0 := a_0 \cdot \cos(\theta)$

$l_1 := a_1 \cdot \cos(\theta) \qquad l_5 := a_5 \cdot \cos(\theta)$

$l_2 := a_2 \cdot \cos(\theta) \qquad l_6 := a_6 \cdot \cos(\theta)$

$l_3 := a_3 \cdot \cos(\theta) \qquad l_7 := a_7 \cdot \cos(\theta)$

$l_4 := a_4 \cdot \cos(\theta) \qquad l_8 := a_8 \cdot \cos(\theta)$

Rate of Petal Length change

$l_{dot} := \tan(\phi) \cdot V_p$

Crack Tip Opening Distance (CTOD)

CTOA

$CTOA \equiv 10 \cdot deg$

$\delta_{c0} := 2 \cdot (a_0 \cdot \sin(CTOA))$

$\delta_{c1} := 2 \cdot (a_1 \cdot \sin(CTOA))$ $\quad \delta_{c5} := 2 \cdot (a_5 \cdot \sin(CTOA))$

$\delta_{c2} := 2 \cdot (a_2 \cdot \sin(CTOA))$ $\quad \delta_{c6} := 2 \cdot (a_6 \cdot \sin(CTOA))$

$\delta_{c3} := 2 \cdot (a_3 \cdot \sin(CTOA))$ $\quad \delta_{c7} := 2 \cdot (a_8 \cdot \sin(CTOA))$

$\delta_{c4} := 2 \cdot (a_4 \cdot \sin(CTOA))$ $\quad \delta_{c8} := 2 \cdot (a_8 \cdot \sin(CTOA))$

Punch Travel

$\delta_{punch0} := \left[\tan(\theta) \cdot (l_0 + r_o)\right]$

$\delta_{punch1} := \left[\tan(\theta) \cdot (l_1 + r_o)\right]$ $\quad \delta_{punch5} := \left[\tan(\theta) \cdot (l_5 + r_o)\right]$

$\delta_{punch2} := \left[\tan(\theta) \cdot (l_2 + r_o)\right]$ $\quad \delta_{punch6} := \left[\tan(\theta) \cdot (l_6 + r_o)\right]$

$\delta_{punch3} := \left[\tan(\theta) \cdot (l_3 + r_o)\right]$ $\quad \delta_{punch7} := \left[\tan(\theta) \cdot (l_7 + r_o)\right]$

$\delta_{punch4} := \left[\tan(\theta) \cdot (l_4 + r_o)\right]$ $\quad \delta_{punch8} := \left[\tan(\theta) \cdot (l_8 + r_o)\right]$

Rate of Work Done at Specified Increment

$$W_{rate0} := \frac{M_{o0}}{m} \cdot l_{dot} \cdot \left[4 \cdot \eta \cdot \left(\frac{l_0 \cdot \tan(\theta)}{\rho} \right) + 3.84 \left(\frac{\delta_{c0}}{t} \right)^{\frac{1}{3}} \cdot \left(\frac{\rho}{t} \right)^{\frac{2}{3}} \cdot (\sin(\theta))^{\frac{-4}{3}} \cdot (\cos(\theta))^{-1} \right]$$

$$W_{rate1} := \frac{M_{o1}}{m} \cdot l_{dot} \cdot \left[4 \cdot \eta \cdot \left(\frac{l_1 \cdot \tan(\theta)}{\rho} \right) + 3.84 \left(\frac{\delta_{c1}}{t} \right)^{\frac{1}{3}} \cdot \left(\frac{\rho}{t} \right)^{\frac{2}{3}} \cdot (\sin(\theta))^{\frac{-4}{3}} \cdot (\cos(\theta))^{-1} \right]$$

$$W_{rate2} := \frac{M_{o2}}{m} \cdot l_{dot} \cdot \left[4 \cdot \eta \cdot \left(\frac{l_2 \cdot \tan(\theta)}{\rho} \right) + 3.84 \left(\frac{\delta_{c2}}{t} \right)^{\frac{1}{3}} \cdot \left(\frac{\rho}{t} \right)^{\frac{2}{3}} \cdot (\sin(\theta))^{\frac{-4}{3}} \cdot (\cos(\theta))^{-1} \right]$$

$$W_{rate3} := \frac{M_{o3}}{m} \cdot l_{dot} \cdot \left[4 \cdot \eta \cdot \left(\frac{l_3 \cdot \tan(\theta)}{\rho} \right) + 3.84 \left(\frac{\delta_{c3}}{t} \right)^{\frac{1}{3}} \cdot \left(\frac{\rho}{t} \right)^{\frac{2}{3}} \cdot (\sin(\theta))^{\frac{-4}{3}} \cdot (\cos(\theta))^{-1} \right]$$

$$W_{rate4} := \frac{M_{o4}}{m} \cdot l_{dot} \cdot \left[4 \cdot \eta \cdot \left(\frac{l_4 \cdot \tan(\theta)}{\rho} \right) + 3.84 \left(\frac{\delta_{c4}}{t} \right)^{\frac{1}{3}} \cdot \left(\frac{\rho}{t} \right)^{\frac{2}{3}} \cdot (\sin(\theta))^{\frac{-4}{3}} \cdot (\cos(\theta))^{-1} \right]$$

$$W_{rate5} := \frac{M_{o5}}{m} \cdot l_{dot} \cdot \left[4 \cdot \eta \cdot \left(\frac{l_5 \cdot \tan(\theta)}{\rho} \right) + 3.84 \left(\frac{\delta_{c5}}{t} \right)^{\frac{1}{3}} \cdot \left(\frac{\rho}{t} \right)^{\frac{2}{3}} \cdot (\sin(\theta))^{\frac{-4}{3}} \cdot (\cos(\theta))^{-1} \right]$$

$$W_{rate6} := \frac{M_{o6}}{m} \cdot l_{dot} \cdot \left[4 \cdot \eta \cdot \left(\frac{l_6 \cdot \tan(\theta)}{\rho} \right) + 3.84 \left(\frac{\delta_{c7}}{t} \right)^{\frac{1}{3}} \cdot \left(\frac{\rho}{t} \right)^{\frac{2}{3}} \cdot (\sin(\theta))^{\frac{-4}{3}} \cdot (\cos(\theta))^{-1} \right]$$

$$W_{rate7} := \frac{M_{o7}}{m} \cdot l_{dot} \cdot \left[4 \cdot \eta \cdot \left(\frac{l_7 \cdot \tan(\theta)}{\rho} \right) + 3.84 \left(\frac{\delta_{c7}}{t} \right)^{\frac{1}{3}} \cdot \left(\frac{\rho}{t} \right)^{\frac{2}{3}} \cdot (\sin(\theta))^{\frac{-4}{3}} \cdot (\cos(\theta))^{-1} \right]$$

$$W_{rate8} := \frac{M_{o8}}{m} \cdot l_{dot} \cdot \left[4 \cdot \eta \cdot \left(\frac{l_8 \cdot \tan(\theta)}{\rho} \right) + 3.84 \left(\frac{\delta_{c8}}{t} \right)^{\frac{1}{3}} \cdot \left(\frac{\rho}{t} \right)^{\frac{2}{3}} \cdot (\sin(\theta))^{\frac{-4}{3}} \cdot (\cos(\theta))^{-1} \right]$$

Total Membrane Work

$$W_{m0} := \left[M_{o0} \cdot \frac{(l_0 - r_o)}{m} \cdot \left[3.84 \left(\frac{\delta_{c0}}{t} \right)^{\frac{1}{3}} \cdot \left(\frac{\rho}{t} \right)^{\frac{2}{3}} \cdot (\sin(\theta))^{\frac{-4}{3}} \cdot (\cos(\theta))^{-1} \right] \right]$$

$$W_{m1} := \left[M_{o1} \cdot \frac{(l_1 - r_o)}{m} \cdot \left[3.84 \left(\frac{\delta_{c1}}{t} \right)^{\frac{1}{3}} \cdot \left(\frac{\rho}{t} \right)^{\frac{2}{3}} \cdot (\sin(\theta))^{\frac{-4}{3}} \cdot (\cos(\theta))^{-1} \right] \right]$$

$$W_{m2} := \left[M_{o2} \cdot \frac{(l_2 - r_o)}{m} \cdot \left[3.84 \left(\frac{\delta_{c2}}{t} \right)^{\frac{1}{3}} \cdot \left(\frac{\rho}{t} \right)^{\frac{2}{3}} \cdot (\sin(\theta))^{\frac{-4}{3}} \cdot (\cos(\theta))^{-1} \right] \right]$$

$$W_{m3} := \left[M_{o3} \cdot \frac{(l_3 - r_o)}{m} \cdot \left[3.84 \left(\frac{\delta_{c3}}{t} \right)^{\frac{1}{3}} \cdot \left(\frac{\rho}{t} \right)^{\frac{2}{3}} \cdot (\sin(\theta))^{\frac{-4}{3}} \cdot (\cos(\theta))^{-1} \right] \right]$$

$$W_{m4} := \left[M_{o4} \cdot \frac{(l_4 - r_o)}{m} \cdot \left[3.84 \left(\frac{\delta_{c4}}{t} \right)^{\frac{1}{3}} \cdot \left(\frac{\rho}{t} \right)^{\frac{2}{3}} \cdot (\sin(\theta))^{\frac{-4}{3}} \cdot (\cos(\theta))^{-1} \right] \right]$$

$$W_{m5} := \left[M_{o5} \cdot \frac{(l_5 - r_o)}{m} \cdot \left[3.84 \left(\frac{\delta_{c5}}{t} \right)^{\frac{1}{3}} \cdot \left(\frac{\rho}{t} \right)^{\frac{2}{3}} \cdot (\sin(\theta))^{\frac{-4}{3}} \cdot (\cos(\theta))^{-1} \right] \right]$$

$$W_{m6} := \left[M_{o6} \cdot \frac{(l_6 - r_o)}{m} \cdot \left[3.84 \left(\frac{\delta_{c6}}{t} \right)^{\frac{1}{3}} \cdot \left(\frac{\rho}{t} \right)^{\frac{2}{3}} \cdot (\sin(\theta))^{\frac{-4}{3}} \cdot (\cos(\theta))^{-1} \right] \right]$$

$$W_{m7} := \left[M_{o7} \cdot \frac{(l_7 - r_o)}{m} \cdot \left[3.84 \left(\frac{\delta_{c7}}{t} \right)^{\frac{1}{3}} \cdot \left(\frac{\rho}{t} \right)^{\frac{2}{3}} \cdot (\sin(\theta))^{\frac{-4}{3}} \cdot (\cos(\theta))^{-1} \right] \right]$$

$$W_{m8} := \left[M_{o8} \cdot \frac{(l_8 - r_o)}{m} \cdot \left[3.84 \left(\frac{\delta_{c8}}{t} \right)^{\frac{1}{3}} \cdot \left(\frac{\rho}{t} \right)^{\frac{2}{3}} \cdot (\sin(\theta))^{\frac{-4}{3}} \cdot (\cos(\theta))^{-1} \right] \right]$$

Total Bending Work

$$W_{b0} := N_p \cdot M_{o0} \cdot (l_0 - r_o)^2 \cdot \frac{\tan(\theta)}{2 \cdot \rho \cdot m}$$

$$W_{b1} := N_p \cdot M_{o1} \cdot (l_1 - r_o)^2 \cdot \frac{\tan(\theta)}{2 \cdot \rho \cdot m} \qquad W_{b5} := N_p \cdot M_{o5} \cdot (l_5 - r_o)^2 \cdot \frac{\tan(\theta)}{2 \cdot \rho \cdot m}$$

$$W_{b2} := N_p \cdot M_{o2} \cdot (l_2 - r_o)^2 \cdot \frac{\tan(\theta)}{2 \cdot \rho \cdot m} \qquad W_{b6} := N_p \cdot M_{o6} \cdot (l_6 - r_o)^2 \cdot \frac{\tan(\theta)}{2 \cdot \rho \cdot m}$$

$$W_{b3} := N_p \cdot M_{o3} \cdot (l_3 - r_o)^2 \cdot \frac{\tan(\theta)}{2 \cdot \rho \cdot m} \qquad W_{b7} := N_p \cdot M_{o7} \cdot (l_7 - r_o)^2 \cdot \frac{\tan(\theta)}{2 \cdot \rho \cdot m}$$

$$W_{b4} := N_p \cdot M_{o4} \cdot (l_4 - r_o)^2 \cdot \frac{\tan(\theta)}{2 \cdot \rho \cdot m} \qquad W_{b8} := N_p \cdot M_{o8} \cdot (l_8 - r_o)^2 \cdot \frac{\tan(\theta)}{2 \cdot \rho \cdot m}$$

Membrane and Bending Work Totals

$W_{m0} = 0\,N \cdot m$ $\qquad$ $W_{b0} = 0\,N \cdot m$

$W_{m1} = 0.641 N \cdot m$ $\qquad$ $W_{b1} = 4.788 \times 10^{-5}\,N \cdot m$

$W_{m2} = 6.54 N \cdot m$ $\qquad$ $W_{b2} = 1.568 \times 10^{-3}\,N \cdot m$

$W_{m3} = 13.648 N \cdot m$ $\qquad$ $W_{b3} = 7.227 \times 10^{-3}\,N \cdot m$

$W_{m4} = 41.295 N \cdot m$ $\qquad$ $W_{b4} = 0.02 N \cdot m$

$W_{m5} = 72.311 N \cdot m$ $\qquad$ $W_{b5} = 0.042 N \cdot m$

$W_{m6} = 113.514 N \cdot m$ $\qquad$ $W_{b6} = 0.076 N \cdot m$

$W_{m7} = 141.606 N \cdot m$ $\qquad$ $W_{b7} = 0.098 N \cdot m$

$W_{m8} = 165.581 N \cdot m$ $\qquad$ $W_{b8} = 0.125 N \cdot m$

Total Work

$$W_{t0} := N_p \cdot (W_{b0} + W_{m0}) \qquad W_{t0} = 0\,J$$

$$W_{t1} := N_p \cdot (W_{b1} + W_{m1}) \qquad W_{t1} = 2.566J$$

$$W_{t2} := N_p \cdot (W_{b2} + W_{m2}) \qquad W_{t2} = 26.167J$$

$$W_{t3} := N_p \cdot (W_{b3} + W_{m3}) \qquad W_{t3} = 54.622J$$

$$W_{t4} := N_p \cdot (W_{b4} + W_{m4}) \qquad W_{t4} = 165.257J$$

$$W_{t5} := N_p \cdot (W_{b5} + W_{m5}) \qquad W_{t5} = 289.409J$$

$$W_{t6} := N_p \cdot (W_{b6} + W_{m6}) \qquad W_{t6} = 454.36J$$

$$W_{t7} := N_p \cdot (W_{b7} + W_{m7}) \qquad W_{t7} = 566.816J$$

$$W_{t8} := N_p \cdot (W_{b8} + W_{m8}) \qquad W_{t8} = 662.824J$$

Estimation of Forces

$$F_0 := 2 \cdot \frac{W_{t0}}{\delta_{punch0}}$$

$$F_1 := 2 \cdot \frac{W_{t1}}{\delta_{punch1}} \qquad F_5 := 2 \cdot \frac{W_{t5}}{\delta_{punch5}}$$

$$F_2 := 2 \cdot \frac{W_{t2}}{\delta_{punch2}} \qquad F_6 := 2 \cdot \frac{W_{t6}}{\delta_{punch6}}$$

$$F_3 := 2 \cdot \frac{W_{t3}}{\delta_{punch3}} \qquad F_7 := 2 \cdot \frac{W_{t7}}{\delta_{punch7}}$$

$$F_4 := 2 \cdot \frac{W_{t4}}{\delta_{punch4}} \qquad F_8 := 2 \cdot \frac{W_{t8}}{\delta_{punch8}}$$

Force and Displacemnt Arrays

$$P := \begin{pmatrix} F_0 \\ F_1 \\ F_2 \\ F_3 \\ F_4 \\ F_5 \\ F_6 \\ F_7 \\ F_8 \end{pmatrix} \qquad \delta := \begin{pmatrix} 0 \\ \delta_{punch1} \\ \delta_{punch2} \\ \delta_{punch3} \\ \delta_{punch4} \\ \delta_{punch5} \\ \delta_{punch6} \\ \delta_{punch7} \\ \delta_{punch8} \end{pmatrix}$$

$$P = \begin{pmatrix} 0 \\ 434.109 \\ 2.77 \times 10^3 \\ 4.208 \times 10^3 \\ 1.001 \times 10^4 \\ 1.443 \times 10^4 \\ 1.926 \times 10^4 \\ 2.235 \times 10^4 \\ 2.444 \times 10^4 \end{pmatrix} \text{ N} \qquad \delta = \begin{pmatrix} 0 \\ 11.821 \\ 18.892 \\ 25.963 \\ 33.034 \\ 40.105 \\ 47.176 \\ 50.712 \\ 54.247 \end{pmatrix} \text{ mm}$$

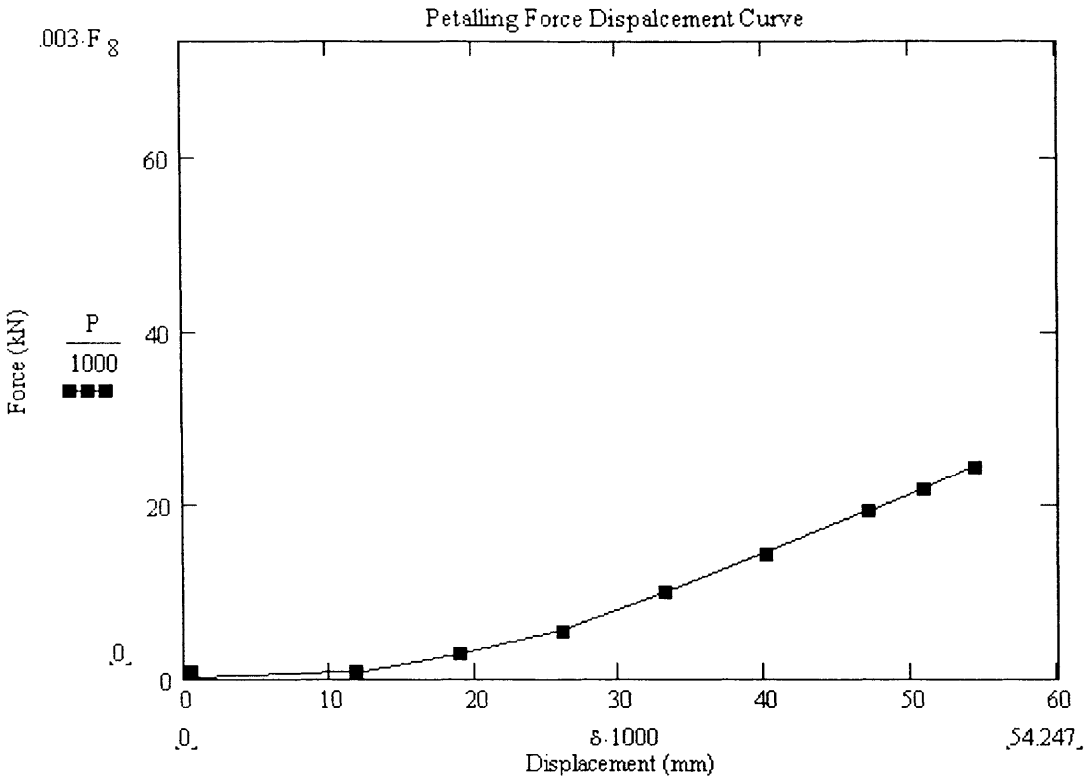
Petalling Force Dispalcement Curve
.003·F 8
60
40
20
0
P
1000
Force (kN)
0
0
10
20
30
40
50
60
0
δ·1000
54.247
Displacement (mm)

Appendix H: LS-DYNA Input File

```
$  .055" plate with 75 mm radius sphere
$
*KEYWORD
*TITLE
Stamping
*PART
 part
       1       2       2
$---+----1----+----2----+----3----+----4----+----5----+----6----+----7----+----8
$                (2) CONTROL CARDS.
$---+----1----+----2----+----3----+----4----+----5----+----6----+----7----+----8
*define curve
$ lcid (x-direction)
    1
$         abscissa         ordinate
             0.0            1000.0
           100.0             1000.0
*control_termination
$  ENDTIM   ENDCYC   DTMIN   ENDNEG   ENDMAS
    1.e-1
*control_timestep
$  DTINIT    SCFT    ISDO  TSLIMT    DTMS    LCTM   ERODE   MS1ST
     .000    .900       0
*CONTROL_SHELL
$  WRPANG   ITRIST   IRNXX   ISTUPD   THEORY     BWC   MITER
   20.000       2      -1       1       2       2       1
*CONTROL_HOURGLASS
$     IHQ      QH
       1    .100
*CONTROL_BULK_VISCOSITY
$      Q2      Q1
    1.500    .060
*CONTROL_ENERGY
$    HGEN    RWEN   SLNTEN    RYLEN
       2       2       1       1
*CONTROL_OUTPUT
$  NPOPT  NEECHO  NREFUP  IACCOP   OPIFS  IPNINT  IKEDIT
       0       0       0       0    .000       0     100
*DATABASE_EXTENT_BINARY
       0       0       3       0       1       1       1       1
       0       0       0       0       0       0
$---+----1----+----2----+----3----+----4----+----5----+----6----+----7----+----8
$                (4) DATABASE CONTROL CARDS FOR ASCII FILE
$---+----1----+----2----+----3----+----4----+----5----+----6----+----7----+----8
```

```
*DATABASE_RWFORC
   1.e-4
*DATABASE_GLSTAT
   1.e-4
*DATABASE_MATSUM
   1.e-4
$---+----1----+----2----+----3----+----4----+----5----+----6----+----7----+----8
$              (5) DATABASE CONTROL CARDS FOR BINARY FILE
$---+----1----+----2----+----3----+----4----+----5----+----6----+----7----+----8
*DATABASE_BINARY_D3PLOT
$ DT/CYCL    LCDT   NOBEAM
   1.e-3
$---+----1----+----2----+----3----+----4----+----5----+----6----+----7----+----8
$              RIGID_SPHERE
$---+----1----+----2----+----3----+----4----+----5----+----6----+----7----+----8
*rigidwall_geometric_sphere_motion
$ NID/NSID
       0
$      xt      yt      zt      xh      yh      zh    fric
      0.    100.    75.7      0.    100.      0.    0.05
$  radius
    75.0
$
$    LCID     OPT      VX      VY      VZ
       1       0      0.      0.    -1.0
$---+----1----+----2----+----3----+----4----+----5----+----6----+----7----+----8
$              BOUNDARY CONDITION
$---+----1----+----2----+----3----+----4----+----5----+----6----+----7----+----8
*BOUNDARY_SPC_SET
$clamped
$ NID/NSID     CID    DOFX    DOFY    DOFZ   DOFRX   DOFRY   DOFRZ
       1         1       1       1       1       1       1
*BOUNDARY_SPC_SET
$symy
$ NID/NSID     CID    DOFX    DOFY    DOFZ   DOFRX   DOFRY   DOFRZ
       2         1                       1       1
*BOUNDARY_SPC_SET
$symx
$ NID/NSID     CID    DOFX    DOFY    DOFZ   DOFRX   DOFRY   DOFRZ
       3                 1         1         1
*BOUNDARY_SPC_SET
$center
$ NID/NSID     CID    DOFX    DOFY    DOFZ   DOFRX   DOFRY   DOFRZ
       4         1       1         1       1       1
$---+----1----+----2----+----3----+----4----+----5----+----6----+----7----+----8
*MAT_PIECEWISE_LINEAR_PLASTICITY
$    MID      RO       E      PR    SIGY    ETAN    EPPF    TDEL
       2 7.800E-09  210.E+03    0.33
```

```
$      C       P     LCSS     LCSR

$    EPS1     EPS2     EPS3     EPS4     EPS5     EPS6     EPS7     EPS8
       0      .02      .04      .06       .1       .5      .75        1
$     ES1      ES2      ES3      ES4      ES5      ES6      ES7      ES8
     240      260      295      330      695      920     1160     2000
*SECTION_SHELL
$HMNAME PROPS       1SectShll1
$     SID   ELFORM     SHRF      NIP    PROPT  QR/IRID    ICOMP    SETYP
       2        2    0.833        5
$      T1       T2       T3       T4     NLOC
    1.397    1.397    1.397    1.397
$---+----1----+----2----+----3----+----4----+----5----+----6----+----7----+----8
$                GEOMETRY
$---+----1----+----2----+----3----+----4----+----5----+----6----+----7----+----8
*NODE
```

Appendix I: Strain Field Worksheet

Strain Field Computation Worksheet

ROW 0

$u_{11\_1\_pt00} \equiv 0$ $\quad u_{11\_2\_pt00} \equiv 0$

$\delta x_{11\_pt00} \equiv 1.0$ $\quad \delta y_{22\_pt00} \equiv 1.0$

$u_{22\_1\_pt00} \equiv 0$ $\quad u_{22\_2\_pt00} \equiv 0$

$\delta u_{11\_pt00} := u_{11\_2\_pt00} - u_{11\_1\_pt00}$ $\quad \delta u_{22\_pt00} := u_{22\_2\_pt00} - u_{22\_1\_pt00}$

$$\varepsilon_{11\_pt00} := \frac{\delta u_{11\_pt00}}{\delta x_{11\_pt00}} \qquad \varepsilon_{22\_pt00} := \frac{\delta u_{22\_pt00}}{\delta y_{22\_pt00}}$$

$$\varepsilon_{12\_pt00} := \frac{1}{2}\left[\left(\frac{\delta u_{11\_pt00}}{\delta y_{22\_pt00}}\right) + \left(\frac{\delta u_{22\_pt00}}{\delta x_{11\_pt00}}\right)\right]$$

$\varepsilon_{11\_pt00} = 0$

$\varepsilon_{22\_pt00} = 0$

$\varepsilon_{12\_pt00} = 0$

Next Point

$u_{11\_1\_pt10} \equiv .8$ $\quad u_{11\_2\_pt10} \equiv 1.0$

$\delta x_{11\_pt10} \equiv .8$ $\quad \delta y_{22\_pt10} \equiv .8$

$u_{22\_1\_pt10} \equiv 0$ $\quad u_{22\_2\_pt10} \equiv 0$

$\delta u_{11\_pt10} := u_{11\_2\_pt10} - u_{11\_1\_pt10}$ $\quad \delta u_{22\_pt10} := u_{22\_2\_pt10} - u_{22\_1\_pt10}$

$$\varepsilon_{11\_pt10} := \frac{\delta u_{11\_pt10}}{\delta x_{11\_pt10}} \qquad \varepsilon_{22\_pt10} := \frac{\delta u_{22\_pt10}}{\delta y_{22\_pt10}}$$

$$\varepsilon_{12\_pt10} := \frac{1}{2}\left[\left(\frac{\delta u_{11\_pt10}}{\delta y_{22\_pt10}}\right) + \left(\frac{\delta u_{22\_pt10}}{\delta x_{11\_pt10}}\right)\right]$$

$\varepsilon_{11\_pt10} = 0.25$

$\varepsilon_{22\_pt10} = 0$

$\varepsilon_{12\_pt10} = 0.125$

Epsilon$_{11}$ Strain Field:

$$\varepsilon_{11} := \begin{pmatrix} \varepsilon_{11\_pt06} & \varepsilon_{11\_pt16} & \varepsilon_{11\_pt26} & \varepsilon_{11\_pt36} & \varepsilon_{11\_pt46} & \varepsilon_{11\_pt56} & \varepsilon_{11\_pt66} & \varepsilon_{11\_pt76} \\ \varepsilon_{11\_pt05} & \varepsilon_{11\_pt15} & \varepsilon_{11\_pt25} & \varepsilon_{11\_pt35} & \varepsilon_{11\_pt45} & \varepsilon_{11\_pt55} & \varepsilon_{11\_pt65} & \varepsilon_{11\_pt75} \\ \varepsilon_{11\_pt04} & \varepsilon_{11\_pt14} & \varepsilon_{11\_pt24} & \varepsilon_{11\_pt34} & \varepsilon_{11\_pt44} & \varepsilon_{11\_pt54} & \varepsilon_{11\_pt64} & \varepsilon_{11\_pt74} \\ \varepsilon_{11\_pt03} & \varepsilon_{11\_pt13} & \varepsilon_{11\_pt23} & \varepsilon_{11\_pt33} & \varepsilon_{11\_pt43} & \varepsilon_{11\_pt53} & \varepsilon_{11\_pt63} & \varepsilon_{11\_pt73} \\ \varepsilon_{11\_pt02} & \varepsilon_{11\_pt12} & \varepsilon_{11\_pt22} & \varepsilon_{11\_pt32} & \varepsilon_{11\_pt42} & \varepsilon_{11\_pt52} & \varepsilon_{11\_pt62} & \varepsilon_{11\_pt72} \\ \varepsilon_{11\_pt01} & \varepsilon_{11\_pt11} & \varepsilon_{11\_pt21} & \varepsilon_{11\_pt31} & \varepsilon_{11\_pt41} & \varepsilon_{11\_pt51} & \varepsilon_{11\_pt61} & \varepsilon_{11\_pt71} \\ \varepsilon_{11\_pt00} & \varepsilon_{11\_pt10} & \varepsilon_{11\_pt20} & \varepsilon_{11\_pt30} & \varepsilon_{11\_pt40} & \varepsilon_{11\_pt50} & \varepsilon_{11\_pt60} & \varepsilon_{11\_pt70} \end{pmatrix}$$

$$\varepsilon_{11} = \begin{pmatrix} 0 & 0.1 & 0.15 & 0 & 0 & 0.2 & 0.4 & 0.25 \\ 0.5 & 0.1 & 0.2 & 0.05 & 0.2 & 0.3 & 0.4 & 0.3 \\ -0.222 & 0.111 & 0.2 & 0.1 & 0.2 & 0.4 & 0.4 & 0.5 \\ -0.25 & 0.222 & 0.222 & 0.278 & 0.333 & 0.444 & 0.722 & 0.579 \\ 0 & 0.111 & 0.167 & 0.222 & 0.333 & 0.444 & 1.056 & 0.842 \\ 0 & 0.111 & 0.25 & 0.25 & 0.5 & 0.5 & 0.625 & 0.941 \\ 0 & 0.25 & 0.25 & 0.375 & 0.571 & 0.75 & 0.5 & 0.75 \end{pmatrix}$$

Epsilon$_{22}$ Strain Field:

$$\varepsilon_{22} := \begin{pmatrix} \varepsilon_{22\_pt06} & \varepsilon_{22\_pt16} & \varepsilon_{22\_pt26} & \varepsilon_{22\_pt36} & \varepsilon_{22\_pt46} & \varepsilon_{22\_pt56} & \varepsilon_{22\_pt66} & \varepsilon_{22\_pt76} \\ \varepsilon_{22\_pt05} & \varepsilon_{22\_pt15} & \varepsilon_{22\_pt25} & \varepsilon_{22\_pt35} & \varepsilon_{22\_pt45} & \varepsilon_{22\_pt55} & \varepsilon_{22\_pt65} & \varepsilon_{22\_pt75} \\ \varepsilon_{22\_pt04} & \varepsilon_{22\_pt14} & \varepsilon_{22\_pt24} & \varepsilon_{22\_pt34} & \varepsilon_{22\_pt44} & \varepsilon_{22\_pt54} & \varepsilon_{22\_pt64} & \varepsilon_{22\_pt74} \\ \varepsilon_{22\_pt03} & \varepsilon_{22\_pt13} & \varepsilon_{22\_pt23} & \varepsilon_{22\_pt33} & \varepsilon_{22\_pt43} & \varepsilon_{22\_pt53} & \varepsilon_{22\_pt63} & \varepsilon_{22\_pt73} \\ \varepsilon_{22\_pt02} & \varepsilon_{22\_pt12} & \varepsilon_{22\_pt22} & \varepsilon_{22\_pt32} & \varepsilon_{22\_pt42} & \varepsilon_{22\_pt52} & \varepsilon_{22\_pt62} & \varepsilon_{22\_pt72} \\ \varepsilon_{22\_pt01} & \varepsilon_{22\_pt11} & \varepsilon_{22\_pt21} & \varepsilon_{22\_pt31} & \varepsilon_{22\_pt41} & \varepsilon_{22\_pt51} & \varepsilon_{22\_pt61} & \varepsilon_{22\_pt71} \\ \varepsilon_{22\_pt00} & \varepsilon_{22\_pt10} & \varepsilon_{22\_pt20} & \varepsilon_{22\_pt30} & \varepsilon_{22\_pt40} & \varepsilon_{22\_pt50} & \varepsilon_{22\_pt60} & \varepsilon_{22\_pt70} \end{pmatrix}$$

$$\varepsilon_{22} = \begin{pmatrix} 0.4 & 0.5 & 0.55 & 0.6 & 0.7 & 0.7 & 0.8 & 0.8 \\ 0 & 0.5 & 0.55 & 0.65 & 0.7 & 0.9 & 1 & 1 \\ 0.2 & 0.3 & 0.45 & 0.45 & 1.7 & 1 & 1 & 1.05 \\ 0.2 & 0.111 & 0.222 & 0.333 & 0.389 & 0.944 & 1 & 1 \\ 0 & 0 & 0.167 & 0.222 & 0.222 & 0.222 & 1.1 & 1.15 \\ 0 & 0 & 0 & 0 & 0.1 & 0.15 & 0.2 & 0.25 \\ 0 & 0 & 0 & 0 & 0 & 0.125 & 0.187 & 0.25 \end{pmatrix}$$

Epsilon$_{12}$ Strain Field:

$$\varepsilon_{12} := \begin{pmatrix} \varepsilon_{12\_pt06} & \varepsilon_{12\_pt16} & \varepsilon_{12\_pt26} & \varepsilon_{12\_pt36} & \varepsilon_{12\_pt46} & \varepsilon_{12\_pt56} & \varepsilon_{12\_pt66} & \varepsilon_{12\_pt76} \\ \varepsilon_{12\_pt05} & \varepsilon_{12\_pt15} & \varepsilon_{12\_pt25} & \varepsilon_{12\_pt35} & \varepsilon_{12\_pt45} & \varepsilon_{12\_pt55} & \varepsilon_{12\_pt65} & \varepsilon_{12\_pt75} \\ \varepsilon_{12\_pt04} & \varepsilon_{12\_pt14} & \varepsilon_{12\_pt24} & \varepsilon_{12\_pt34} & \varepsilon_{12\_pt44} & \varepsilon_{12\_pt54} & \varepsilon_{12\_pt64} & \varepsilon_{12\_pt74} \\ \varepsilon_{12\_pt03} & \varepsilon_{12\_pt13} & \varepsilon_{12\_pt23} & \varepsilon_{12\_pt33} & \varepsilon_{12\_pt43} & \varepsilon_{12\_pt53} & \varepsilon_{12\_pt63} & \varepsilon_{12\_pt73} \\ \varepsilon_{12\_pt02} & \varepsilon_{12\_pt12} & \varepsilon_{12\_pt22} & \varepsilon_{12\_pt32} & \varepsilon_{12\_pt42} & \varepsilon_{12\_pt52} & \varepsilon_{12\_pt62} & \varepsilon_{12\_pt72} \\ \varepsilon_{12\_pt01} & \varepsilon_{12\_pt11} & \varepsilon_{12\_pt21} & \varepsilon_{12\_pt31} & \varepsilon_{12\_pt41} & \varepsilon_{12\_pt51} & \varepsilon_{12\_pt61} & \varepsilon_{12\_pt71} \\ \varepsilon_{12\_pt00} & \varepsilon_{12\_pt10} & \varepsilon_{12\_pt20} & \varepsilon_{12\_pt30} & \varepsilon_{12\_pt40} & \varepsilon_{12\_pt50} & \varepsilon_{12\_pt60} & \varepsilon_{12\_pt70} \end{pmatrix}$$

$$\varepsilon_{12} = \begin{pmatrix} 0.2 & 0.3 & 0.35 & 0.3 & 0.35 & 0.45 & 0.6 & 0.525 \\ 0.25 & 0.3 & 0.375 & 0.35 & 0.45 & 0.6 & 0.7 & 0.65 \\ 0.011 & 0.217 & 0.325 & 0.275 & 0.95 & 0.7 & 0.7 & 0.775 \\ 0.025 & 0.167 & 0.222 & 0.306 & 0.361 & 0.694 & 0.881 & 0.801 \\ 0 & 0.063 & 0.167 & 0.222 & 0.278 & 0.333 & 1.086 & 1.005 \\ 0 & 0.063 & 0.125 & 0.125 & 0.263 & 0.294 & 0.375 & 0.547 \\ 0 & 0.125 & 0.125 & 0.187 & 0.25 & 0.437 & 0.344 & 0.5 \end{pmatrix}$$

Rotating the strain field in order to align coordinate sysytem with crack:

$$\varepsilon_{\eta\eta} := \varepsilon_{22} \cdot \cos(22 \cdot \text{deg}) \qquad \varepsilon_{\xi\xi} := \frac{\varepsilon_{22}}{\cos(22 \cdot \text{deg})} \qquad \varepsilon_{\xi\eta} := \varepsilon_{12} \cdot \cos(22 \cdot \text{deg})$$

Final Crack-Oriented Strain Fields:

$$\varepsilon_{\eta\eta} = \begin{pmatrix} 0.371 & 0.464 & 0.51 & 0.556 & 0.649 & 0.649 & 0.742 & 0.742 \\ 0 & 0.464 & 0.51 & 0.603 & 0.649 & 0.834 & 0.927 & 0.927 \\ 0.185 & 0.278 & 0.417 & 0.417 & 1.576 & 0.927 & 0.927 & 0.974 \\ 0.185 & 0.103 & 0.206 & 0.309 & 0.361 & 0.876 & 0.927 & 0.927 \\ 0 & 0 & 0.155 & 0.206 & 0.206 & 0.206 & 1.02 & 1.066 \\ 0 & 0 & 0 & 0 & 0.093 & 0.139 & 0.185 & 0.232 \\ 0 & 0 & 0 & 0 & 0 & 0.116 & 0.174 & 0.232 \end{pmatrix}$$

$$\varepsilon_{\xi\xi} = \begin{pmatrix} 0.431 & 0.539 & 0.593 & 0.647 & 0.755 & 0.755 & 0.863 & 0.863 \\ 0 & 0.539 & 0.593 & 0.701 & 0.755 & 0.971 & 1.079 & 1.079 \\ 0.216 & 0.324 & 0.485 & 0.485 & 1.834 & 1.079 & 1.079 & 1.132 \\ 0.216 & 0.12 & 0.24 & 0.36 & 0.419 & 1.019 & 1.079 & 1.079 \\ 0 & 0 & 0.18 & 0.24 & 0.24 & 0.24 & 1.186 & 1.24 \\ 0 & 0 & 0 & 0 & 0.108 & 0.162 & 0.216 & 0.27 \\ 0 & 0 & 0 & 0 & 0 & 0.135 & 0.202 & 0.27 \end{pmatrix}$$

$$\varepsilon_{\xi\eta} = \begin{pmatrix} 0.185 & 0.278 & 0.325 & 0.278 & 0.325 & 0.417 & 0.556 & 0.487 \\ 0.232 & 0.278 & 0.348 & 0.325 & 0.417 & 0.556 & 0.649 & 0.603 \\ 0.01 & 0.201 & 0.301 & 0.255 & 0.881 & 0.649 & 0.649 & 0.719 \\ 0.023 & 0.155 & 0.206 & 0.283 & 0.335 & 0.644 & 0.816 & 0.743 \\ 0 & 0.058 & 0.155 & 0.206 & 0.258 & 0.309 & 1.007 & 0.932 \\ 0 & 0.058 & 0.116 & 0.116 & 0.243 & 0.272 & 0.348 & 0.507 \\ 0 & 0.116 & 0.116 & 0.174 & 0.232 & 0.406 & 0.319 & 0.464 \end{pmatrix}$$

$$
\text{stacking\_ratio} := \begin{bmatrix}
\left[\left(\frac{z_{11\_p06}}{z_{22\_p06}}\right)+\frac{1}{2}\right] & \left[\left(\frac{z_{11\_p16}}{z_{22\_p16}}\right)+\frac{1}{2}\right] & \left[\left(\frac{z_{11\_p26}}{z_{22\_p26}}\right)+\frac{1}{2}\right] & \left[\left(\frac{z_{11\_p36}}{z_{22\_p36}}\right)+\frac{1}{2}\right] & \left[\left(\frac{z_{11\_p\#6}}{z_{22\_p\#6}}\right)+\frac{1}{2}\right] & \left[\left(\frac{z_{11\_p56}}{z_{22\_p56}}\right)+\frac{1}{2}\right] & \left[\left(\frac{z_{11\_p\%6}}{z_{22\_p\%6}}\right)+\frac{1}{2}\right] & \left[\left(\frac{z_{11\_p76}}{z_{22\_p76}}\right)+\frac{1}{2}\right] \\
\left[\frac{1}{2}\left(\frac{z_{11\_p06}}{z_{22\_p06}}\right)+1\right] & \left[\frac{1}{2}\left(\frac{z_{11\_p16}}{z_{22\_p16}}\right)+1\right] & \left[\frac{1}{2}\left(\frac{z_{11\_p26}}{z_{22\_p26}}\right)+1\right] & \left[\frac{1}{2}\left(\frac{z_{11\_p36}}{z_{22\_p36}}\right)+1\right] & \left[\frac{1}{2}\left(\frac{z_{11\_p\#6}}{z_{22\_p\#6}}\right)+1\right] & \left[\frac{1}{2}\left(\frac{z_{11\_p56}}{z_{22\_p56}}\right)+1\right] & \left[\frac{1}{2}\left(\frac{z_{11\_p\%6}}{z_{22\_p\%6}}\right)+1\right] & \left[\frac{1}{2}\left(\frac{z_{11\_p76}}{z_{22\_p76}}\right)+1\right] \\
\left[\left(\frac{z_{11\_p05}}{z_{22\_p06}}\right)+\frac{1}{2}\right] & \left[\left(\frac{z_{11\_p15}}{z_{22\_p15}}\right)+\frac{1}{2}\right] & \left[\left(\frac{z_{11\_p25}}{z_{22\_p25}}\right)+\frac{1}{2}\right] & \left[\left(\frac{z_{11\_p35}}{z_{22\_p35}}\right)+\frac{1}{2}\right] & \left[\left(\frac{z_{11\_p\#5}}{z_{22\_p\#5}}\right)+\frac{1}{2}\right] & \left[\left(\frac{z_{11\_p55}}{z_{22\_p55}}\right)+\frac{1}{2}\right] & \left[\left(\frac{z_{11\_p\%5}}{z_{22\_p\%5}}\right)+\frac{1}{2}\right] & \left[\left(\frac{z_{11\_p75}}{z_{22\_p75}}\right)+\frac{1}{2}\right] \\
\left[\frac{1}{2}\left(\frac{z_{11\_p05}}{z_{22\_p06}}\right)+1\right] & \left[\frac{1}{2}\left(\frac{z_{11\_p15}}{z_{22\_p15}}\right)+1\right] & \left[\frac{1}{2}\left(\frac{z_{11\_p25}}{z_{22\_p25}}\right)+1\right] & \left[\frac{1}{2}\left(\frac{z_{11\_p35}}{z_{22\_p35}}\right)+1\right] & \left[\frac{1}{2}\left(\frac{z_{11\_p\#5}}{z_{22\_p\#5}}\right)+1\right] & \left[\frac{1}{2}\left(\frac{z_{11\_p55}}{z_{22\_p55}}\right)+1\right] & \left[\frac{1}{2}\left(\frac{z_{11\_p\%5}}{z_{22\_p\%5}}\right)+1\right] & \left[\frac{1}{2}\left(\frac{z_{11\_p75}}{z_{22\_p75}}\right)+1\right] \\
\left[\left(\frac{z_{11\_p04}}{z_{22\_p04}}\right)+\frac{1}{2}\right] & \left[\left(\frac{z_{11\_p14}}{z_{22\_p14}}\right)+\frac{1}{2}\right] & \left[\left(\frac{z_{11\_p24}}{z_{22\_p24}}\right)+\frac{1}{2}\right] & \left[\left(\frac{z_{11\_p34}}{z_{22\_p34}}\right)+\frac{1}{2}\right] & \left[\left(\frac{z_{11\_p\#4}}{z_{22\_p\#4}}\right)+\frac{1}{2}\right] & \left[\left(\frac{z_{11\_p54}}{z_{22\_p54}}\right)+\frac{1}{2}\right] & \left[\left(\frac{z_{11\_p\%4}}{z_{22\_p\%4}}\right)+\frac{1}{2}\right] & \left[\left(\frac{z_{11\_p74}}{z_{22\_p74}}\right)+\frac{1}{2}\right] \\
\left[\frac{1}{2}\left(\frac{z_{11\_p04}}{z_{22\_p04}}\right)+1\right] & \left[\frac{1}{2}\left(\frac{z_{11\_p14}}{z_{22\_p14}}\right)+1\right] & \left[\frac{1}{2}\left(\frac{z_{11\_p24}}{z_{22\_p24}}\right)+1\right] & \left[\frac{1}{2}\left(\frac{z_{11\_p34}}{z_{22\_p34}}\right)+1\right] & \left[\frac{1}{2}\left(\frac{z_{11\_p\#4}}{z_{22\_p\#4}}\right)+1\right] & \left[\frac{1}{2}\left(\frac{z_{11\_p54}}{z_{22\_p54}}\right)+1\right] & \left[\frac{1}{2}\left(\frac{z_{11\_p\%4}}{z_{22\_p\%4}}\right)+1\right] & \left[\frac{1}{2}\left(\frac{z_{11\_p74}}{z_{22\_p74}}\right)+1\right] \\
\left[\left(\frac{z_{11\_p03}}{z_{22\_p03}}\right)+\frac{1}{2}\right] & \left[\left(\frac{z_{11\_p13}}{z_{22\_p13}}\right)+\frac{1}{2}\right] & \left[\left(\frac{z_{11\_p23}}{z_{22\_p23}}\right)+\frac{1}{2}\right] & \left[\left(\frac{z_{11\_p33}}{z_{22\_p33}}\right)+\frac{1}{2}\right] & \left[\left(\frac{z_{11\_p\#3}}{z_{22\_p\#3}}\right)+\frac{1}{2}\right] & \left[\left(\frac{z_{11\_p53}}{z_{22\_p53}}\right)+\frac{1}{2}\right] & \left[\left(\frac{z_{11\_p\%3}}{z_{22\_p\%3}}\right)+\frac{1}{2}\right] & \left[\left(\frac{z_{11\_p73}}{z_{22\_p73}}\right)+\frac{1}{2}\right] \\
\left[\frac{1}{2}\left(\frac{z_{11\_p03}}{z_{22\_p03}}\right)+1\right] & \left[\frac{1}{2}\left(\frac{z_{11\_p13}}{z_{22\_p13}}\right)+1\right] & \left[\frac{1}{2}\left(\frac{z_{11\_p23}}{z_{22\_p23}}\right)+1\right] & \left[\frac{1}{2}\left(\frac{z_{11\_p33}}{z_{22\_p33}}\right)+1\right] & \left[\frac{1}{2}\left(\frac{z_{11\_p\#3}}{z_{22\_p\#3}}\right)+1\right] & \left[\frac{1}{2}\left(\frac{z_{11\_p53}}{z_{22\_p53}}\right)+1\right] & \left[\frac{1}{2}\left(\frac{z_{11\_p\%3}}{z_{22\_p\%3}}\right)+1\right] & \left[\frac{1}{2}\left(\frac{z_{11\_p73}}{z_{22\_p73}}\right)+1\right] \\
\left[\left(\frac{z_{11\_p02}}{z_{22\_p02}}\right)+\frac{1}{2}\right] & \left[\left(\frac{z_{11\_p12}}{z_{22\_p13}}\right)+\frac{1}{2}\right] & \left[\left(\frac{z_{11\_p22}}{z_{22\_p22}}\right)+\frac{1}{2}\right] & \left[\left(\frac{z_{11\_p32}}{z_{22\_p32}}\right)+\frac{1}{2}\right] & \left(\frac{z_{11\_p\#2}}{z_{22\_p\#2}}+\frac{1}{2}\right) & \left[\left(\frac{z_{11\_p52}}{z_{22\_p52}}\right)+\frac{1}{2}\right] & \left[\left(\frac{z_{11\_p\%2}}{z_{22\_p\%2}}\right)+\frac{1}{2}\right] & \left[\left(\frac{z_{11\_p72}}{z_{22\_p72}}\right)+\frac{1}{2}\right] \\
\left[\frac{1}{2}\left(\frac{z_{11\_p02}}{z_{22\_p02}}\right)+1\right] & \left[\frac{1}{2}\left(\frac{z_{11\_p12}}{z_{22\_p13}}\right)+1\right] & \left[\frac{1}{2}\left(\frac{z_{11\_p22}}{z_{22\_p22}}\right)+1\right] & \left[\frac{1}{2}\left(\frac{z_{11\_p32}}{z_{22\_p32}}\right)+1\right] & \left[\frac{1}{2}\left(\frac{z_{11\_p\#2}}{z_{22\_p\#2}}\right)+1\right] & \left[\frac{1}{2}\left(\frac{z_{11\_p52}}{z_{22\_p52}}\right)+1\right] & \left[\frac{1}{2}\left(\frac{z_{11\_p\%2}}{z_{22\_p\%2}}\right)+1\right] & \left[\frac{1}{2}\left(\frac{z_{11\_p72}}{z_{22\_p72}}\right)+1\right] \\
\left[\left(\frac{z_{11\_p01}}{z_{22\_p01}}\right)+\frac{1}{2}\right] & \left[(0)+\frac{1}{2}\right] & \left[(0)+\frac{1}{2}\right] & \left[(0)+\frac{1}{2}\right] & \left[\left(\frac{z_{11\_p\#1}}{z_{22\_p\#1}}\right)+\frac{1}{2}\right] & \left[\left(\frac{z_{11\_p51}}{z_{22\_p51}}\right)+\frac{1}{2}\right] & \left[\left(\frac{z_{11\_p\%1}}{z_{22\_p\%1}}\right)+\frac{1}{2}\right] & \left[\left(\frac{z_{11\_p71}}{z_{22\_p71}}\right)+\frac{1}{2}\right] \\
\left[\frac{1}{2}\left(\frac{z_{11\_p01}}{z_{22\_p01}}\right)+1\right] & \left[\frac{1}{2}(0)+1\right] & \left[\frac{1}{2}(0)+1\right] & \left[\frac{1}{2}(0)+1\right] & \left[\frac{1}{2}\left(\frac{z_{11\_p\#1}}{z_{22\_p\#1}}\right)+1\right] & \left[\frac{1}{2}\left(\frac{z_{11\_p51}}{z_{22\_p51}}\right)+1\right] & \left[\frac{1}{2}\left(\frac{z_{11\_p\%1}}{z_{22\_p\%1}}\right)+1\right] & \left[\frac{1}{2}\left(\frac{z_{11\_p71}}{z_{22\_p71}}\right)+1\right] \\
\left[\left(\frac{z_{11\_p00}}{z_{22\_p00}}\right)+\frac{1}{2}\right] & \left[(0)+\frac{1}{2}\right] & \left[(0)+\frac{1}{2}\right] & \left[(0)+\frac{1}{2}\right] & \left[(0)+\frac{1}{2}\right] & \left[\left(\frac{z_{11\_p50}}{z_{22\_p50}}\right)+\frac{1}{2}\right] & \left[\left(\frac{z_{11\_p\%0}}{z_{22\_p\%0}}\right)+\frac{1}{2}\right] & \left[\left(\frac{z_{11\_p70}}{z_{22\_p70}}\right)+\frac{1}{2}\right] \\
\left[\frac{1}{2}\left(\frac{z_{11\_p00}}{\cdots}\right)+1\right] & \left[\frac{1}{2}(0)+1\right] & \left[\frac{1}{2}(0)+1\right] & \left[\frac{1}{2}(0)+1\right] & \left[\frac{1}{2}(0)+1\right] & \left[\frac{1}{2}\left(\frac{z_{11\_p50}}{\cdots}\right)+1\right] & \left[\frac{1}{2}\left(\frac{z_{11\_p\%0}}{\cdots}\right)+1\right] & \left[\frac{1}{2}\left(\frac{z_{11\_p70}}{\cdots}\right)+1\right]
\end{bmatrix}
$$